NEST

National Enterprise for nanoScience and nanoTechnology

Laboratories

LABORATORIO NEST

NATIONAL ENTERPRISE FOR NANOSCIENCE AND NANOTECHNOLOGY

LABORATORIO NEST

Scientific report and five-year proposal

Index

Executive summary

The present document provides a scientific, financial and institutional report of Laboratorio NEST, the National Enterprise for nanoScience and nanotechnology, for the period 2008-2013 and a proposal for its development lines for the next five years.

The report illustrates the evolution of the NEST initiative at the Scuola Normale Superiore: NEST has grown into a multi-institutional enterprise through formal long-term partnerships with Consiglio Nazionale delle Ricerche, Istituto Italiano di Tecnologia, and Scuola Superiore Sant'Anna. This evolution was motivated by the objective to make available a competitive, well-equipped multidisciplinary research environment ideally suited to train undergraduate and graduate students in the dynamic field of nanoscience and nanotechnology. Critical mass was impossible to reach with staff and resource from SNS only, but the multi-institution format chosen is believed to have achieved this goal. This will be illustrated also by providing a description of the laboratory facilities available at NEST.

A description of the main research activities and a complete list of publications are provided that demonstrate the degree of success and the breadth of the scientific activities: from the bibliographical point of view, in the period here examined the number of yearly NEST citations more than doubled (in fact it increased by about 120%). Proponents wish to underline the direct involvement of SNS students in all activities and the fruitful interactions within Scuola Normale Superiore (particularly with biologists, chemists, and, of course, physicists). In general, since this report is designed for the evaluation of Laboratorio NEST, only publications, activities, and projects that see the *direct* involvement of Scuola Normale Superiore people are included. All activities presented here were largely based on external funding and proponents wish to stress the degree of success of NEST in attracting national and European resources. More recently an increasing presence of NEST in the Regional community (and beyond) as a technology transfer center can be reported. NEST is now a regional "Centro di competenza" for industries and the scientific reference for the Capannori Science Park "Toscana Nanotech", we foresee that this aspect will pay an increasing role in the near future.

The impact of NEST on SNS educational activities remains one of the main indicators of success for us and will be addressed in several points, in particular by providing the complete list of students that carried out their thesis work (laurea or PhD theses) at NEST.

Finally, the proposed development lines will be put forward. The foreseen evolution of NEST will be presented and the main scientific and technological directions schematically described within the vast and rapidly evolving fields of nanoscience and nanotechnology.

1. Scientific report

2008 - 2013

1.1 The NEST initiative

NEST, the National Enterprise for nanoScience and nanoTechnology, is an interdisciplinary research and training centre where physicists, chemists and biologists investigate scientific issues at the nanoscale. This knowledge is exploited to develop innovative nanobiotechnological tools, nanoelectronic and photonic devices and architectures.

NEST is located in the San Silvestro building, the seat of Scuola Normale Superiore at the time of its foundation in 1810. Scuola Normale Superiore decided to enter the field of nanoscience in 2001 by applying to the Istituto Nazionale per la Fisica della Materia (INFM) for the establishment of one of its Excellence centers. The proposal was selected and funded, as a result NEST was created. Since then a number of institutional changes occurred and INFM itself does not exist anymore, but was absorbed by the Consiglio Nazionale delle Ricerche. Scuola Normale Superiore, however, never abandoned its target of creating a competitive center for research and training in nanoscience and nanotechnology. This objective was pursued by consistently investing in this initiative, but, more importantly, by forming a stable network of collaborations that made NEST an attractor for other institutions that found it the ideal location to establish related and closely integrated research entities that all share the NEST "brand".

Today the NEST initiative comprises four distinct institutions: Scuola Normale Superiore, Istituto Italiano di Tecnologia, Consiglio Nazionale delle Ricerche and, a very recent addition, Scuola Superiore Sant'Anna. Although each institution has its own staff and administration (Laboratorio NEST of SNS, IIT@NEST Center for Nanotechnology Innovation of IIT, the Istituto Nanoscienze of CNR, and nanoPlant of Scuola Sant'Anna) facilities and activities are closely coordinated and scientists team up for specific scientific objectives regardless of their affiliation.

This concentration of efforts and flexibility allows NEST scientist to address a rather broad range of experimental and theoretical research activities that span from semiconductor/superconductor nanostructure design, growth and investigation to single-molecule studies in live cells and tissues. Despite this broad scope, NEST scientists adopt a unified approach thanks to the close cultural integration of its multidisciplinary teams.

From the point of view of Scuola Normale Superiore this format represents a unique opportunity to reach critical mass and offer a truly state-of-the-art environment for its students that find at NEST research and training conditions that are at the highest level and fully comparable to the best university laboratories worldwide.

1.2 People and facilities @ NEST

The following data are relative to year 2013.

1.2.1 People at NEST

The Scuola Normale Superiore staff comprises:

Professors	Fabio Beltram Rosario Fazio	Vittorio Giovannetti
Ricercatori (tenured)	Stefano Luin	
Ricercatori	Silvia Landi	Davide Rossini
Assegnisti (Fellows)	Pietro Artoni Marco Brondi Alberto Carlini Antonella De Pasquale Andrea Gamucci Emanuela Jacchetti Jiasen Jin Laura Marchetti Andrea Mari Leonardo Mazza Victor Mukherjee	Michele Nobile Francesca Pederzoli Francesco Pellegrino Alessandro Pitanti Francesco Rossella Sebastian Sulis Sato Ilaria Tonazzini Vladimir Voccoli Valerio Voliani Ji-Hua Xu
PhD students	Gerardo Abbandonato Matteo Agostini Simone Barbarino Alberto Biella Fulvio Bonsignore Matteo Carrega Subhra Kanti De Teresa De Nadai Giacomo De Palma Giuseppe De Vito Carmine Di Rienzo Alessandro Farace Antonio Fornieri Umesh Prasad Gomes Aliaj Ilirjan Ang Li Sara Macchi Subrata Mal Luca Masini Sandro Meucci	Domenico Montemurro Francesco Mazza Antonella Negro Paola Parlanti Libero Pizza Enrico Pracucci David Porciani Lorenzo Romeo Alberto Ronzani Fabrizio Salomone Melissa Santi Thomas Satzoukidis Barbara Storti Marco Travagliati Fabio Trovato Francesco Trovato Stefano Valentini Andrea Ursic Simone Zanotto

Undergraduate students	Rosy Amodeo	Stefano Guiducci
	Lorenzo Baldacci	Matteo Ippoliti
	Luca Matteo Barbieri	Ludovico Lami
	Vezio Bianchi	Carlo Maria Lazzarini
	Anna Bochicchio	Davide Orsucci
	Domenico Cassano	Luca Pesce
	Martino Alfredo Cappelluti	Angelo Piga
	Tommaso Cavallucci	Alessandro Ranalli
	Alessandra Cecchini	Luca Rigovacca
	Alessandro David	Antonio Rossi
	Sergio Lucio De Bonis	Lorenzo Scipioni
	Gianmarco Ferri	Andrea Sonnellini
	Leonardo Filareti	Giulia Spampinato
	Emanuele Fiorino	Francesco Tavanti
	Marco Galimberti	Davide Toniolo
	Andrea Giuntoli	Leonardo Viti
	Francesco Gobbo	

Technical Staff	Pietro Barnini	Bruno Guidi
	Franco Carillo	Claudio Lelli
	Daniele Ercolani	Pasqualantonio Pingue
	Paolo Faraci	

Administrative staff	Antonella Sagramoni

For what concerns the whole NEST community the following chart shows the numbers relative to the three main institutions. Under "Researcher staff" we provide the total number of ricercatori, professors and assegnisti (fellows).

NEST staff
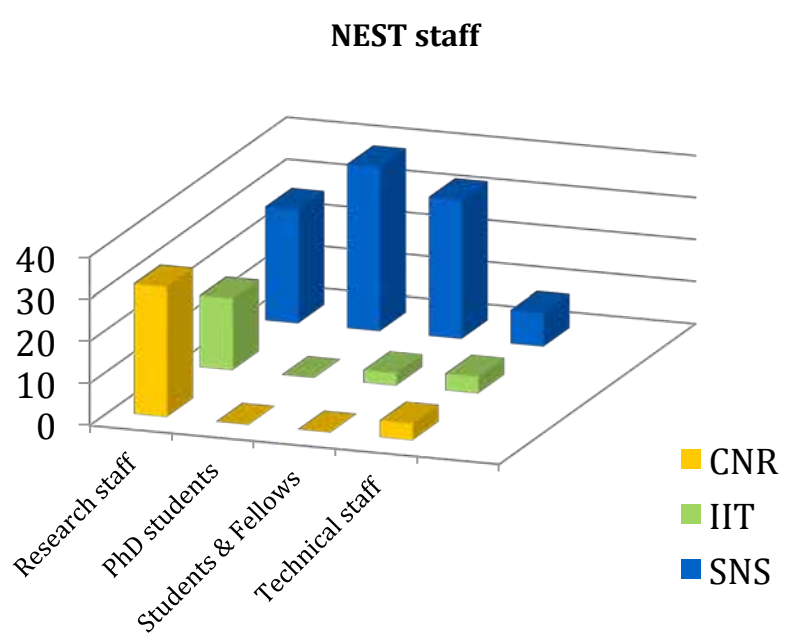
1.2.2 Research facilities at NEST

A detailed description of each laboratory is available on the Laboratory's web site (www.laboratorionest.it/facilities), in this section floor maps and a synthetic description of the present destination of each room/laboratory are provided.

Ground Floor

A Offices
B Offices
C Reception
D Meeting Room

0.1 Low-temperature magneto transport and optics
0.2 Scanning Gate Microscopy
0.3 Graphene growth
0.4 Transmission Electron Microscopy
0.5 CBE, Plasma etching and Deposition
0.6 Coherent Anti-Stokes Raman Spectroscopy (CARS)
0.7 Superconductivity
0.8 Microfluidics and cell mechano-trasduction

First floor

1.1 Clean Room Facility
1.2 Wedge bonding
1.3 Spatially-resolved Raman and two-photon microscopy
1.4 UHV-STM
1.5 Confocal Microscopy
1.6 THz Quantum Cascade Laserr
1.7 Nuclear Magnetic Resonance
1.8 BSL2 Facility
1.9 Synthesis Facility
1.10 Graphene ink and NPsRoom
1.11 Tissue Culture
1.12 Bio Chemistry and Molecular
1.13 Technical Bio Services
1.14 NanoPlant
1.15 In vivo Two Photon Imaging
1.16 Primary Cells Colture

1.3 Research highlights 2008-2013

In the following sections the activities carried out in some selected research lines are reported. Each section includes the main NEST publications that appeared in the scientific literature during the reference period.
The complete list of NEST publications for the period is provided in Section 1.4.

- 1.3.1   Terahertz photonics
- 1.3.2   Cell-penetrating peptides and endosomal trafficking
- 1.3.3   Lab on a chip - SAW fluidics
- 1.3.4   Quantum Hall Interferometry – Scanning Gate Microscopy
- 1.3.5   Green-fluorescent protein photophysics
- 1.3.6   Semiconductor nanowires: VLS growth and quantum transport
- 1.3.7   Nanotechnology for guided cell differentiation
- 1.3.8   Advanced microscopy techniques in living cells
- 1.3.9   Quantum coherent dynamics of solid state devices
- 1.3.10   Quantum simulators
- 1.3.11   Quantum transport and Majorana fermions in hybrid systems
- 1.3.12   Quantum thermal machines
- 1.3.13   Limits and properties of Bosonic Quantum Communication Channels
- 1.3.14   Open quantum systems: theoretical characterization and experimental proposals
- 1.3.15   Quantum Metrology
- 1.3.16   Quantum Optomechanics
- 1.3.17   Quantum Algorithms

1.3.1 Terahertz photonics

Quantum cascade (QC) lasers [1] are semiconductor devices in which radiation is generated by electronic transitions within an artificial crystal, a so-called heterostructure. This heterostructure consists of alternating layers of two semiconductor materials, with the layer thickness determining the electronic states inside the crystal, and thereby the frequency of the emitted light as well as the electrical transport. The operation of QC lasers in the range of frequencies 1-10 THz was demonstrated and patented at Laboratorio NEST, by employing superlattice active material and developing a waveguide concept based on interface modes called surface plasmons [2]. Here we present recent results in the implementation of THz QCLs into advanced photonic structures and novel applications, as well as in the investigation of the fundamental limits of the emission linewidth. Furthermore, THz research at NEST has evolved towards new concepts in the detection of radiation exploiting nanowire and graphene nanostructures.

The present high level of interest in THz laser sources is driven by their many potential applications. These are found in fields such as gas sensing and spectroscopy, the provision of local oscillators for heterodyne detection in astronomy and in advanced imaging techniques. Although each specific application has its own set of associated performance requirements, the majority require single mode laser light, with good beam quality and high powers. The Fabry-Perot cavities commonly used for THz QCLs tend to be intrinsically multi-
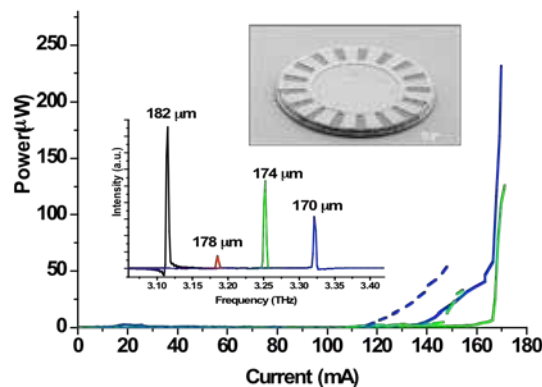

Figure 1. Light-current characteristics of ~ 3.2 THz microdisk DFB lasers. Solid lines refer to disks with 17 grating periods, dashed lines to 16. The insets show a SEM picture of the finished device and single-mode emission spectra for disks with different diameter.

mode and, equally important, their precise emission frequency cannot be determined a priori by device construction.

Distributed feedback (DFB) resonators were realized in recent past to achieve stable and predictable single mode emission. A number of different approaches were developed, all based on inserting a grating right at the top metal - semiconductor interface [3,4]. Surface-plasmon waveguides, in fact, present the nice feature of having the mode intensity peaked at the surface; any patterning of this interface is then bound to heavily affect the propagating mode. The use of higher order gratings is especially interesting for vertically emitting devices, which would otherwise be impossible, owing to the intersubband selection rules. This aspect is of relevance also to enhance the extraction of light from double-metal waveguides, which is typically quite low due to the

impedance mismatch between the guided mode and free space. We have now applied this concept to whispering gallery microdisk lasers, as exemplified in Fig. 1. By defining a circular second-order metal grating along the circumference, a single lasing whispering gallery mode can be selected and light collected in the vertical direction. Furthermore, the use of gratings with prime number circular symmetry forces the device to operate on the mode with highest vertical outcoupling, providing efficient vertical emission. The measured slope efficiency of 50 mW/A is in fact the largest observed to date for vertically emitting THz QC lasers. The beam profile is also circularly symmetric, which is an important feature for practical use in optical set-ups, and its divergence is mainly determined by the disk size [5]. To optimize this aspect, we have then modeled and fabricated THz QCLs in a ring DFB resonator of much larger diameter [6]. A second order grating with a double slit configuration was found to offer the best compromise between electrical and optical properties of the top electrode. Figure 2 shows the L-I characteristics and the measured far-field of a fabricated device. Even without collection optics employed, the devices show peak powers up to 10 mW, with a slope efficiency of ~25 mW/A, demonstrating the good radiative efficiency of this resonator and the directionality of the emitted power.
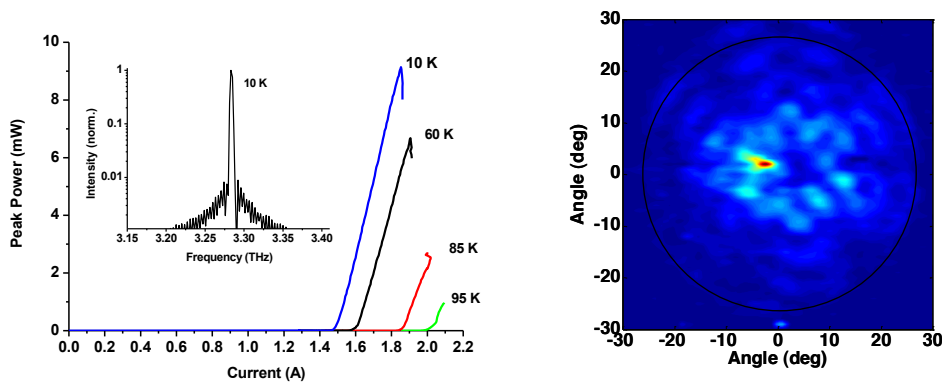

Figure 2. Left: Light-current characteristics of a ring device at different temperatures. The inset shows the spectrum of the same device on a logarithmic scale at 1.8A. Right: Measured far-field of another ring device. The black circle corresponds to the cryostat window.

An alternative concept being investigated is based on quasi-periodic linear gratings generated with a deterministic rule [7]. Single-mode THz lasers have been realized employing a specially designed Fibonacci sequence. High-power collimated emission is achieved at an angle of nearly 50° from the surface normal, and can be tailored by grating design.

Tuning of the emission line is also an important aspect for spectroscopic applications. We have recently demonstrated the first THz QC lasers operating in an external cavity. A simple configuration with a controllable end mirror placed near the laser facet without collimating optics was adopted, and the emission tuned by changing the cavity length [8]. Typical performances are reported in Fig. 3 for a 4.7 THz laser. At the moment this configuration, while simple, allows tuning ranges of ~ 2 % of the emission frequency. A different approach we have developed is instead based on using a movable-microcavity coupled with a laser through a second-order grating [9].

Interestingly, a similar set-up was also used for the first measurement of the linewidth enhancement factor in a THz QC laser using a self-mixing technique [10]. The gain dynamics within the active region of THz QC lasers was further studied through time-resolved pump-probe measurements of the gain recovery time. These were performed at the FELIX free electron laser source, monitoring the time evolution of the photocurrent induced by the THz pulses in a saturation regime of the transition [11]. The results are consistent with estimates of electron transit times in the QC superlattice.

On the other hand, we have investigated the fundamental limits to the laser emission linewidth, by analyzing its frequency noise spectrum. At high frequencies, where the 1/f contribution becomes negligible, a plateau is found, corresponding to a base floor < 100 Hz compatible with the Schawlow-Townes formula, corrected to include the contribution of thermal photons [12]. Finally, an important portion of THz research at NEST is now devoted to the development of practical applications of the THz quantum cascade technology through their implementation in sensing and imaging (including near-field) systems [13-14].

On the detection side, we have pioneered the use of field-effect nanotransistors as THz sensors, in which the rectification of the incoming signal originates from the non-linearity of the transfer characteristics. Both InAs nanowires [14-16] and graphene detectors [17-18] have been developed, with room-temperatures performances already competitive with commercial devices.

References

[1] Quantum cascade laser, Science **264**, 553 (1994). J. Faist *et al*.

[2] Terahertz semiconductor-heterostructure laser, Nature **417**, 156 (2002). R. Köhler, A. Tredicucci, F. Beltram, H. E. Beere, E. H. Linfield, A. G. Davies, D. A. Ritchie, R. C. Iotti, F. Rossi.

[3] High performance operation of single mode terahertz quantum cascade lasers with metallic gratings, Appl. Phys. Lett. **87**, 181101 (2005). L. Mahler, A. Tredicucci, R. Köhler, F. Beltram, H.E. Beere, E.H. Linfield, D.A. Ritchie.

[4] Finite size effects in surface emitting terahertz quantum cascade lasers, Opt. Express **17**, 6703 (2009). L. Mahler, A. Tredicucci, F. Beltram, C. Walther, H. E. Beere, and D. A. Ritchie.

[5] Vertically emitting microdisk lasers, Nature Photonics **3**, 46 (2009). L. Mahler, A. Tredicucci, F. Beltram, C. Walther, J. Faist, B. Witzigmann, H. E. Beere, and D. A. Ritchie.

[6] Distributed feedback ring resonators for vertically emitting terahertz quantum cascade lasers, Opt. Express **17**, 13031 (2009). L. Mahler, M. I. Amanti, C. Walther, A. Tredicucci, F. Beltram, J. Faist, H. E. Beere, and D. A. Ritchie.

[7] Quasi-periodic distributed feedback laser, Nature Photon. **4,** 165 (2010). L. Mahler, A. Tredicucci, F. Beltram, C. Walther, J. Faist, H. E. Beere, and D. A. Ritchie.

[8] Tunable terahertz quantum cascade lasers with an external cavity, Appl. Phys. Lett. **91**, 121104 (2007) J. Xu, J. M. Hensley, D. B. Fenner, R. P. Green, L. Mahler, A. Tredicucci, M. G. Allen, F. Beltram, H. E. Beere, and D. A. Ritchie.

[9] Tuning a distributed feedback laser with a coupled microcavity, Opt. Express **18**, 19185 (2010). L. Mahler, A. Tredicucci, F. Beltram, H. E. Beere, D. A. Ritchie.

[10] Linewidth enhancement factor of terahertz quantum cascade lasers, Appl. Phys. Lett. **92**, 071106 (2008). R. P. Green, J. Xu, L. Mahler, A. Tredicucci, F. Beltram, G. Giuliani, H. E. Beere, and D. A. Ritchie.

[11] Gain recovery dynamics of a terahertz quantum cascade laser, Phys. Rev. B **80**, 075303 (2009). R. P. Green, A. Tredicucci, N. Q. Vinh, B. Murdin, C. Pidgeon H. E. Beere, and D. A. Ritchie.

[12] Quantum-limited frequency fluctuations in a terahertz laser, Nature Photon. **6**, 525 (2012). M. S. Vitiello, L. Consolino, S. Bartalini, A. Taschin, A. Tredicucci, M. Inguscio, P. De Natale.

[13] Terahertz confocal microscopy with a quantum cascade laser source, Opt. Exp. **20**, 21924 (2012). U. Siciliani de Cumis, J. Xu, L. Masini, R. Degl'Innocenti, P. Pingue, F. Beltram, A. Tredicucci, M. S. Vitiello, P. Benedetti, H. E. Beere, D. A. Ritchie.

[14] Room temperature Terahertz detectors based on semiconductor nanowire field-effect transistors, Nano Letters **12**, 96 (2012). M. S. Vitiello, D. Coquillat, L. Viti, D. Ercolani, F. Teppe, A. Pitanti, F. Beltram, L. Sorba, W. Knap, and A. Tredicucci

[15] Semiconductor nanowires for highly sensitive, room-temperature detection of Terahertz quantum cascade laser emission, Appl. Phys. Lett. **100**, 241101 (2012). M. S. Vitiello, L. Viti, L. Romeo, D. Ercolani, G. Scalari, J. Faist, F. Beltram, L. Sorba, and A. Tredicucci.

[16] Terahertz detection by heterostructured InAs/InSb nanowire based field effect transistors, Appl. Phys. Lett. **101**, 141103 (2012). A. Pitanti, D. Coquillat, D. Ercolani, L. Sorba, F. Teppe, W. Knap, G. De Simoni, F. Beltram. A. Tredicucci, M.S. Vitiello.

[17] Graphene field-effect transistors as room-temperature terahertz detectors, Nature Mat. **11**, 865 (2012). L. Vicarelli, M. S. Vitiello, D. Coquillat, A. Lombardo, A. C. Ferrari, W. Knap, M. Polini, V. Pellegrini, A. Tredicucci.

[18] Photocurrent-based detection of terahertz radiation in graphene, Appl. Phys. Lett. **103**, 211120 (2013). A. Tomadin, A. Tredicucci, V. Pellegrini, M. S. Vitiello, M. Polini.

1.3.2 Cell-penetrating peptides and endosomal trafficking

The selective permeability of the plasma membrane prevents most exogenous agents from gaining cellular access, thus severely hindering drug delivery attempts. Engineering of molecular vectors able to successfully tackle this issue is one of the most intriguing challenges in nanomedicine. Our strategy is focused on the design and production of modular, biocompatible molecular nanomachines capable of reaching chosen compartments in specific cells. Such a modular system may comprise: i) a molecular motif(s) capable of interacting with cellular membranes, promoting vector internalization (e.g. by endocytosis) and effective translocation to the interior of the cell.; ii) a sequence allowing vector selective localization to the desired intracellular targets; iii) an active payload (e.g. DNA for gene therapy, a probe for diagnostic imaging), and iv) a scaffold moiety (e.g. dendrimer, gold nanoparticle) allowing multiple and controlled functionalization of the single components. Our 2008-2013 research activity describes the demonstration of several of the desired modules and provides further information on their use as part of nanosystems addressing specific issues of biological/clinical relevance. The acquired knowledge will open the way to combine the advantages of the single modules into more efficient supramolecular assemblies.

High-delivery yields, low toxicity, and the possibility to successfully enter a wide range of target cells make cell-penetrating peptides (CPPs) excellent candidates as transporters for drug-delivery applications, in many aspects superior to commonly used delivery agents and techniques (e.g. liposomes, microinjection, electroporation, viral systems). Unfortunately, CPP-attached cargoes are usually taken up by endocytosis and consequently trapped (and degraded) into acidic endosomal compartments [1]: this severely limiting the efficacy of this strategy. In order to overcome this problem, we devised a modular peptidic moiety comprising a motif that enables effective translocation through the cell membrane and a motif that promotes endosomal escape. We screened a number of candidate sequences selected from natural sources (i.e. toxins, viral proteins and antimicrobics) for their ability to disrupt the vesicular membrane and release its content. Among others, the Cecropin-A and Mellitin hybrid peptide CM_{18} (KWKLFKKIGAVLKVLTTG) proved to be among the smallest and most effective candidates with membrane-perturbing abilities. When fused to Tat_{11}
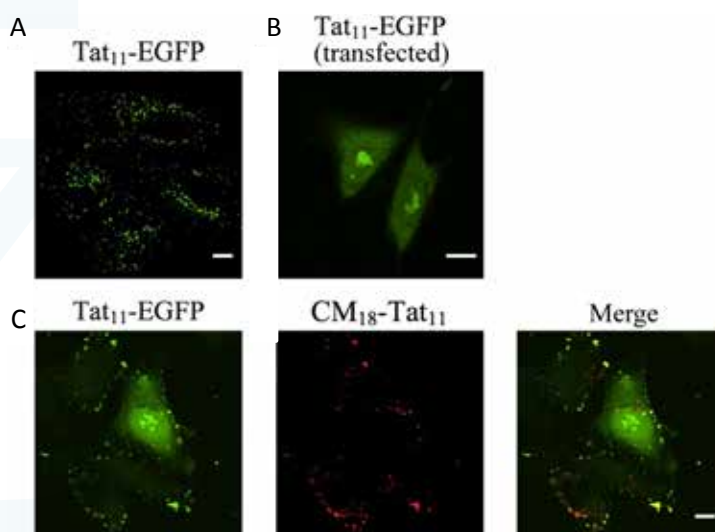

Figure 1. CM_{18}-Tat_{11}-driven cytosolic release of Tat_{11}-EGFP recombinant protein. *A*, treatment with 5 μM Tat_{11}-EGFP alone results in extensive vesicular staining, which accumulates at the perinuclear region. *B*, cells transiently transfected with Tat_{11}-EGFP plasmid. *C*, in co-treatment with 0.5 μM atto-633-labeled CM_{18}-Tat_{11}, Tat_{11}-EGFP is promptly released from vesicles into the cytoplasm, thus showing its typical intracellular localization. Scale bars: 10 μm.

peptide (YGRKKRRQRRR), it is readily taken up by macropinocytosis and concomitantly promotes membrane destabilization of the formed vesicles, thus promoting the release of co-localized membrane-impermeable molecules [2]. For instance, as shown in Fig. 1, in the presence of CM_{18}-Tat_{11} membrane impermeable Tat_{11}-EGFP recombinant protein is promptly released from vesicles into the cytoplasm, thus showing its typical intracellular localization. By means of this innovative endosomolityc peptide, we successfully delivered plasmidic DNA into cultured cells, obtaining transfection efficiencies comparable to golden standards (e.g. lipofectamine) [3].

Selective targeting of a subcellular compartment is another important aspect of peptide-mediated delivery. In the past years we demonstrated that the Tat_{11} peptide mediates nuclear transport of cargo proteins through passive diffusion and showed that rational mutagenesis of Tat sequence affords variants (e.g. Tat_{GGG}) with finely tuned inter-compartmental dynamics and controllable nuclear delivery properties [4,5]. During the reference period we identified the determinants of this intracellular targeting property. Fluorescence-based measurements (FRAP and FRET), calibration of protein concentrations, and *in vitro* binding assays were exploited to address the physicochemical mechanisms of Tat-peptide recognition by the classical Importin α (Impα) and Importin β (Impβ) receptors, as compared to the classical nuclear localization sequence from SV40 [6]. We showed that wild-type Tat peptide is an unconventional nuclear localization sequence that binds directly to both Impα and Impβ carriers in the absence of competitors (*in vitro*) (Fig. 2), whereas this property is silenced in the actual cellular environment.
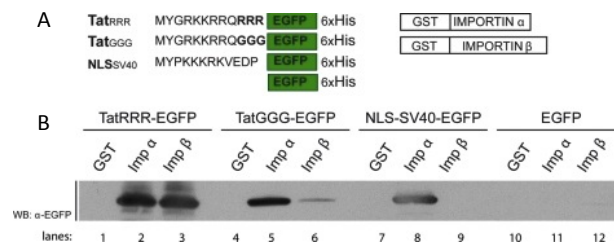

Figure 2. *A*, purified His-tagged proteins composed by Tat_{RRR}, Tat_{GGG}, and NLS_{SV40} sequences fused to EGFP and purified recombinant Impα and Impβ fused to glutathione *S*-transferase. *B*, Western blot (*WB*) filter showing the direct interaction of Tat_{RRR} and Tat_{GGG} with Impα and Impβ. The NLS of SV40 was used as a control for the interaction with Impα and not Impβ, whereas the His-tagged EGFP protein was used as a control for the absence of interaction with import carriers.

In the latter case, Impα/β-dependent nuclear import can be successfully restored by replacing the "RRR" stretch with "GGG"[7]. Based on these results, we rationalized previous controversial reports on Tat peptide transport properties and also provided general guidelines for the design of novel intracellular targeting sequences with controlled biochemistry [8,9].

Once identified peptides as vector building blocks capable to both cross cell membranes and direct cargo intracellular localization, we investigated possible

candidates as multifunctionalizable scaffold moieties. In particular, our recent research focused on dendrimers and gold nanoparticles (NPs). The former represent an exciting new class of macromolecular architecture and they are very promising tools for therapeutic and diagnostic purposes. Besides having a high degree of molecular uniformity, narrow molecular weight distribution, specific size/shape characteristics, and a highly-functionalized terminal surface, they are also endowed with cell-penetrating properties. We elucidated the intracellular trafficking properties of PAMAM dendrimers with high spatial and temporal resolution in living cells by confocal fluorescence microscopy. Macromolecules of different chemical functionality, size, and surface charge were investigated and their internalization properties correlated with the molecular structure. Toxicity data allowed the identification of dendrimers maximizing intracellular uptake with the minimum effect on cell viability. Time-lapse imaging and colocalization assays with fluorescent biomarkers for endocytic vesicles demonstrated that dendrimers are internalized by both clathrin-dependent endocytosis and macropinocytosis and are eventually delivered to the lysosomal compartment [10]. In parallel, the hyperbranched architecture of PAMAM dendrimers was exploited to label them with multiple organic fluorophores, thus enhancing fluorescent response to environmental changes [11]. Notably dual labeling with sensing and reference dyes provided ratiometric readout of physicochemical parameters such as calcium and potassium ion concentrations, or pH (Fig. 3). We evaluated these probes both *in vitro* and *in vivo*. For instance, we demonstrated that a dual labeled dendrimer is able to report quantitatively on blood acidification in brain parenchyma in a murine model subjected to CO_2 challenge [12].
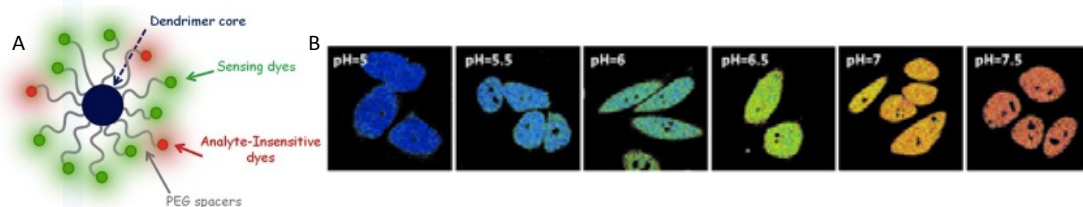

Figure 3. *A*, schematic diagram of the nanosensor, composed by a dendrimer core, and a PEG spacer functionalized with both a pH-sensitive dye (fluorescein) and a pH-insensitive one (rhodamine) . *B*, ratiometric imaging of living CHO cells clamped at different pH with the ionophore nigericin

Unlike dendrimers, gold nanoparticles require surface coating in order to become suitable as scaffold moieties. We developed several single-step methods to coat and functionalize water-reduced NPs with up to three distinct reactive groups (e.g. carboxylic acids, amines, and alkynes) [13,14]. These processes yield stable, non-cytotoxic NPs presenting multi-reactive groups on the surface; these allow rapid, selective and modular conjugation of virtually any chosen biomolecule or fluorophore. Functionalized and conjugated nanostructures were analyzed by electrophoresis, SEM, SERS; their biocompatibility and delivery capability were tested by cellular-uptake experiments. Based on this knowledge, we developed a novel nanostructured system designed for controlled (photo)release of biomolecular payloads in living cells [15, 16].
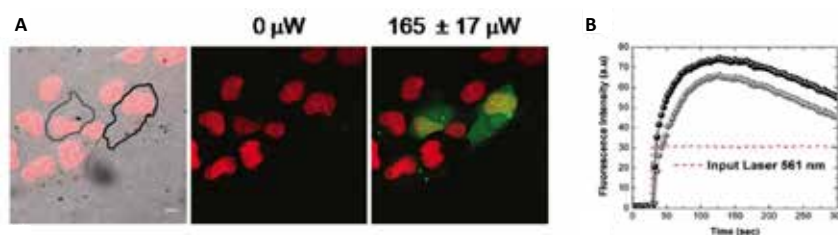
Figure 4. *A*, Cells loaded with functionalized NPs and exposed to 561 nm radiation monitored by confocal fluorescence imaging. Hoechst staining of nuclei is identified by the red LUT; green LUT describes fluorescein localization; gray LUT identifies transmission bright-field imaging. Left image: superposition of Hoechst staining and bright field; middle and right images: two frames showing Hoechst staining and fluorescein channels before 561 nm laser irradiation and after ≈ 100 s of continuous irradiation. The power of the 561 nm laser used is indicated at the top of the images. Scale bar: 10 μm. *B*, Typical average intensity traces (black/gray curves) in the fluorescein channel within the regions of interest (ROIs) shown with corresponding colors to the left image of (A). The red dashed line indicates the off and on times for the 561 nm laser light.

The system consists of a gold nanoparticle able to covalently link payloads by click-chemistry reactions. Irradiation of NP with light of suitable wavelength induces three-photon uncaging by means of photolytical triazole degradation. Owing to a non-linear effect promoted by the plasmonic resonance of the metal nanoparticle, the process can be accomplished by laser power orders of magnitude lower than that usually required for multiphoton processes. As a proof of concept, irradiation of fluorescein-conjugated NPs in living cells with low laser power at 561nm in a standard confocal microscope allowed efficient and highly controllable uncaging of the fluorescent payload within few seconds (**Fig. 4**) [15]. Moreover, when doxorubicin (a common but toxic cancer chemotherapeutic agent) is caged on the NPs with the same technique and released by irradiation with a high temporal and spatial control in osteosarcoma cells, this causes their death only in the selected area [16].

References
[1] Real-time measurement of endosomal acidification by a novel genetically encoded biosensor, Anal. Bioanal. Chem. **393**, 1123 (2009). M. Serresi, R. Bizzarri, F. Cardarelli, and F. Beltram.
[2] A novel chimeric cell-penetrating peptide with membrane-disruptive properties for efficient endosomal escape, J. Controlled Release **163**, 293 (2012). F. Salomone, F. Cardarelli, M. Di Luca, C. Boccardi, R. Nifosì, G. Bardi, L. Di Bari, M. Serresi, F. Beltram.
[3] In Vitro Efficient Transfection by CM_{18}-Tat_{11} Hybrid Peptide: A New Tool for Gene-Delivery Applications, PlosOne **8**, 7 (2013). F. Salomone, F. Cardarelli, G. Signore, C. Boccardi, F. Beltram.
[4] In vivo study of HIV-1 Tat arginine-rich motif unveils its transport properties, Mol Ther **7**, 1313 (2007). F. Cardarelli, M. Serrese, R. Bizzarri, M. Giacca, F. Beltram.
[5] Tuning transport properties of HIV-1 Tat arginine-rich motif in living cells, Traffic **9**, 528 (2008) F. Cardarelli, M. Serresi, R. Bizzarri, and F. Beltram
[6] Probing nuclear localization signal-Importin alpha binding equilibria in living cells, J. Biol. Chem. **284**, 36638 (2009). F. Cardarelli, R. Bizzarri, M. Serresi, L. Albertazzi, and F. Beltram.
[7] Quantitative analysis of Tat peptide binding to import carriers reveals unconventional nuclear transport properties, J. Biol. Chem. **286**, 12292 (2011). F. Cardarelli, M. Serresi, A. Albanese, R. Bizzarri, and F. Beltram
[8] Fluorescence recovery after photobleaching (FRAP) analysis of nuclear export rates indentifies intrinsic features of nucleocytoplasmic transport, J. Biol. Chem. **287**, 5554 (2012). F. Cardarelli, L. Tosti. M. Serresi, F. Beltram, R. Bizzarri.

[9] Fuorescence recovery after photobleaching reveals the biochemistry of nucleocytoplasmic exchange, Anal. Bioanal. Chem. **403**, 2339 (2012) R. Bizzarri, F. Cardarelli, M. Serresi, and F. Beltram.

[10] Dendrimer Internalization and Intracellular Trafficking in Living Cells, Mol. Pharm. **7**, 680 (2010). L. Albertazzi, M. Serresi, A. Albanese, F. Beltram.

[11] Delivery and Subcellular Targeting of Dendrimer-Based Fluorescent pH Sensors in Living Cells, J. Am. Chem. Soc. **132**, 18158 (2010). L. Albertazzi, B. Storti, L. Marchetti, F. Beltram.

[12] Dendrimer-based fluorescent indicators: in vitro and in vivo applications, PLoS ONE **6**, e28450 (2011). L. Albertazzi, M. Brondi, G.M. Pavan, S. Sulis Sato, G. Signore, B. Storti, G.M. Ratto, F. Beltram.

[13] Single-step bifunctional coating for selectively conjugable nanoparticles, Nanoscale **2**, 2783 (2010). V. Voliani, S. Luin, F. Ricci, and F. Beltram.

[14] Peptidic coating for gold nanospheres multifunctionalizable with photostable and photolabile moieties, J. Materials Chem. **22**, 14487 (2012). V. Voliani, F. Ricci, S. Luin, F. Beltram.

[15] Multiphoton molecular photorelease in click-chemistry-functionalized gold nanoparticles, Small **7**, 3271 (2011). V. Voliani, F. Ricci, G. Signore, R. Nifosì, S. Luin, F. Beltram

[16] Cancer phototherapy in living cells by multiphoton release of doxorubicin from gold nanospheres, J. Materials Chem. **1**, 4225 (2013). V. Voliani, G. Signore, O. Vittorio, P. Faraci, S. Luin, J. Peréz-Prieto, F. Beltram

1.3.3 Lab on chip - SAW fluidics

The increasing demand for low-cost and portable devices for biomedical applications has stimulated the development of advanced micro-total-analysis systems (μTAS) [1]. For a full exploitation of the advantages of microfluidics one needs highly controlled liquid flows into biochips. In the common case of hydrophobic capillaries, polar fluids must be forced through microchannels by means of active pumping elements, in order to overcome the large resistance to flow due to the small microchannel sections. The existing pumping systems typically rely on external pressurized lines, which unavoidably limit the portability of microfluidic systems. In the last years, the interaction between surface acoustic waves (SAWs) and liquids was explored as a pumping approach, relying on the streaming effect that drives the fluid flow in the direction of SAW propagation [2]. SAW methods have been mainly limited to mixing, localization or transport of droplets deposited on planar substrates, preferably patterned by regions of different wettability. The main issues of such open digitalized microfluidic architectures are the liquid evaporation and a remarkable sensitivity to surface contamination.
Lab-on-a-Chip research activity at NEST lab aims to the design and realization of handheld, battery-operated chips based on SAW-driven micropumps and closed microchannel networks suitable for automated, high-throughput, cost-effective architectures.

We investigated the application of SAW based pumping methods to microchannel environments fully compatible with μTAS applications, studying the flow of water and protein solutions in prototypical devices made by a piezoelectric $LiNbO_3$ substrate and elastomeric polymer patterns defining the capillary circuits.

We employed a combination of photo- and soft lithography to fabricate devices with different fluidic geometries. The basic layout consisted of two layers. The bottom layer was a $LiNbO_3$ substrate, with two microfabricated interdigital transducers (IDTs) for SAW excitation and detection. The IDTs were composed by 20 pairs of 500-μm-long Al fingers with 24 μm periodicity (~160 MHz resonance frequency on $LiNbO_3$), placed at a distance of 3.4 μm. The upper layer was a patterned polydimethylsiloxane (PDMS) film. Channel geometries with lateral dimensions between 120 and 520 μm and relative heights between 10 and 50 μm were transferred onto PDMS replicas. Final devices were straightforwardly assembled by conformal bonding of the two layers (Fig. 1): the hybrid microchannels were thus defined by the $LiNbO_3$ bottom wall and the PDMS lateral and top walls.
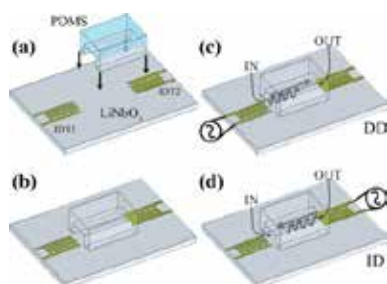

Figure 1. Scheme for the assembling of microfluidic devices and the activation of the liquid motion into microchannels: (a) and (b) final devices were fabricated by the superposition of a PDMS textured element and a $LiNbO_3$ substrate layer with IDTs for SAW excitation and detection; (c) DD and (d) ID experimental arrangements.
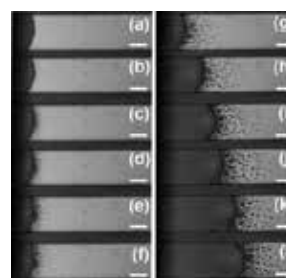

Figure 2. Photographs of the water withdrawing micropumping at different times (*t*). From (a) to (l): *t* = 0.00, 0.05, 0.06, 0.08, 0.09, 0.13, 0.53, 1.51, 2.46, 3.48, 4.49, and 5.49 s, respectively. Marker = 100 μm.

The liquid reservoirs consisted in de-ionized water drops of about 2 ml released at the entrance of the microchannels. Continuous SAWs were excited, and the position of the water-air interface within the channel was monitored as a function of time and power of the signal applied to the IDT (P_{SAW}). We analyzed two different experimental arrangements. First, SAWs were excited from one IDT to the channel entrance and, hence, along the channel toward its outlet [direct drive (DD)] [Fig. 1(c)]. Second, the SAWs were launched in the opposite direction, i.e., from the other IDT, so that SAWs propagated from the channel outlet toward its inlet [inverted drive (ID)] [Fig. 1(d)]. In case of conventional DD, with increasing P_{SAW}, we observed droplet deformation caused by acoustic streaming and, finally, a rather slow movement of the liquid into the channel (P_{SAW} = 20 dBm). At these power values, however, significant droplet atomization occurred that strongly affected the droplet outside the channel, where incoming SAW power was maximum. This led to fast evaporation of the water reservoir and prevented the filling of the microchannel.

ID showed a very different behavior [3]. For P_{SAW} >14 dBm, a fast liquid transfer from the reservoir droplet into the microchannel (Fig. 2) was observed. We stress that the liquid was driven in the opposite direction with respect to the SAW propagation direction. In view of the known SAW-fluid interaction properties[2] so far leading to liquid drag only along the SAW direction, this phenomenon was quite unexpected. Figure 2 displays a typical filling process, where water nebulization was visible at the meniscus position. ID pumping is surprising in light of the fact that any momentum transfer to the liquid must be in the opposite direction with respect to actual fluid flow. Conventional acoustic-streaming physics, therefore, does not apply. In order to understand this dramatic difference between the ID and DD behaviors we must consider the different positions where the SAW-liquid interaction occurs. In the ID configuration, the interaction is maximum within the capillary and leads to a drastically enhanced water nebulization rate at the meniscus position. This atomization leads to the formation and growth of water particles sprayed off the main fluid drop within the channel (Fig. 2). The evolution of these droplets and their interaction with the liquid meniscus determine the observed pumping phenomenon: small droplet generation is followed by coalescence and final merging with the meniscus. The latter phenomenon changes the position of the liquid-air interface, resulting in a net fluid movement in the opposite direction with respect to SAW propagation. The filling velocity (v_{fill}) could be controlled up to a maximum value of 1.24 mm/s (i.e., about 0.3 ml /min for the present channel geometry) by varying P_{SAW} up to 20 dBm, yielding rapid filling (t=0.9 s) of the whole channel, without significant evaporation of the droplet reservoir.

We also tested the compatibility of this pumping method with biological solutions [4]. Efficient microchannel filling was easily obtained also for solutions of fluorescent proteins (Fig. 3). For sake of example, in case of a channel with section 200 x 20 μm^2 coupled to an IDT working at a resonance frequency of 151 MHz, a filling velocity of about 50 mm s^{-1} was measured (for W = 21.5 dBm).

Importantly, the protein fluorescence intensity and spectral characteristics (peak wavelength, λ_{E1GFP}, and emission full width at half maximum, $\Delta\lambda_{E1GFP}$ were not

significantly affected by the interaction with the SAW and with the hybrid channel during the entire filling process (Fig. 9). The unaltered protein fluorescence confirms the suitability of SAW withdrawing in microchannels for biological applications.
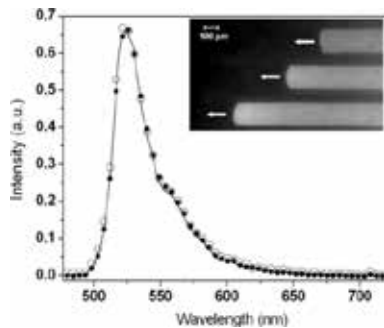

Figure 3. E1GFP emission spectra at the entrance of SAW microchannels (open dots), within microchannels during SAW withdrawing (solid line), and at the exit of the microchannels (full dots). No significant intensity or spectral differences were observed during and after the filling process. For all the spectra, l_{E1GFP} = 524 nm and Dl_{E1GFP} = 29 nm. Inset: fluorescence images of E1GFP solution withdrawing micropumping at different times (t). From top to bottom: t=0.00, 10.15, 19.45 s.
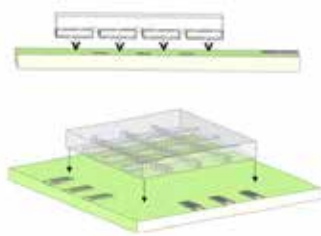

Figure 4. Schematization of a microfluidic chip based on a PDMS microchannel network and IDTs as integrated micropumps.

ID appears to be very promising for the fabrication of integrated micropumps for microfluidic chips and μTAS. Indeed, the present approach requires only an external signal generator set at the IDT resonance frequency. Importantly, impedance matching and device geometry optimization (i.e., channel shape, IDT periodicity/aperture, IDT position, etc.) will enable battery-operated systems.

$t_0 = 0$ N5$_{on}$
$t_1 = 44s$ N5$_{off}$, W3$_{on}$
$t_2 = 2m42s$ W3$_{off}$, N4$_{on}$
$t_3 = 3m05s$ N4$_{off}$, W2$_{on}$
$t_4 = 4m10s$ W2$_{off}$, N3$_{on}$
$t_5 = 4m23s$ N3$_{off}$, W1$_{on}$
$t_6 = 4m59s$ W1$_{off}$, N2$_{on}$
$t_7 = 6m04s$ N2$_{off}$, N4$_{on}$
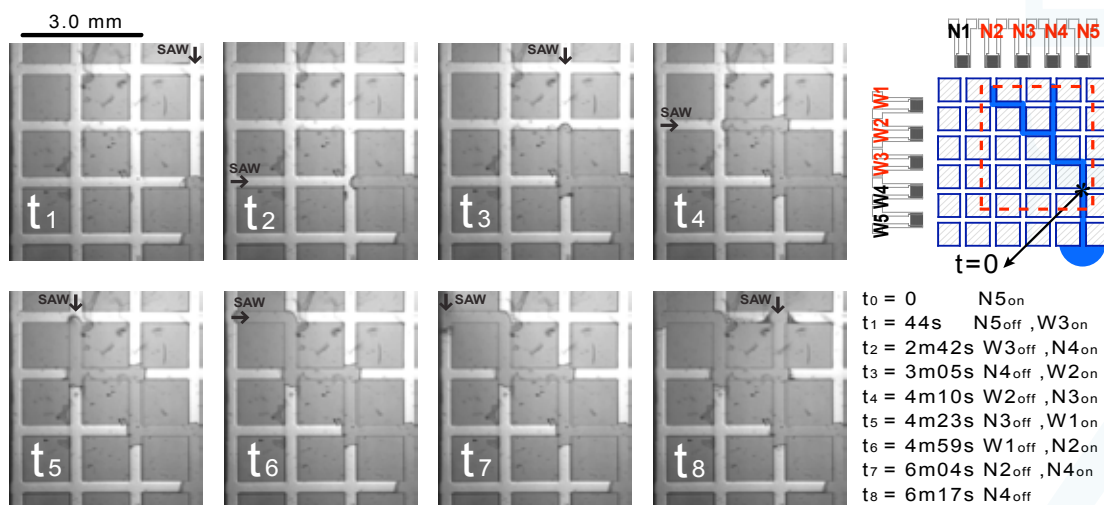$t_8 = 6m17s$ N4$_{off}$

Figure 5. Micropumping cycle exploiting 7 different SAW micropumps acting along a network of 7 microchannels, containing 6 cross areas for a total fluidic volume of 500 nl. The final liquid pattern (t_8) was achieved by inducing 6 direction changes (from t_2 to t_7) and one fluid split (t_8).

Work is in progress to extend this approach to more complex microfluidic networks by integrating several IDTs on the same chip to drive fluids along specific diagnostic paths (Fig. 4). SAW-based counterflow was successfully exploited to control liquids in hydrophobic microchannel arrays. The devices were formed by a 5×5 orthogonal array of hybrid $LiNbO_3$/PDMS microchannels (20 input/output ports, 25 crossing areas) and 20 IDTs for SAW excitation and detection. SAW-induced acoustic counterflow was demonstrated capable of: i) filling discontinuous microchannels; ii) inducing 90° flow direction changes; iii) extracting fluid laterally from filled microchannels; and iv) flow splitting and simultaneous multichannel filling. Finally, one example of a complex filling sequence was given showing 6 direction changes and one fluid split (Fig. 5).

Finally, we recently demonstrated a new protocol based on spatiotemporal image correlation spectroscopy to map velocity fields in microfluidic devices[7-8], and automated architectures for on-chip routing of fluids that we believe nicely show the potential for practical implementations based on our pumping mechanism [9].

References
[1] Microfluidics: Fluid physics at the nanoliter scale, Rev. Mod. Phys. **77**, 977 (2005). T M Squires and S R Quake.
[2] Planar chip device for PCR and hybridization with surface acoustic wave pump, Lab. Chip **5** 308 (2005). Z Guttenberg, H Muller, H Habermuller, A Geisbauer, J Pipper, J Felbel, M Kielpinski, J Scriba and A Wixforth
[3] Acoustic-counter-flow micro-fluidics by surface acoustic waves, Appl. Phys. Lett. **92**, 104103 (2008). M. Cecchini, S. Girardo, D. Pisignano, R. Cingolani, and F. Beltram
[4] Polydimethylsiloxane-LiNbO₃ surface acoustic wave hybrid micropump devices for fluid control into microchannels, Lab Chip **8**, 1557 (2008). S. Girardo, M. Cecchini, F. Beltram, R. Cingolani, and D. Pisignano
[5] F Beltram, M Cecchini, R Cingolani, S Girardo, D Pisignano "Micro/nanofluidic channels structure fluid motion controlling device for chips (e.g. micromixers) for e.g. biological applications has polydimethylsiloxane structured volume, and piezoelectric substrate having active control mechanism" International Patent WO2009013705-A1 (2007)
[6] Surface-acoustic-wave counterflow micropumps for on-chip liquid motion in two-dimensional microchannel arrays, Lab Chip **10**, 1997 (2010). L. Masini, M. Cecchini, S. Girardo, D. Pisignano, F. Beltram.
[7] Easy monitoring of velocity fields in microfluidic devices using spatiotemporal image correlation spectroscopy, Anal Chem **85**, 8080 (2013). M. Travagliati, S. Girardo, D. Pisignano, F. Beltram, and M. Cecchini.
[8] Fabrication, operation and flow visualization in surface-acoustic-wave-driven acoustic-counterflow microfluidics, JoVE **78**, e50524 (2013). M. Travagliati, R. Shilton, F. Beltram, and M. Cecchini.
[9] Interaction-free, automatic, on-chip fluid routing by surface acoustic waves, Lab chip **12**, 2621 (2012). M. Travagliati, G. De Simoni, C. M. Lazzarini, V. Piazza, F. Beltram, M. Cecchini.

1.3.4 Quantum Hall Interferometry – Scanning Gate Microscopy

Two-dimensional electron systems based on GaAs/AlGaAs heterostructures in a strong magnetic field were used to investigate the physics of edge modes in the quantum Hall regime. These electron states realize an ideal chiral one-dimensional electron beam which can be used both for the study of transport phenomena in one dimension and as a building block for the construction of advanced electron interferometers.

The interest in the development of solid state quantum devices goes well beyond fundamental research on many-body systems. An example is the quantum mechanics concept of *entanglement*. In the last decade entanglement has become synonymous with quantum computing. A number of physical systems were already proposed as possible candidates as quantum computing hardware. In this context, the peculiar properties of quantum Hall (QH) systems can be very useful. First of all, since these are implemented within solid state devices, they can be easily miniaturized and integrated on chip by means of well-established semiconductor-technology fabrication methods. More importantly, QH circuits operate with electrons: due to their fermionic statistics, it is much easier to obtain a single-electron rather than a single-photon source. Moreover, in QH systems, the Lorentz force compels electrons to move along counter-propagating chiral channels at sample edges. When Landau levels (LLs) in the bulk are fully occupied, backscattering between counter-propagating edge states is drastically suppressed. When several LLs are populated, edge channels consist of a series of dissipationless edge states that can be easily separated and independently contacted much like a computer bus [1]. Edge channels in the fractional QH regime are even more interesting, since their excitations are expected to display anyonic statistics.

A two-particle entangler can in principle be obtained in a two-channel conductor, for example employing two edge channels in the integer QH regime. Coherent mixing between two counter-propagating edge states was achieved by means of quantum point contacts and employed to realize an all-electronic Mach-Zehnder interferometer. Such devices have nevertheless several drawbacks caused by their non-simply connected topology. It is not obvious how to concatenate many devices in series, i.e. how to achieve scalability. On the contrary, Giovannetti and coworkers recently theoretically showed that if a coherent mixer between co-propagating edges is realized, scalable simply-connected interferometers can be build. Such devices could in principle work with many modes, if implemented in QH systems with filling factor v > 2. This advantage, along with the scalability, could be pivotal to practically access the potential of quantum circuits as electron entanglers and open the way to an innovative class of quantum computing devices.

The application of this scheme to the quantum computation of anyonic qubits crucially depends on the ability to determine (i) how parallel edge channels can be mixed, and whether this mixing is coherent or not, and (ii) the inner structure of edges, and in particular to determine possible fractional components that could be used as a bus of anyonic quasi-particles. Work at NEST is aimed at experimentally addressing these challenging questions. To this end, we combine transport measurements and a scanning probe microscopy technique to directly manipulate edge channels [2,3].

To explore the inner (fractional) structure of (integer) edges, we used the scanning gate microscopy (SGM) technique [2]. Our SGM maps provided the first images of the fractional features (corresponding to filling factors 1/3, 2/5, 3/5, and 2/3) that form the inner edge structure [4]. SGM maps showed that the edge consists of a series of alternating compressible and incompressible stripes (see Fig. 1). The high resolution of the SGM technique allowed us to directly measure stripe widths and compare them with the predictions of the edge-reconstruction theory. The experimental demonstration of fractional structures within integer edge channels represents the conclusive answer to long-time debated issues: the stripe structure explains how edge channels behave at the interface between an integer and a fractional QH phase. In this case, an integer edge is partitioned into its fractional components, so that there is continuity between the fractional incompressible stripe and the corresponding macroscopic fractional phase. This also elucidates the non-fermionic characteristics observed at NEST via finite bias measurements on point-like junctions between integer QH phases [5].
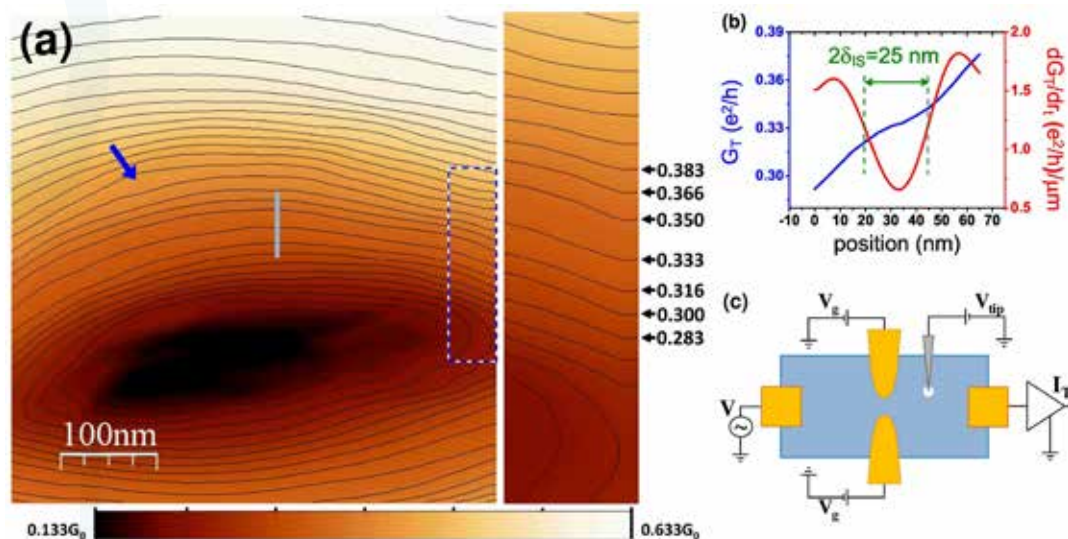

Figure 1. (a) SGM scan at the center of a QPC in a quantum Hall system at integer filling factor 1. The map shows the transmitted differential conductance as a function of the tip position, together with contour lines at constant differential conductance. On the right, a zoom of the 50 x 200 nm region corresponding to the dashed rectangle is displayed. (b) Profile of the differential conductance along the light blue line in (a), together with its derivative. (c) Scheme of the SGM experimental setup.

In these experiments we also demonstrated how to accurately control edge-channel trajectories [2]. This ability introduces a new degree of freedom in transport measurements: the device geometry itself can become a tunable experimental parameter, controllable in real time at low temperature. The unprecedented flexibility of this method has opened the way to a number of experimental opportunities, such as a QH circuit whose geometry can be controlled at low temperature by moving the tip: we used such a size-tunable QH circuit to locally investigate the microscopic processes that are responsible for the charge equilibration of bias imbalanced co-propagating channels [6,7]. These measurements clarified important findings of previous transport experiments:

on one hand our data unambiguously showed the link between inter-edge scattering and the presence of potential fluctuations [6]. On the other hand, they allowed us to explain the puzzling reduction of the threshold voltage for the onset of radiative emission [7]. Finally, our results suggest that one such device can indeed be exploited as a beam mixer for co-propagating edge channels in simply-connected Mach-Zehnder interferometers.
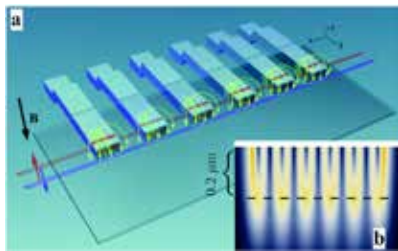

Figure 2. Schematics of the device studied. The Cobalt fingers produce a fringing field resulting in an in-plane, oscillatory, magnetic field at the level of the 2DEG residing below the top surface. The field induces charge transfer between the spin up (red line) and spin down (blue line) edge channels.

A related activity at NEST aims at experimentally demonstrating a new method to artificially couple spin-resolved edge states of a quantum-Hall insulator and induce inter-edge charge transfer associated to spin-flip scattering events. The process exploits the coupling of the electron spin with a spatially-dependent periodic in-plane magnetic field created by an array of Cobalt nano-magnets placed at the boundary of the two-dimensional electron gas (see Fig. 2). This approach could be used for the realization of scalable quantum information processing based on the spin degree of freedom of topologically-protected edge states [8].

Our results open the way to the realization of simply-connected Mach-Zehnder interferometers based on co-propagating edge channels. Our SGM work on the fractional sub-structure of edge channels furthermore indicates how to operate the interferometer with individual fractional stripes instead of single integer-edge channels. The impact of such a result can be vast since it may represent a valid step forward towards the achievement of an interferometer operating with exotic quasi-particles, like the non-abelian excitations of the ν=5/2 QH phase. Such an advance would in perspective lead to the implementation of fault-tolerant quantum computers, because of the nonlocal encoding of the quasiparticle states, which makes them immune to errors caused by local perturbations.

References
[1] Charge down and heat up, Nature Phys. **8**, 640 (2012). S. Heun.
[2] Selective control of edge channel trajectories by scanning gate microscopy. Physica E **42**, 1038 (2010). N. Paradiso, S. Heun, S. Roddaro, L. N. Pfeiffer, K. W. West, L. Sorba, G. Biasiol, F. Beltram.
[3] Imaging backscattering through impurity-induced antidots in quantum Hall constrictions, Phys. Rev. B **86**, (2012). N. Paradiso, S. Heun, S. Roddaro, G. Biasiol, L. Sorba, D. Venturelli, F. Taddei, V. Giovannetti, F. Beltram.
[4] Imaging Fractional Incompressible Stripes in Integer Quantum Hall Systems, Phys. Rev. Lett. **108**, 246801 (2012). N. Paradiso, S. Heun, S. Roddaro, L. Sorba, F. Beltram, G. Biasiol, L. N. Pfeiffer, K.W. West.
[5] Tuning non-linear charge transport between integer and fractional quantum Hall states, Phys. Rev. Lett. **103**, 016802 (2009). S. Roddaro, N. Paradiso, V. Pellegrini, G. Biasiol, L. Sorba, F. Beltram.

[6] Spatially resolved analysis of edge-channel equilibration in quantum Hall circuits, Phys. Rev. B **83**, 155305 (2011). N. Paradiso, S. Heun, S. Roddaro, D. Venturelli, F. Taddei, V. Giovannetti, R. Fazio, G. Biasiol, L. Sorba, F. Beltram.

[7] Impact of electron heating on the equilibration between quantum Hall edge channels, Phys. Rev. B **84**, 235318 (2011). N. Paradiso, S. Heun. S. Roddaro, L. Sorba, F. Beltram, G. Biasiol.

[8] Controlled coupling of spin-resolved quantum Hall edge states, Phys. Rev. Lett. **107**, 236804 (2011). B. Karmakar, D. Venturelli, L. Chirolli, F. Taddei, V. Giovannetti, R. Fazio, S. Roddaro, G. Biasiol, L. Sorba, V. Pellegrini, and F. Beltram.

1.3.5 Fluorescent proteins and their chromophore analogues: photophysics and biosensing

The complex photophysics of fluorescent proteins (FPs) in conjunction with advanced spectroscopic and microscopic techniques makes it possible to map several biochemical parameters (e.g. pH and concentration of ions) at submicrometric resolution. Furthermore 3D imaging of living cells within intact tissues, organs, and whole animals, is accessible through multiphoton excitation. Here we report our results on the photophysics of photoactivation/deactivation of some FPs and of their synthetic chromophore analogues. We exploites this knowledge for nano-resolution imaging and for the development of new reversibly-switchable FP mutants. Finally, we report our findings on FP multiphoton excitation spectra, in particular in light of the implementation of FP-based sensors for pH and chloride suitable for in vivo applications.

Photoswitching and cis-trans photoisomerization

Novel imaging techniques emerged in recent times thanks to the development of new FPs that can be reversibly or irreversibly photoconverted between two optical states that added a "temporal dimension" to imaging of proteins at intracellular level also *in vivo*. The most impressive results were obtained by using *reversibly* switchable FPs (RSFPs) [1-4], as they allow repeated activation events, thus prolonging the observation of biological dynamics, and the photo-labeling of several subcellular regions one after the other. Furthermore, RSFPs stand as excellent fluorophores for novel nano-resolution imaging techniques based on the regioselective activation/deactivation of emissive states at the nanoscale.

We linked the photoswitching behavior of certain FPs to chromophore *cis-trans* photoisomerization. We investigated also the spectral and structural modification of synthetic chromophore analogues upon irradiation, and determined for the first time the optical, NMR and Raman spectra of neutral *trans* isomers (Fig. 1), along with photoconversion quantum yields φ_c. Surprisingly, φ_c ranges from 0.1 to 1.0, demonstrating that photoconversion is a general and very efficient intrinsic photophysical mechanism of FP chromophores, whose efficiency is modulated by the mutant-specific protein environment [1,4]. Starting from these results, we developed butenolide derivatives structurally related to the GFP chromophore; we examined in detail the photophysics of these structures, with particular attention paid to their solvatochromic and photoswitching behavior [5,6]. Butenolide derivatives show ratiometric read-out of their fluorescence emission related to polarity of the environment, and fluorescence emission related to its dielectric constant; their straightforward engineering in bio-derivatized structures for membrane and intracellular targeting and their scarce cytotoxicity were exploited in the measurement of dielectric constant in different subcellular domains (Fig. 2) [6].
Pre-resonant Raman experiments are able to determine the vibrational features of the chromophore also when embedded in the proteins (Fig. 1g,h). We studied the Raman signatures of different chromophore states in GFP mutants and compared them to those of the isolated chromophores. Our experiments allowed us to demonstrate that the *cis-trans* isomerization is responsible for the photoswitching behaviour of at least two RSFPs, namely EYQ1 (a newly developed GFP variant with T203Y E222Q) and BFPF (Y66F) [4]. In particular,

for the case of EYQ1 we showed that at pH=8 the chromophore is anionic in the native form and neutral *trans* in the photoconverted form; it is neutral *cis* in the native form at lower pH. Our investigation highlights the relevance of Raman spectroscopy for the study of the ground and metastable states of optically-active portions of proteins.
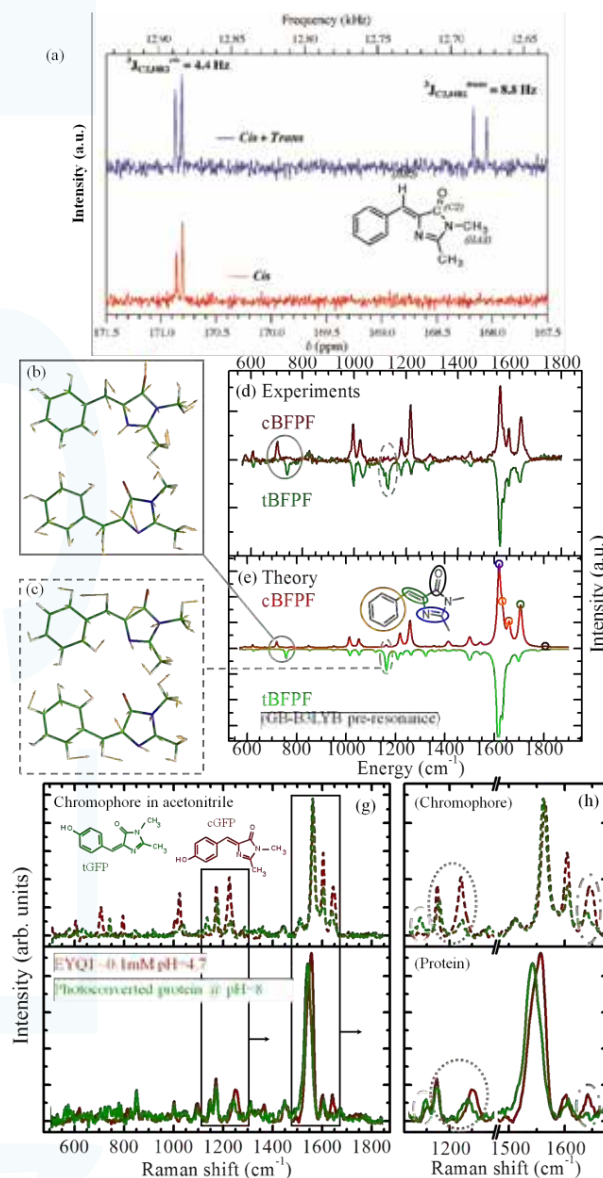

Figure 1. (a) ^{13}C-NMR spectra of native and photoconverted cBFPF while adopting selective decoupling between the methyl protons HA3 and C2: the detected $^3J_{C2,HB2}$ values in the photoproduct correspond to those expected for the *cis* and *trans* isomers. MIDDLE: Experimental (d) and calculated in vacuo (e) pre-resonant Raman spectra of the isolated chromophore of BFPF in *cis* and *trans* forms (cBFPF, tBFPF); the spectra of the photoconverted form are shown inverted around the x-axis. Solid and dashed gray ellipses highlight two of the modes that change significantly in the cis-trans transition, and that are described in panels (b) and (c). Small circles emphasize stretching modes localized on double bonds in the chromophore region, highlighted in the inset of panel (e) with corresponding color: black, C=O; green, C=C on the bridge; orange, C=C on the phenylic ring; blue, C=N. BOTTOM: The dark red solid curves represent the Raman spectrum of native EYQ1 at pH=4.7 after the subtraction of the baseline, and the dark green solid curves represent the spectrum of the photoconverted form at pH=8. For comparison are reported the Raman spectra of its neutral chromophores in *cis* and *trans* forms (cGFP and tGFP, dark red and dark green dashed curves, respectively). Panel (g) contains magnifications of the highlighted regions in panel (h); the ellipses emphasize peaks with similar behavior for isolated and protein-embedded chromophores
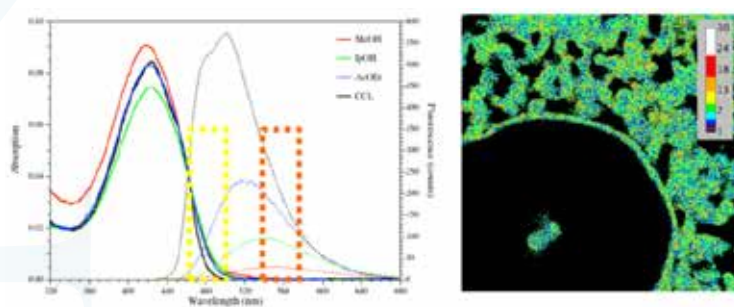

Figure 2. LEFT: absorption and fluorescence emission spectra of a butenolide derivative. The two channels selected for ratiometric analysis are highlited. RIGHT: dielectric constant map of butenolide dye in living cell.

In order to develop more efficient RSFPs, we focused on residues adjacent to the chromophore that can hinder this "intrinsic" photochromic behaviour. Hybrid QM/MM methods were applied to FPs to understand their structure/function relationship, i.e. how different chromophore structures and the amino acids surrounding the chromophore tune the excitation/emission spectrum [7]. Also with the help of these computational studies, we demonstrated that the E222Q replacement induces reversible photoswitching in four GFPs otherwise differing in the mutation pattern, and yields switching 2-3 orders of magnitude faster than in any other previously reported photoswitchable GFP [2,3]. We assessed the utility of the new RSFPs for intracellular studies *e.g.* by inverse Fluorescence Recovery After Photobleaching (iFRAP), a technique that relies on the localized photoactivation of a fluorophore and the real-time monitoring of its subsequent dynamics. EYQ2 (S65T/T203Y/E222Q) was conjugated to a short peptide sequence that acts as a nuclear localization signal (NLS), *i.e.* it is recognized by the cellular importin system and actively transported to the nucleus. Then, the dynamics of the nucleocytoplasmic shuttling of NLS-EYQ2 was determined by iFRAP (Fig. 3d). EYQ2 allowed for the long-term repetition of the experiment in the same cell, thus increasing the accuracy of kinetic measurements and ideally providing the correlation of transport dynamics with different cell states. iFRAP on NLS-EYQ2 yielded a shuttling time-constant (t=117±3 s) in excellent agreement with the value measured by conventional FRAP on NLS-EGFP.
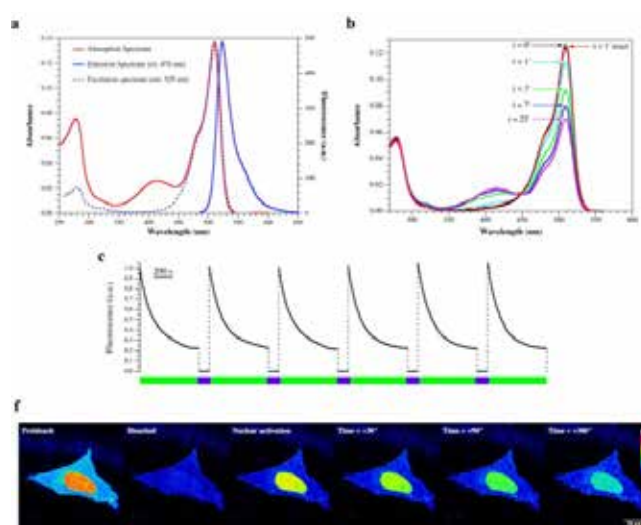

Figure 3. (a) Absorption (red line), emission (solid blue line), and excitation (dashed blue line) of EYQ1 (T203Y/E222Q) at pH 7.2; (b) Absorption spectrum photoconversion of EYQ1 at pH 8.7: following 514 nm-illumination (0.5 W/cm^2) the anionic chromophore band (510 nm) decreases its intensity and the dark state band at 410 emerges (t=0' to 25'); 405 nm-illumination (0.06 W/cm^2) for 1' is sufficient to restore the original absorption (t=1' react); (c) photoswiching on/off cycles of EYQ1 in transfected HeLa cells by means of 514-nm (*bleaching cycle: green*) and 403-nm (*reactivation step: violet*) laser light; (d) iFRAP of NLS-EYQ2 in one HeLa cell: initially fluorescence is bleached off cell-wide by 514 nm scan-irradiation; then, fluorescence is reactivated only in the nucleus by means of short (1s) 405-nm point-irradiation and the cell is imaged by using low power 514 scan-excitation

pH/chloride biosensing

The chromophore of E^{n}GFP can exist into two optically-distinguishable forms

(neutral and anionic) that are both fluorescent; such a dual fluorescence property makes possible the fabrication of ratiometric (i.e. concentration independent) pH sensors tailored to the 5-9 pH range [8,9]. Moreover, the S65T mutation introduces a specific anion-binding site in E^nGFP [8,10]. We thus decided to exploit this peculiarity in the development of a novel chloride sensor. Monitoring these parameters is of much relevance: pH is a remarkable modulator of cell structure and function, and Cl^- participates in many physiological functions including stabilization of neuronal resting potential, charge balance in vesicular acidification, and regulation of cell volume. Our sensor was conceived as ratiometric, genetically-encoded and capable to simultaneously measure $[Cl^-]$ and pH. To this end, a monomeric red protein insensitive to chloride and pH (DsRed) was fused to E^2GFP via a peptide linker, creating the sensor called Clophensor in Fig. 4 [10]. In vitro and results in living cells demonstrated the functionality of the sensor in the physiological range of pH and for Cl^- concentration ranging from 300mM down to less than 1 mM.
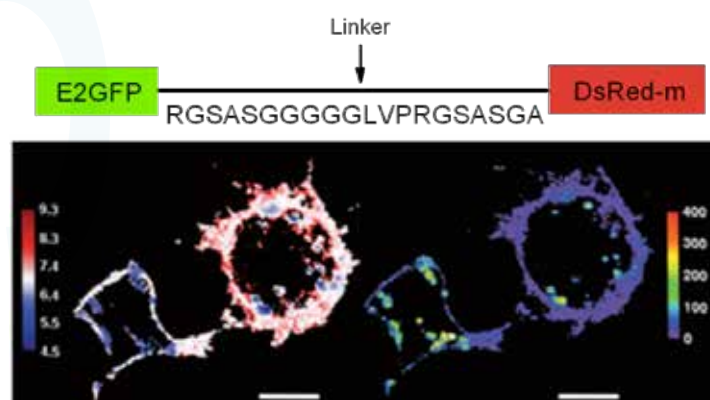

Figure 4. TOP: Cartoon scheme of the ClopHensor: E2GFP is the pH and Cl^- sensing portion, DsRed-m is the reference portion of the sensor; BOTTOM: pH (left) and $[Cl^-]$ (right) maps in living hek293 cells. The sensor was targeted to the membrane and to large dense core vesicles by means of suitable labeling (gap43 and neuropeptide Y, respectively). White bar: 5μm

We are pursuing the use of this biosensor in deep-tissue mapping, aiming at *in-vivo* experiment that can be performed via two-photon excitation microscopy. To this end, two-photon excitation and photoconversion spectra have been measured [8] and, in view of actual invio applications, an *in-utero* electroporation technique was demonstrated to control the localization for the expression of exogenous proteins in the brain of living mice [11].

From a computational point of view, we investigated the two-photon absorption (TPA) properties of various fluorescent proteins (BFP, CFP, GFP, DsRed, mOrange, zFP and Kaede), and compared them with one-photon properties, using computational methods based on Density Functional Theory. This technique allowed us to calculate excitation wavelengths and cross sections for various model chromophores. A general relationship between excitation wavelength and structure was extracted, based on the variation of electric dipole upon excitation, and ultimately connected with the extension of the π-conjugated system (an example in Fig. 5b) [7]. The two-photon calculations shed light on the peculiar TPA features of DsRed (Fig. 5a), and predicted the presence of high-energy (500-700 nm) TPA bands in several other FPs. These excitation bands, later confirmed by experiments, can provide researchers with useful, and yet unexploited, spectral windows for two-photon imaging.
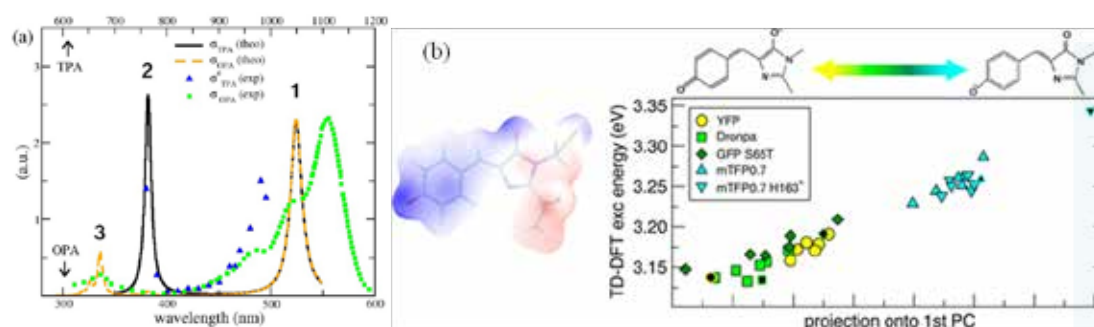
Figure 5. (a) Comparison between experimental and theoretical spectra of DsRed. The two-photon measured cross section (blue triangles) displays a strong increase below 800 nm (band **2**), whereas the one photon spectrum (green squares) is rather featureless in that region. The calculated TPA cross section (black solid line) reproduces this band, as due to excitation at a higher excited state. The blue shift between the theoretical and experimental **1** band is due to having considered the isolated model chromophore instead of the entire protein, to intrinsic errors of the theory, and to neglect of vibronic features. (b) Left: Electrostatic potential of the surrounding protein matrix mapped onto the chromophore molecular surface. Right: QM/MM TD-DFT excitation energy as a function of chromophore structure (described by a suitable linear combination of bond lengths) for various FP structures.

References

[1] Cis-trans photoisomerization of fluorescent-protein chromophores. J. Phys. Chem. B **112**, 10714 (2008). V. Voliani, R. Bizzarri, R. Nifosì, S. Abbruzzetti, E. Grandi, C, Viappiani, and F. Beltram

[2] Photoswitching of E222Q GFP mutants: "concerted" mechanism of chromophore isomerization and protonation, Photochem Photobiol. Sci. **9**, 1307 (2010). S. Abbruzzetti, R. Bizzarri, S. Luin, R. Nifosì, B. Storti, C. Viappiani, F. Beltram.

[3] Single aminoacid replacement makes Aequorea Victoria fluorescent proteins reversibly photoswitchable, J. Am. Chem. Soc. **132**, 85 (2010). R. Bizzarri, M. Serresi, F. Cardarelli, S. Abbruzzetti, B. Campanini, C. Viappiani, F. Beltram.

[4] Raman Study of Chromophore States in Photochromic Fluorescent Proteins. J. Am. Chem. Soc. **131**, 96 (2009). S. Luin, V. Voliani, G. Lanza, R. Bizzarri, R. Nifosì, P. Amat, V. Tozzini, M. Serresi, F. Beltram.

[5] Cis–trans photoisomerization properties of GFP chromophore analogs, Eur Biophys J. **40**, 1205 (2011). G. Abbandonato, G. Signore, R. Nifosì, V. Voliani, R. Bizzarri, F. Beltram.

[6] Imaging the static dielectric constant in vitro and in living cells by a bioconjugable GFP chromophore analog, Chem. Commun. **49**, 1723 (2013). G. Signore, G. Abbandonato, B. Storti, M. Stockl, V. Subramaniam, R. Bizzarri.

[7] Spectral "fine" tuning in fluorescent proteins: the case of the gfp-like chromophore in the anionic protonation state, J Chem Theory Comput **9**, 497 (2013), P. Amat, R. Nifosì.

[8] Green Fluorescent Protein-based pH indicators for in vivo use: a review, Anal. Bioanal. Chem. 393, 1107 (2009). R. Bizzarri, M. Serresi, S. Luin, F. Beltram.

[9] Real-time measurement of endosomal acidification by a novel genetically encoded biosensor, Anal. Bioanal. Chem. **393**, 1123 (2009). M. Serresi, R. Bizzarri, F. Cardarelli, and F. Beltram.

[10] Simultaneous intracellular chloride and pH measurements using a GFP-based sensor, Nature Methods **7**, 516 (2010). D. Arosio, F. Ricci, L. Marchetti, R. Gualdani, L. Albertazzi, F. Beltram.

[11] High-performance and site-directed in utero electroporation by a triple-electrode probe, Nat Commun. **3**, 960 (2012). M. dal Maschio, D. Ghezzi, G. Bony, A. Alabastri, G. Deidda, M. Brondi, S. Sulis Sato, R.P. Zaccaria, E. Di Fabrizio, G.M. Ratto, L. Cancedda.

1.3.6 Semiconductor nanowires: VLS growth and quantum transport

Self-assembled nanowires (NWs) are emerging as a versatile and powerful tool for the investigation of transport phenomena at the nanometer scale. NWs are strongly anisotropic monocrystalline nanostructures that can be fabricated by exploiting a nanoparticle-mediated growth technique known as vapor-solid-liquid (VLS) mechanism. This nanofabrication approach yields complex axial/radial nano-heterostructures in which materials that are incompatible in standard epitaxy can be combined with large flexibility. These peculiar properties make NWs attractive for what concerns both innovative fundamental research directions [1] and device implementations beyond current CMOS technology [2]. NW-related activities at NEST started in 2008, but in few years they have led to various high-impact publications that today make NEST an important player in the international NW community. Here we describe in particular our investigations on growth physics and on the development of InAs/InP single-electron transistors and superconductor-semiconductor hybrid devices.

NWs are promising demonstration of the bottom-up approach to nanoscience and nanotechnology [1,2]. The VLS mechanism for NW growth is a unique nanofabrication tool that makes it possible to design and create complex free-standing nanostructures with no need for delicate patterning procedures and complex device architectures typical of other top-down strategies. This allows the parallel fabrication of high-quality nanostructures and opens the way to large-scale production of advanced nanomaterials and nanodevices. NEST research activities on NWs started in 2008, in parallel with the installation of a chemical beam epitaxy (CBE) facility dedicated to the growth of semiconducting NWs. Since then, investigation efforts at NEST focused on two complementary fronts: (i) the progress of growth science and technology for the fabrication of innovative nanostructures; (ii) the development of novel devices based on NWs designed and realized at NEST.

Growth activities. Our Riber Compact-21 CBE system was installed in 2008 and it is still exclusively dedicated to the growth of III-V semiconductor NWs. The growth chamber is equipped with three reconfigurable injectors for the precursors of the group III (In, Ge), group V (As, P) and for the doping species (Se). The specific epitaxy technique was chosen based on the experience of leading groups worldwide and on the good trade-off between the degree of control and flexibility offered by this technology. Protocols for the fabrication of optimized InAs NWs were quickly established during few months following the installation and state-of-the-art technology for the growth of InAs/InP nano-heterostructures was established at NEST during the first two years of activity.
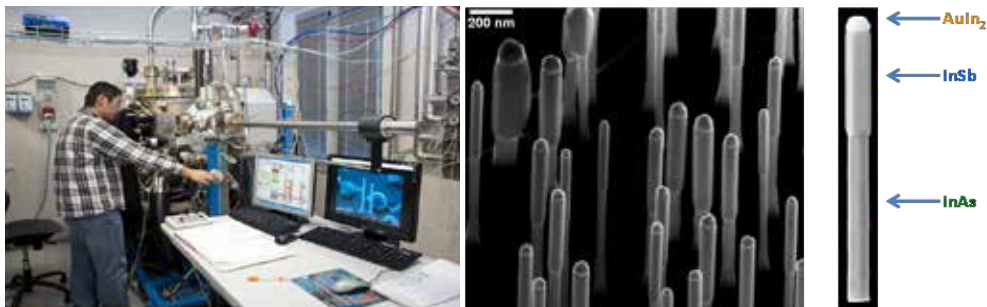

Figure 1. Left hand side, picture of the growth laboratory and of the Riber Compact-21 chemical beam epitaxy system. Right hand side: monocrystalline InAs/InSb NW heterojunctions recently developed at NEST. The nanoparticle catalyzing the growth process is clearly visible on the top of the NWs.

Subsequent research efforts further focused on: (i) new challenging materials such as InSb-based NW heterostructures (see Fig. 1), which are particularly attractive because of their high carrier mobility, small effective mass and strong quantum confinement and spin-related effects [3-8]; (ii) non-standard growth techniques, for instance based on alternative catalyst metals such as Pd [9,10]; (iii) the fine calibration of the NW parameters and structural properties of grown NWs, which are of course crucial to device implementations [11,12].

Quantum transport phenomena and devices in NWs. The VLS technology offers a practical method to produce nanostructures whose electron Hamiltonian and behavior can be designed with great freedom, thanks to the controlled definition of nanometer-scale artificial potential barriers and to the combination of different material systems. In particular, NWs can be used to strongly confine carriers in three-dimensional axial/radial heterostructures and to obtain device architectures with properties that it would be impossible or impractical to achieve using more standard epitaxy and nanofabrication methods. In addition, NW are free-standing nanostructures which can be easily removed from the growth substrate and coupled with different materials such as for instance superconductors or ferromagnets. This possibility can be exploited to induce, investigate and control transport phenomena in the NWs.

One of the main driving ideas behind NW research activities at NEST in 2008-2013 was the investigation of transport phenomena based on the combination between strongly correlated electron-systems found in superconductors and the quantum systems attainable using NWs. In hybrid nanodevices, strong electron correlations can be induced in NW-based quantum conductors and used to explore a wide range of fundamental charge and heat transport phenomena as well as device applications, including innovative transistor concepts and high-sensitivity detectors. In this context, NWs provide a valuable enabling technology to realize unique device architectures. Research efforts at NEST successfully demonstrated advanced hybrid devices based on uniform InAs NWs in which the charge flow can be controlled using quantum pumping [13], superconductive quantum interference [14] as well as out-of-equilibrium effects [15]. In order to fully exploit the possibility offered by the VLS approach, an important part of the activities was also devoted to the investigation of single-electron physics in strongly confined quantum dots based on InAs/InP heterostructured NWs, building on the established expertise of the laboratory staff on the field [16,17]. In this specific case, we successfully demonstrated the field-effect control of the charge and spin configuration of quantum dots up to an electronic temperature of about 50K [18-20], opening a new route to the implementation of single-electron transistors and detectors which are able to work at room temperature, without the need of a cryogenic equipment. Finally, NEST research activities addressed additional relevant NW transport aspects which are expected to be important for practical device applications, in particular for what concerns the role of telegraph noise [21], the interaction between charge transport and mechanical degrees of freedom [22], and perspectives for the realization of large-scale NW devices [23].

References
[1] Nanoelectronics from the bottom up, Nature Mater. 6, 841 (2007). W. Lu, C. M. Lieber.

[2] International Technology Roadmap for Semiconductors 2012, Emerging Research Devices (http://www.itrs.net/)

[3] InAs/InSb nanowires heterostructures grown by chemical beam epitaxy, Nanotechnology **20**, 505605 (2009). D. Ercolani, F. Rossi, A. Li, S. Roddaro, V. Grillo, G. Salviati, F. Beltram, L. Sorba.

[4] Growth mechanism of InAs–InSb heterostructured nanowires grown by chemical beam epitaxy, J. Crystal Growth **323**, 304 (2011). L. Lugani, D. Ercolani, F. Beltram, L. Sorba.

[5] Growth of InAs/InAsSb heterostructured nanowires, Nanotechnology **23**, 115606 (2012). D. Ercolani, M. Gemmi, L. Nasi, F. Rossi, M. Pea, A. Li, G. Salviati, F. Beltram and L. Sorba.

[6] Electron beam induced current in InSb-InAs nanowire type-III heterostructures, Appl. Phys. Lett. **101**, 063116 (2012). C. Y. Chen, A. Shik, A. Pitanti, A. Tredicucci, D. Ercolani, L. Sorba, F. Beltram, H. E. Ruda.

[7] Faceting of InAs-InSb heterostructured nanowires, Crystal Growth and Design **10**, 4038 (2010). L. Lugani, D. Ercolani, F. Rossi, G. Salviati, F. Beltram, and L. Sorba.

[8] Modeling of InAs-InSb nanowires grown by Au-assisted chemical beam epitaxy, Nanotechnology **23,** 095602 (2012). L. Lugani**,** D. Ercolani, L. Sorba, N. V. Sibirev, M. A. Timofeeva, V. G. Dubrovskii

[9] Pd–assisted growth of InAs nanowires, Crystal Growth and Design **10**, 4197 (2010). S. Heun, B. Radha, D. Ercolani, G. U. Kulkarni, F. Rossi, V. Grillo, G. Salviati, F. Beltram, and L. Sorba.

[10] Coexistence of Vapor-Liquid-Solid and Vapor-Solid-Solid Growth Modes in Pd-Assisted InAs Nanowires, Small **6**, 1935 (2010). S. Heun, B. Radha, D. Ercolani, G. U. Kulkarni, F. Rossi, V. Grillo, G. Salviati, F. Beltram, and L. Sorba

[11] Raman sensitivity to crystal structure in InAs nanowires, Appl. Phys. Lett. **100,** 143101 (2012). J. K. Panda, A. Roy, A. Singha, M. Gemmi, D. Ercolani, V. Pellegrini, L. Sorba

[12] Se-doping dependence of the transport properties in CBE-grown InAs nanowire field effect transistors, Nanoscale Res. Lett. **7,** 1 (2012). L. Viti, M. S. Vitiello, D. Ercolani, L. Sorba, A. Tredicucci.

[13] A Josephson quantum electron pump, Nature Phys. **7**, 857 (2011). F. Giazotto, P. Spathis, S. Roddaro, S. Biswas, F. Taddei, M. Governale, and L. Sorba

[14] Hybrid InAs nanowire-vanadium proximity SQUID, Nanotechnology **22**, 105201 (2011). P. Spathis, S. Biswas, S. Roddaro, L. Sorba, F. Giazotto, F. Beltram.

[15] Hot-electron effects in InAs nanowire Josephson junctions, Nano Research **4**, 259 (2011). S. Roddaro, A. Pescaglini, D. Ercolani, L. Sorba, F. Giazotto, and F. Beltram.

[16] Singlet-triplet transition in a few-electron lateral $In_{0.75}Ga_{0.25}As/In_{0.75}Al_{0.25}As$ quantum dot, Appl. Phys. Lett. **96**, 142107 (2010). F. Deon, V. Pellegrini, F. Carillo, F. Giazotto, G. Biasiol, L. Sorba, F. Beltram.

[17] Electronic properties of quantum dot systems realized in semiconductor nanowires, Semicond. Sci. Technol. **25**, 024007 (2010). J. Salfi, S. Roddaro, D. Ercolani, L. Sorba, I. Saverlyev, M. Blumin, H. E. Ruda, F. Beltram.

[18] Electrostatic spin control in InAs/InP nanowire quantum dots, Nano Lett. **12**, 4490 (2012). L. Romeo, S. Roddaro, A. Pitanti, D. Ercolani, L. Sorba, and F. Beltram.

[19] Manipulation of electron orbitals in hard-wall InAs/InP nanowire quantum dots, Nano Lett. **11**, 1695 (2011). S. Roddaro, A. Pescaglini, D. Ercolani, L. Sorba, F. Beltram.

[20] Contacts shielding in nanowire field effect transistors, J. Appl. Phys. **111,** 064301 (2012). A. Pitanti, S. Roddaro, M. S. Vitiello, A. Tredicucci

[21] Probing the Gate-Voltage-Dependent Surface Potential of Individual InAs Nanowires Using Random Telegraph Signals, ACS Nano **5**, 2191 (2011). J. Salfi, N. Paradiso, S. Roddaro, S. Heun, S. V. Nair, I. G. Savelyev, M. Blumin, F. Beltram, H. E. Ruda.

[22] Charge pumping in InAs nanowires by surface acoustic waves, Semicond. Sci. Technol. **25**, 024013 (2010). S. Roddaro, E. Strambini, V. Piazza, F. Beltram.

[23] Large-Area Ohmic Top Contact to Vertically Grown Nanowires Using a Free-Standing Au Microplate Electrode, ACS Appl. Mat. & Int. **4,** 1860 (2012). B. Radha, D. Jayaraj, G.U. Kulkarni, S. Heun, D. Ercolani, L. Sorba.

1.3.7 Nanotechnology for guided cell differentiation

The morphogenesis of mammalian organs and tissues relies on the ability of individual cells to respond to a vast range of extracellular signals. Among these are gradients of soluble molecules such as growth factor and cell-secreted mitogens encoding for preferential directions over long distances. A second class of signals is provided by the chemical and physical properties of the extracellular matrix (ECM) in the cell proximity. These guidance cues are read by cells in a process that requires the activity of specific cell-adhesion machinery and leads to the remodeling of cell shape. Several cellular responses such as polarization, migration, proliferation, and apoptosis are elicited by a direct cell-ECM interaction in virtually all cell types. A pivotal role in this process is played by the substrate nanotopography. In order to unravel the mechanisms by which differentiating cells read the local topography it is crucial to decouple its effects from those stemming from other chemical and physical stimuli. Thanks to recent advances in biomaterial nanofabrication, selected morphological aspects of the ECM are now reproducible in vitro through the realization of artificial scaffolds with controlled topography (Fig. 1). The related research activity at NEST lab follows two strategies: (i) improving the chemical and morphological properties of biomimetic two-dimensional (2D) scaffolds with nanostructured surface modifications (ii) understanding the cellular mechanisms regulating topographical guidance (iii) evaluate the impact of "noisy" guidance and investigate ways to enhance resistance to such "noise".

We established successful protocols to fabricate anisotropic nano-textures (i.e. nanogratings, alternating lines of grooves and ridges of submicron size) on thermoplastic materials. Particular attention was paid to the biocompatibility of the resulting cell scaffold. To this aim tissue-culture polystyrene (TCPS) was initially chosen [1]. The desired topography could be induced by nanoimprint lithography (NIL) [1, 2]. No further surface chemical functionalization was performed (Fig. 1A) and the resulting imprinted substrates proved optimal for the growth of PC12 cells, a well-established model of neuronal differentiation [3]. Cell-nanograting interaction on TCPS substrates was investigated specifically focusing on two aspects: the efficiency of neurite alignment (Fig. 1B) and cell polarity state (Fig. 1C-E) as induced by nanogratings with varying geometries [1, 2]. As previously reported for other cell types, PC12 cells were only marginally affected by larger structures (>1 µm linewidth) whereas sub-micron topography led to highly increased non-isotropic differentiation. Figure 1 displays the degree of axon outgrowth control determined by 750 and 500 nm linewidth gratings. The latter was found to be more effective, leading to over 90% of the axons aligning within 3 degrees to the gratings, and almost 70% of axons aligned within 10 degrees. For what concerns 750 nm linewidth substrates, 75% of axons were aligned within 30 degrees and the 36% within 10. For comparison, the same analysis was performed on cells differentiating on flat, unpatterned TCPS where no preferential directionality was observed (Fig. 1B).

Nanogratings reduced to two the number of neurites produced by PC12 cells upon treatment with NGF (Fig. 1D). Neuronal bipolarity was correlated with an increased stretching of the cell body and a reduced length of the cell protrusions (Fig. 1E).

We next analyzed the mechanisms governing the interaction between differentiating neuronal cells and our nanoimprinted topographies [4, 5]. Our work aimed at defining a biological link between the topographical configuration
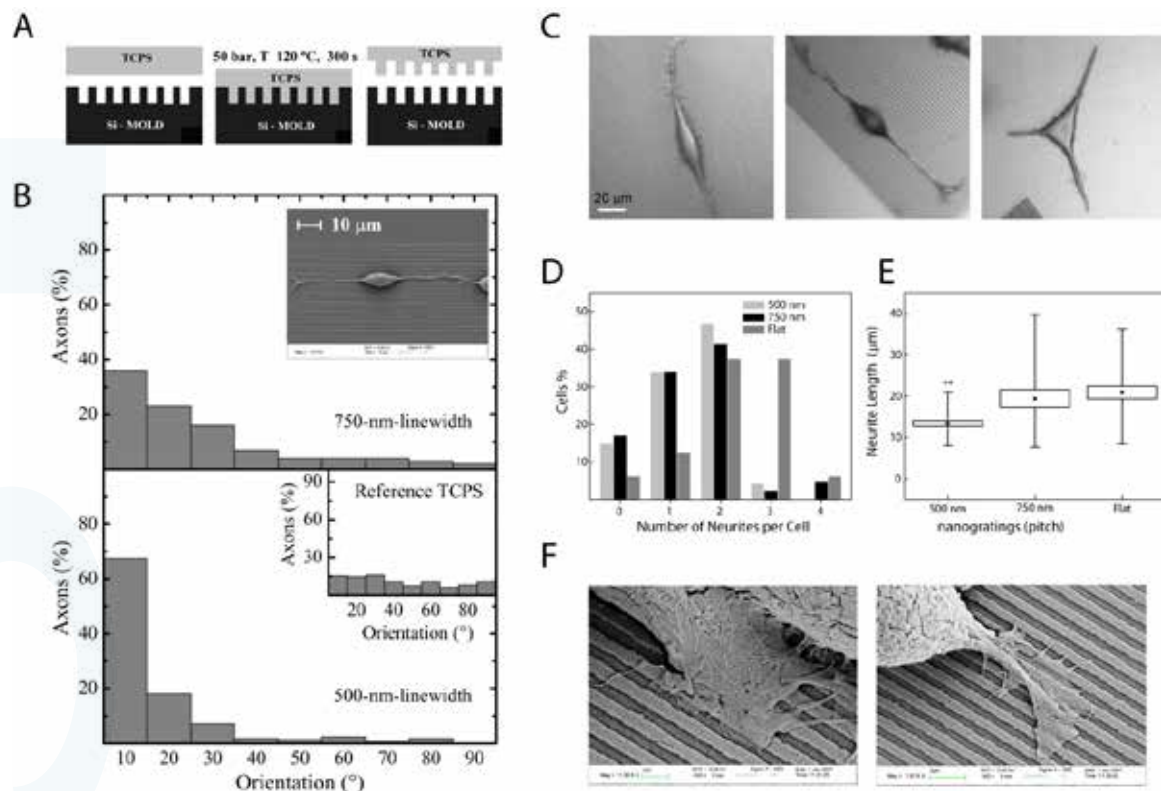
Figure 1. A) Fabrication process of TCPS-nanostructures and their characterization. TCPS were placed on top of the silicon mold and softened by increasing the temperature up to 120 ◦C (left). 20 bar pressure was applied for 5 min before cooling down to 70 ◦C (middle). The pressure was finally released and mold and TCPS detached (right). B) Quantitative analysis of guided axon outgrowth on TCPS nanogratings: percentage of axons as a function of the angle between the axon and grating-line directions for 750 nm (upper panel) and 500 nm (lower panel) linewidth gratings. The same analysis is reported in the inset of the lower panel for cell differentiation on flat TCPS. Inset of upper panel: scanning electron microscope image of a PC12 cell on a nanograting showing bipolar conformation, enhanced body elongation and guided axon outgrowth. C) Typical cell phenotype on 500 nm grating (left), 750 nm grating (center), and flat surface (right). D) Distribution of the number of neurites per cell. E) Average neurite length. Neurite lengths are reported as 10-90 percentile distribution. F) SEM images of PC12 cells differentiating on nanopatterned substrates: details of sprouting filopodia and lamellipodia.

of the substrate and the resulting cell polarity. For this activity we evaluated the use of new biocompatible materials with enhanced optical properties allowing the use of high-resolution live-cell microscopy in physiological conditions [6]. In this direction the nanoimprint protocol defined for TCPS could be further developed to obtain similar nanogratings imprinted on COC. Using these improved substrates we revealed the role played by integrin-based adhesion complexes, the focal adhesions, during neuronal differentiation on anisotropic nanotopographies [4]. First, we showed that during neuronal differentiation, topographical anisotropies control focal-adhesion maturation. Modulation of adhesions was the driving mechanism that selected the properly aligned neurites.

Notably, by varying a single topographical parameter of the substrate, orientation and maturation of focal adhesions could be finely modulated yielding independent control over the final number and the outgrowth direction of neurites [7]. Second, we demonstrated that a guiding topography can induce and consolidate a single polarity state by regulating the cell differentiation machinery. Hence, differentiating neurons can not only 'read' the topographical guidance cues, but can also re-localize specific cellular activities along preferential directions and thus 'learn' to achieve a committed differentiation.
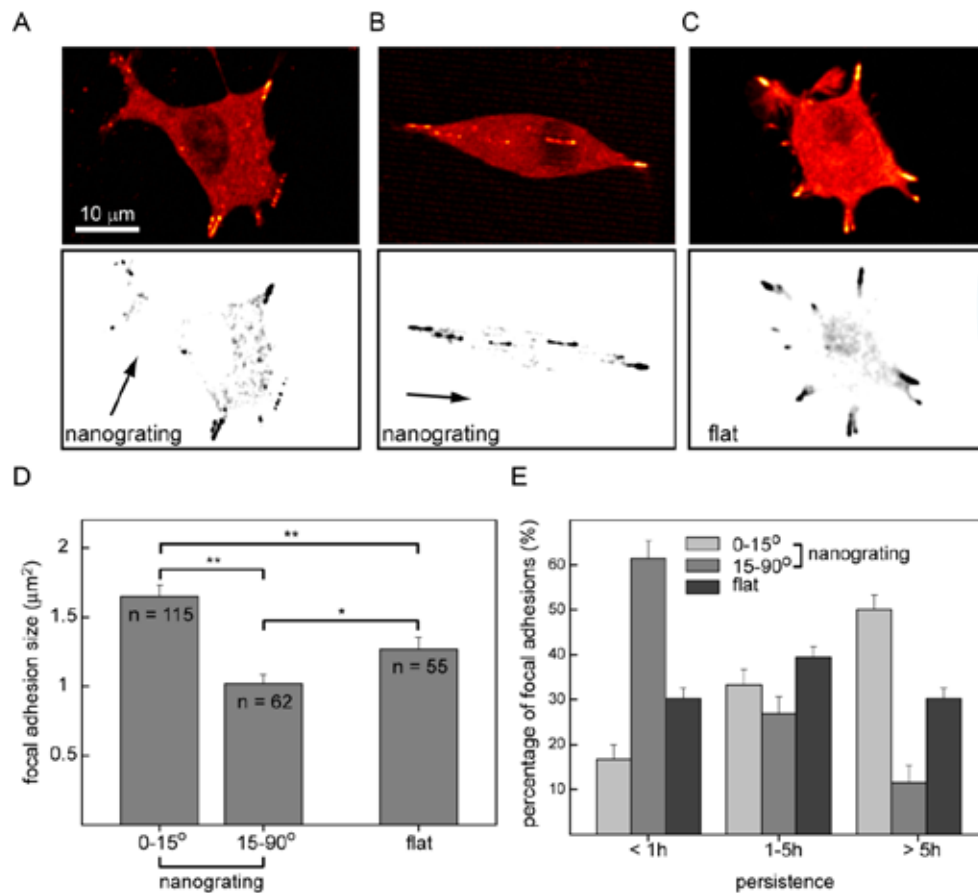
Figure 2. Angular modulation of focal-adhesion size and persistence. **A**) and **B**) Distribution of paxillin-EGFP fluorescent signal in PC12 cells differentiating on nanogratings, and [**C**)] on flat substrates. Statistical comparison of focal adhesion size **D**) and persistence **E**) on nanogratings and on flat substrates.

Moreover, we addressed the effect of nanogratings on the migration properties of differentiating PC12 cells and correlated their behavior with the polarity state induced by the substrate. During neuronal differentiation, cell-substrate interaction is sufficient to induce directional migration along the nanogratings (Fig. 3). Control cells contacting flat substrates migrated freely in all directions while cells differentiating on nanogratings showed slower migration characterized by an angular restriction that confined cell movements. Finally, we

showed that directional migration on nanogratings is linked to a specific organization of the cell cytoskeleton reflecting the nanograting directionality [8].
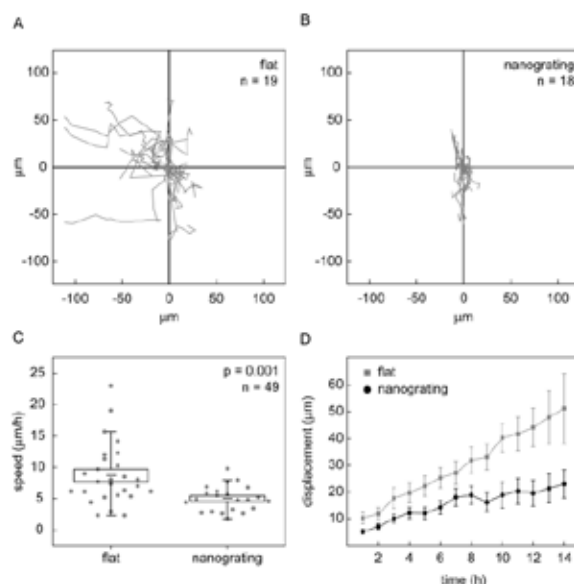

Figure 3. Migration of PC12 cells differentiating on nanogratings or on flat substrates. **A)** Individual trajectories of PC12 cells (n=19) migrating on flat substrate. **B)** Individual trajectories of PC12 cells (n=18) migrating on nanogratings. For each trajectory (gray lines in panels A and B) the initial cell position was translated into the origin of the graph. **C)** Statistical analysis of cell speed during migration on nanogratings and flat substrates. The 5 to 95 percentile distribution (vertical line) was derived from individual data points (gray circles). The population mean is reported as a horizontal black line enclosed in a rectangular box whose length represents the standard error of the mean. The reported p-value was obtained performing a Mann-Whitney test. For this analysis 49 cells were considered. **D)** Cell displacement during migration. The average distance traveled from the origin is reported for cells migrating on flat substrates (gray squares) and on nanogratings (black circles) for each time of measure (_t = 1 h), for a total of 14 hours.

We also studied neuronal cell response to directional stimuli by exploiting nanogratings with a controlled amount of random nanotopographical noise [9]. We showed that the loss of neurite guidance is not linear with noise, but exhibits a threshold effect, correlating with changes in FA maturation and spatial organization. Remarkably, by acting pharmacologically on cell contractility, we could promote aligned FA maturation, and improve neurite-guidance tolerance to noise [10].

Finally, the human neuroblastoma cell line SH-SY5Y was interfaced with plastic nanogratings and contact guidance was investigated under proliferating conditions and upon differentiation after treatment with retinoic acid (RA) and brain-derived neurotrophin factor (BDNF), and compared with mouse primary hippocampal neurons (HNs). RA/BDNF improved SH-SY5Y responsiveness to NG directional cues, and significantly enhanced the alignment to the nanograting lines. HNs behaved similarly, showing a marked change in network organization if cultured on NGs [11].
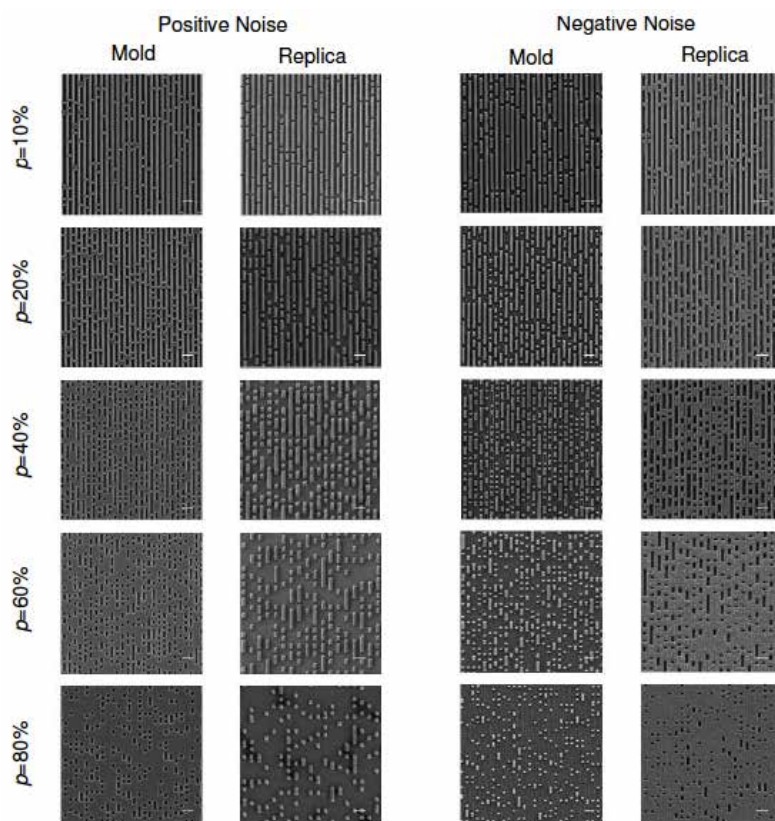
Figure 4. Scanning electron microscope images of the noisy molds and replicas. p indicates the noise level. Scale bars = 2 μm

References

[1] PC12 differentiation on biopolymer nanostructures, Nanotechnology **18**, 505103 (2007). M. Cecchini, G. Bumma, M. Serresi, and F. Beltram.

[2] PC12 polarity on biopolymer nanogratings. J. Phys. C **100**, 012003 (2008). M. Cecchini, A. Ferrari, and F. Beltram.

[3] Signaling pathways for PC12 cell differentiation: making the right connections. Science **296**, 1648 (2002). D. Vaudry, P. J. Stork, P. Lazarovici, L.E. Eiden.

[4] Neuronal polarity selection by topography-induced focal-adhesion control, Biomaterials **31**, 4682 (2010). A. Ferrari, M. Cecchini, D. Pisignano, F. Beltram.

[5] The effect of alternative neuronal differentiation pathways on PC12 cell adhesion and neurite alignment to nanogratings, Biomaterials **31**, 2565 (2010). A. Ferrari, P. Faraci, M. Cecchini, F. Beltram.

[6] High-resolution poly(ethylene terephthalate) (PET) hot embossing at low-temperature: thermal, mechanical and optical analysis of nanopatterned films, Langmuir **24**, 12581 (2008). M. Cecchini, F. Signori, P. Pingue, S. Bronco, F. Ciardelli, and F. Beltram.

[7] Nanotopographic control of neuronal polarity, Nanoletters **11**, 505 (2011). A. Ferrari, M. Cecchini, A. Dhawan, S. Micera, I. Tonazzini, R. Stabile, D. Pisignano, F. Beltram

[8] Directional PC12 cell migration along plastic nanotracks. IEEE Trans. Biomed. Eng. **56**, 2692 (2009). A. Ferrari, M. Cecchini, R. Degl'Innocenti, F. Beltram.

[9] Biocompatible noisy nanotopographies with specific directionality for controlled anisotropic cell cultures. Soft Matter **8**, 1109 (2012). S. Meucci, I. Tonazzini, F. Beltram, M. Cecchini.

[10] Neuronal differentiation on anisotropic substrates and the influence of nanotopographical noise on neurite contact guidance. Biomaterials **34**, 6027 (2013). I. Tonazzini, S. Meucci, P. Faraci, F. Beltram, and M. Cecchini.

[11] Interaction of SH-SY5Y cells with nanogratings during neuronal differentiation: comparison with primary neurons. Advanced Healthcare Materials doi: 10.1002/adhm.201300216 (2013). I. Tonazzini , A. Cecchini , Y. Elgersma, and M. Cecchini

1.3.8 Advanced microscopy techniques in living cells

Progress in fluorescence imaging is enabling the study of biological events at unprecedented detail, thanks to novel microscopy techniques that provide imaging and mapping of several parameters in the environment down to the nanoscale resolution. In the NEST laboratory we have carried out both the development of novel fluorescent nanotools for biosensing and of novel techniques in order to study dynamics and interaction of several moieties on the membrane and in other internal organelles and vesicles of living cells. Some of these techniques may have interesting application in diagnostic based on ultrasensitive techniques.

An important area of activity at NEST regards the implementation and development of epifluorescence, confocal and TIRF microscopy techniques and their application to the study of bioevents (such as protein dynamics, oligomerization state, and interactions). This often requires the development of novel fluorescent indicators, which is done in our laboratory also by a chemical synthesis approach. On the other side, new image acquisition and analysis methods (e.g. based on fluorescence correlation spectroscopy, FCS, or on single particle tracking, SPT) can increase the amount of biological information that can be recovered compared to conventional strategies based on perturbation (e.g. FRAP). These methods are now routinely used in several research projects, as shortly described in the following.

The development of new fluorescent probes can in principle conjugate the extremely high sensitivity of fluorescence (down to single molecule) to its intrinsic sensitivity to any molecular factor capable to affect the long-living excited state. Molecular recognition events in living systems, or structural rearrangements in specific domains (e.g. cell membranes), are often related to transient changes of the physicochemical properties of their local (nm-scale) environment. Thus, environmentally-sensitive probes may help understanding subtle biological phenomena. By rational molecular design, we successfully developed a palette of intracellular fluorescent reporters, based on coumarin, butenolide, and styryl cores, endowed with excellent brightness and photostability, and provided with functional groups for conjugation to biomolecules [1-4]. As an example, for a new "molecular rotor", a viscosity sensitive dye, we demonstrated strong absorption in the green region of the spectrum, very little solvatochromism, and strong emission sensitivity to local viscosity [4]. Actually the emission increase was paralleled by an increase in emission lifetime; owing to its concentration-independent nature, fluorescence lifetime is particularly suitable to image environmental properties, such as viscosity, at the intracellular level. Accordingly, we demonstrated that intracellular viscosity measurements could be efficiently carried out by lifetime imaging with our probe and phasor analysis, an efficient method for measuring lifetime-related properties (e.g., bionalyte concentration or local physicochemical features) in living cells (Fig. 1) [4]. Moreover, we analyzed the interactions between organic dyes and the possible scaffolds that can be functionalized; in particular, we studied surface enhanced Raman scattering (SERS) for fluorophores conjugated to metallic nanoparticles, and how the use of dendrimers (reproducible ramified polymers, which carry on their surface

functionalizable moieties) can increase the versatility of fluorescence-based approaches [5].
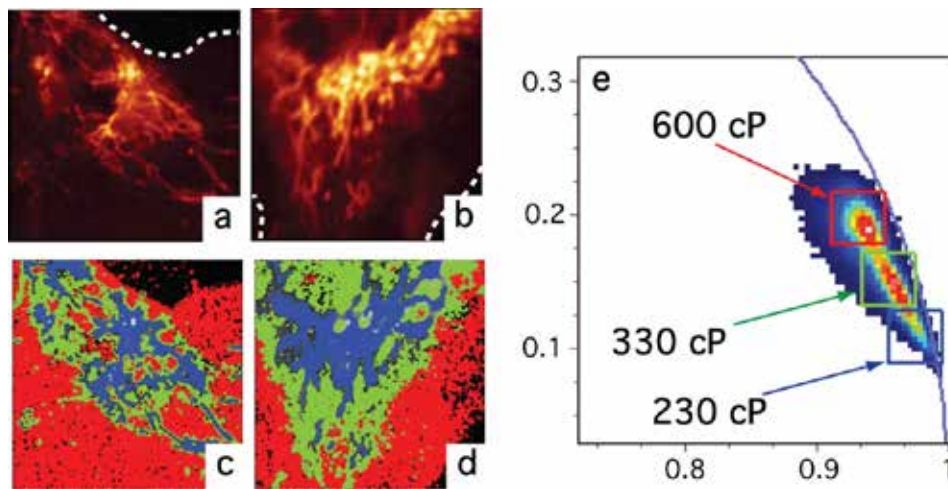

Figure 1 Cultured HUVEC cells treated with our styryl molecular rotor [4]. Panels a-b: fluorescence intensity images. Panels c,d: "phasor" (lifetime) images corresponding to a,b; the color code is: red for membrane, green for lysosomes, blue for mitochondria. Panel e: phasor plot for images c,d; the three different regions corresponding to membrane (red), lysosomes (green) and mitochondria (blue) are enclosed in colored squar
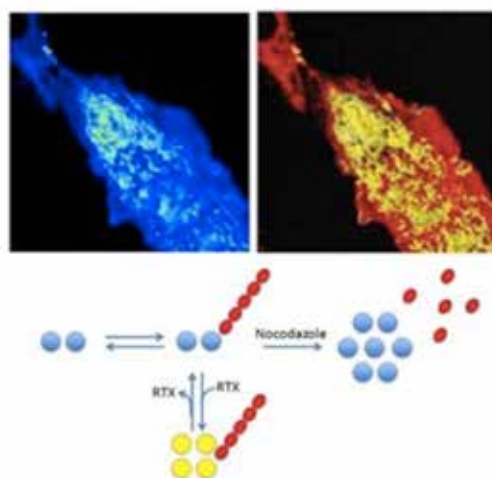
es and the related viscosities are added.

Figure 2. Intensity (left) and N&B map (right) of TRPV1 upon activation. Red pixels correspond to dimers, yellow pixels to functional tetramers. Schematic representation of TRPV1 oligomerization state under different conditions.

In one of the approach to study the dynamics of molecules in living cells, classical FCS and its recently developed variants have been introduced to study protein diffusion, aggregation state, and interactions in the context of a living cell sample and in presence of many molecules. For example, the Number&Brightness (N&B) fluctuation analysis has been used to quantitatively investigate the aggregation state of the transient receptor potential cation channel subfamily V member 1 (TRPV1), a non-selective membrane protein activated by heat and capsaicin and involved in nociception [6]. By N&B we demonstrated that TRPV1 is dimeric under physiological conditions whereas it mostly converts into a functional tetramer under ligand-binding conditions (Fig. 2). Moreover, fast spatiotemporal correlation spectroscopy allowed us to determine the lateral diffusion laws of a GFP-tagged transmembrane transferrin receptor in live Chinese hamster ovary cells, a well-known benchmark of membrane-skeleton–dependent transiently confined diffusion; this approach can be used also with dim and dense molecole and represents a powerful tool for the determination of

kinetic and thermodynamic parameters over very wide spatial and temporal scales. [7]
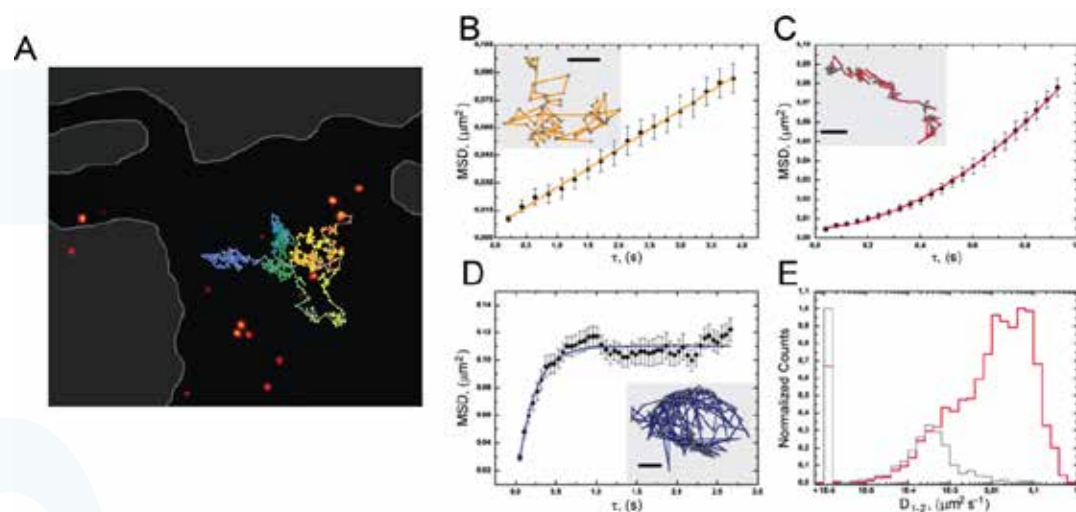

Figure 3. TrkA SM trajectories at the basal membrane of living cells. A) TIRF microimage showing single Qdot-labelled ACP-TrkA receptor molecules at the basal plasma membrane. The border of the basal membrane is depicted as a light-grey line and areas outside the cell are grayed. A typical trajectory recorded for TrkA molecules is superimposed to a spot of the image; the color code represents the trajectory time progression. B–E) MSD vs lag-time (t) plots for trajectories (insets) epitomizing three diffusive regimes associated to individual ACP-TrkA receptors: (B) Brownian (yellow curve), (C) drifted (red curve) and (D) confined (blue curve) regimes. Bar: 0.16 mm (1 pixel). (E) Global distribution of average diffusivities (D_{1-2}) associated to each single trajectory (red curve) and D_{1-2} distribution of Qdot immobilized to the glass surface (gray curve). The bin "<1E-6" includes negative values for D_{1-2}, mostly arising from cases where the uncertainty is higher than the absolute value.

In a parallel approach, SPT in combination with TIRF microscopy have been used to address the study of tropomyosin receptor kinase A (TrkA) lateral diffusion in the membrane of living cells. TrkA is the high-affinity nerve growth factor (NGF) receptor, and cooperates with the low-affinity p75 neurotrophin co-receptor (p75NTR) to transduce NGF signals in neuronal cells. The dynamic interplay between NGF, TrkA and p75NTR is critically involved in several physio-pathological processes. The quantitative description of the early steps of NGF-induced TrkA and p75NTR separate and concerted responses at the cell plasma membrane is currently a hot topic studied by our laboratory. We have demonstrated that the insertion of the acyl carrier protein (ACP) tag at the extracellular domain of TrkA receptor allows for the specific labeling of the receptor pool exposed at the cell surface, when the construct is transfected in living cells [8]. The ACP tag has shown to not interfere with TrkA receptor function, both in terms of ligand responsiveness and downstream signalling. Eventually coupled to semiconductor quantum dots (Qdots) or to fluorophores, the ACP-TrkA construct has allowed recording heterogeneous diffusion patterns of receptor single molecules (SMs) at the cell plasma membrane, with a localization precision down to 10 nm and a temporal resolution in the ms time scale (Fig. 3) [8]. Software has been implemented and developed for almost automated analysis of the obtained SM trajectories. Algorithms currently available at NEST process trajectories obtained by one-color SMs temporal series and calculate: i) the most significant diffusion and confinement parameters,

starting from the mean square displacement (MSD) of trajectories or subtrajectories; ii) the fraction and dynamic changes of all monomers and/or homo-oligomers detected by measuring fluorescence intensities of the tracked objects [8, 9].

The heterogeneous movements of TrkA at the membrane have also been correlated to its function, in particular with the binding of different biologically relevant ligands: NGF, NGF R100E HSANV mutant, proNGF and NT-3 [9]. We have provided evidence that a close correlation exists between the initial receptor membrane dynamics triggered upon binding and the specific biological outcomes induced by different ligands for the same receptor. Indeed, in the absence of ligands, most of TrkA receptors are fast moving monomers (D≈0.47 μm^2/s); about 20% TrkA molecules are moving at least an order of magnitude slower and around 4% are almost immobile within regions of about 0.6 μm in diameter. Ligand binding results in increased slow and/or immobile populations over the fast one, slowing down of non-immobile trajectories and reduction of confinement areas, observations which are consistent with the formation of receptor dimeric and oligomeric states. Notably, the extent of TrkA lateral mobility modification is strictly ligand-dependent and each ligand promotes distinct trajectory patterns of TrkA receptors at the cell membrane (ligand "fingerprinting" effect, Figure 4). This ligand-signature of receptor dynamics results from a differential combination of receptor-binding affinity, intracellular effectors recruited in the signalling platforms and formation of signalling/recycling endosome precursors [9].
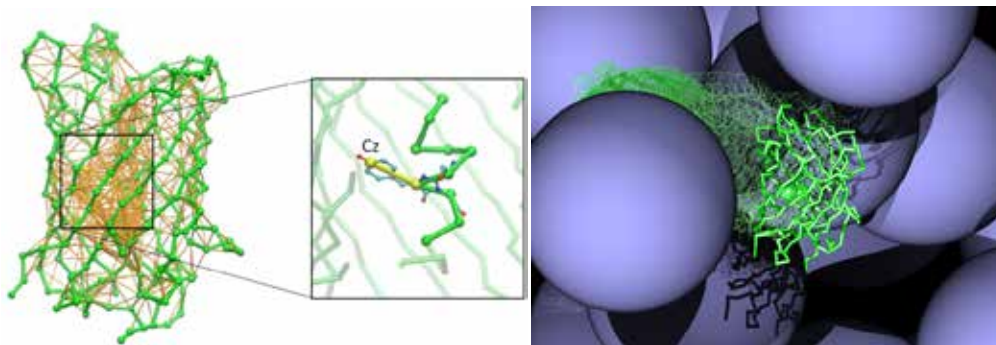
Figure 5. Left: CG Minimalist model for the GFP (green ball&sticks); an indicative representation of the local interactions topology (*T*) is reported as orange bonds. An expanded view of the chromophore surrounding is shown, with the atomistic structure of the chromophore superimposed. The chromophore beads are in yellow. Right: artistic representation of the diffusion of a single GFP molecule in a crowded environment.

Efforts were also dedicated to the simulation of the dynamics of proteins in crowded environments, such as cytoplasm and plasmamembrane. As a benchmark, the dynamic of GFP was addressed. After the development of a strategy for developing corse grained (CG) "minimalist" models for biopolymers, and its application to the theoretical study of RNA, DNA, and polypeptides [10], a minimalist model for the GFP was optimized by combining statistics-, physics- and structure-based information by means of a Genetic Algorithm, resulting in

accurate monomer internal fluctuations and homodimer binding modes [11]. The diffusive dynamics of GFP in concentrated environments was addressed by embedding the protein in a simplified cytoplasm-like solution consisting of spherical crowding agents. Thanks to the extreme simplifications of both the tracer and crowding agents and the rigorous procedure to evaluate the inter-molecular interactions, µs-long multiscale simulations of the GFP were easily accessible at different crowders concentrations and reproduced the *in vivo* measured diffusion coefficients (Fig. 5) [11].

References

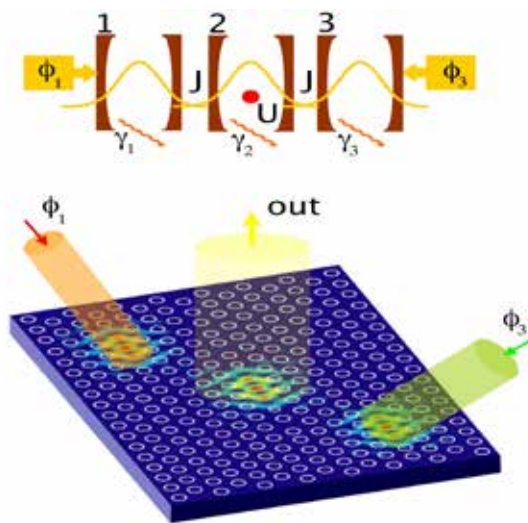[1] Engineering the excited state of fluorophores for high resolution imaging of bio- and soft-matter, Eur Biophys. J. **40**, 147 (2011). R. Bizzarri, G. Signore, P. Bianchini, G. Abbandonato, A. Battisti, A. Pucci, R. Nifosì, A. Diaspro, F. Beltram.

[2] A Novel Coumarin Fluorescent Sensor to Probe Polarity Around Biomolecules, J. Biomed. Nanotech. **5**, 722 (2009). G. Signore, R. Nifosì, L. Albertazzi, R. Bizzarri.

[3] Polarity-Sensitive Coumarins Tailored to Live Cell Imaging, J. Am. Chem. Soc. **132**, 1276–1288 (2010). G. Signore, Ri. Nifosì, L. Albertazzi, B. Storti, R. Bizzarri.

[4] Imaging intracellular viscosity by a new molecular rotor suitable for phasor analysis of fluorescence lifetime, Anal. Bioanal. Chem. **405**, 6223, (2013). A. Battisti, S. Panettieri, G. Abbandonato, E. Jacchetti, F. Cardarelli, G. Signore, F. Beltram, R. Bizzarri.

[5] Dendrimer-based fluorescent indicators: in vitro and in vivo applications, PLoS ONE **6**, e28450 (2011). L. Albertazzi, M. Brondi, G.M. Pavan, S. Sulis Sato, G. Signore, B. Storti, G.M. Ratto, F. Beltram.

[6] Intact microtubules preserve transient receptor potential vanilloid 1 TRPV1 functionality through receptor binding, J. Biol. Chem. **287**, 7803 (2012). B. Storti, R. Bizzarri, F. Cardarelli, F. Beltram.

[7] Fast spatiotemporal correlation spectroscopy to determine protein lateral diffusion laws in live cell membranes, PNAS **110**(30), 12307 (2013). C. Di Rienzo, E. Gratton, F. Beltram, F. Cardarelli.

[8] Single particle tracking of acyl carrier protein (ACP)-tagged TrkA receptors in PC12nnr5 cells, J. Neurosci. Methods 204, 82 (2012). A. Callegari, S. Luin, L. Marchetti, A. Duci, A. Cattaneo, F. Beltram.

[9] Ligand signature in the membrane dynamics of single TrkA receptor molecules, J. Cell Sci. 126, 4445 (2013). L. Marchetti, A. Callegari, S. Luin, G. Signore, A. Viegi, F. Beltram, A. Cattaneo.

[10] Evolutionary Algorithm in the Optimization of a Coarse-Grained Force Field, J. Chem. Theory Comput. **9**(11), 4874 (2013) F. Leonarski, F. Trovato, V. Tozzini, A. Leś, J. Trylska.

[11] A minimalist model of proteins diffusion and interactions: the Green Fluorescent Protein within the cytoplasm, Macromolecules **46**(20), 8311 (2013). F. Trovato, R. Nifosi, A. Di Fenza, V. Tozzini.

1.3.9 Quantum coherent dynamics of solid state devices

Superconducting nanostructures offer the unique opportunity to explore a wealth of different quantum effect at mesoscopic level. Coupled to mechanical moving parts these systems realize interesting quantum nano-electro-mechanical devices. Circuit-QED systems based on superconducting co-planar resonators are ideal systems to investigate the dynamics of photon blockade. Besides their interest in fundamental science, superconducting nano-circuits are among the most promising implementations of solid state quantum information processing.

Cavity quantum electrodynamics (QED) experiments in solid-state systems have lead to the observation of the photon blockade effect, where nonlinearities at the single-photon level alter the quantum statistics of light emitted by the cavity [1]. Motivated by the success of single-cavity QED experiments, the focus has recently shifted to the exploration of the rich physics promised by strongly-correlated quantum optical systems in multi-cavity and extended photonic media. The interplay between coherent tunnel coupling and on-site interactions in dissipation-free bosonic systems has lead to many spectacular observations, ranging from the demonstration of number-phase uncertainty relation to quantum phase transitions. To explore the effect of dissipation and coherent drive on tunnel coupled interacting bosonic systems, we proposed a device that is the quantum optical analog of a Josephson interferometer [2]. It is briefly sketched in the figure. It consists of two coherently driven linear optical cavities connected via a central cavity with a single-photon nonlinearity. The Josephson-like oscillations in the light emitted from the central cavity as a function of the phase difference between two pumping fields can be suppressed by increasing the strength of the nonlinear coupling. The interplay between the phase dependence of the light emitted and the strength of the non-linearities present in the system is a manifestation of the number-phase uncertainty relation Remarkably, we found that in the limit of ultra-strong interactions in the center-cavity, the coupled system maps on to an effective Jaynes-Cummings system with a nonlinearity determined by the tunnel coupling strength. In the limit of a single nonlinear cavity coupled to two linear waveguides, the degree of photon antibunching from the nonlinear cavity provides an excellent measure of the transition to the nonlinear regime where Josephson oscillations are suppressed. Photon correlation measurements for this device reveal a sharp threshold from Poissonian to sub-Poissonian statistics that is almost insensitive to the strength of the tunnel-coupling. On the other hand, in the case of a linear array of cavities coupled to a non-linear center cavity, the anti-bunching threshold is found to depend strongly on the tunnel-coupling. This observation signifies that photon correlation measurements are

very effective in revealing the interplay of coherent tunneling and on-site interactions and may contain the key to interpret and probe possible phases of extended cavity-arrays which operate under non-equilibrium conditions.

Another very interesting manifestation of quantum coherent effects in nanostructure is Cooper pair pumping. In a mesoscopic conductor a dc charge current can be obtained, in the absence of applied voltages, by cycling in time two parameters which characterize the system [3]. In the scattering approach to transport the pumped charge per cycle can be expressed in terms of derivatives
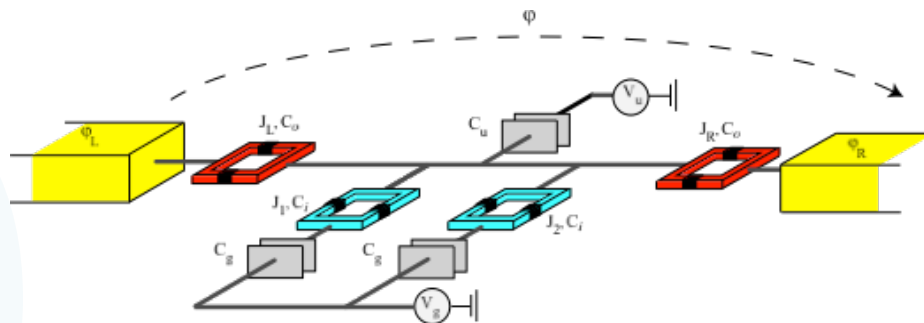
of the scattering amplitudes with respect to the pumping parameters [4]. If only superconducting leads are present and at low enough temperature, pumping is due to the adiabatic transport of Cooper pairs. Besides the dependence of the pumped charge on the cycle, in the superconducting pumps there is a dependence on the superconducting phase difference(s) (the overall process is coherent). A connection between Berry phase and pumped charge has been established also in this case thus opening the possibility to detect geometric phases in superconducting nanocircuits. We studied Cooper pair pumping in superconducting nanocircuits in the regime of Coulomb blockade. The new feature we considered was the possibility to pump in a degenerate subspace [5]. This generalization is known to have important consequences on the adiabatic evolution of quantum systems [6]. Indeed we showed that it leads to important modifications to adiabatic pumping as well. We derived an expression for the pumped charge in the presence of a degenerate spectrum and relate it to the non-Abelian connection of Wilczek and Zee. Furthermore we proposed a superconducting network (see the figure above) where this relation can be tested and discussed two clear signatures of non-abelian holonomies. First, under appropriate conditions to be discussed below, the pumped charge per cycle is quantized. Second and most important here the pumped charge depends both on the cycle and the point where the cycle starts. If tested experimentally this would be a clear proof of the non-Abelian nature of pumping.

References
[1] K.M. Birnbaum, A. Boca, R. Miller, A.D. Boozer, T.E. Northuop, and J. Kimble, Nature **436**, 87 (2005); C. Lang, D. Bozyigit, C. Eichler, L. Steffen, J. M. Fink, A. A. Abdumalikov, M. Baur, S. Filipp, M. P. da Silva, A. Blais, and A. Wallraff, Phys. Rev. Lett. **106**, 243601 (2011).
[2] D. Gerace, H.E. Tureci, A. Imamoglu, V. Giovannetti, and R. Fazio, Nature Phys. **5**, 281 (2009).
[3] D. J. Thouless, Phys. Rev. B **27**, 6083 (1983).
[4] P. W. Brouwer, Phys. Rev. B **58**, R10135 (1998).
[5] V. Brosco, R. Fazio, F.W.J. Hekking, and A. Joye, Phys. Rev. Lett. **100**, 027002 (2008)
[6] F. Wilczek and A. Zee, Phys. Rev. Lett. **52**, 2111 (1984).

1.3.10 Quantum simulators

Artificial many-body systems can be also employed as quantum simulators, i.e. to simulate other quantum systems [as forecasted by Feynmann more that three decades ago]. Crucial for all these applications is the ability to manipulate many-body systems in a controlled fashion.

Recent theoretical advances in cavity quantum-electrodynamics (QED) have shown that arrays of coupled nonlinear cavities are potential candidates to explore quantum many-body phenomena of light. The initial proposals [1] to realize a Mott phase of polaritons have initiated an intense activity to investigate the properties of cavity QED arrays. Cavity arrays, periodic arrangements of neighbouring QED cavities, have been introducedas prototype systems to study many-body states of light. Their very rich phenomenology arises from the interplay between strong local non-linearities and photon hopping.

Cavity arrays are ideal open system quantum simulators. Indeed experiments in cavity-QED are typically performed under non-equilibrium conditions, with an external source acting on the system to compensate for the loss of photons due to the finite quality factor of the cavities. Hence, particle number per cavity is determined by a dynamical balance between the external drive and loss instead of a chemical potential. It is therefore of paramount importance to find signatures of the different phases of an array of cavities under non-equilibrium conditions. In addition it is very interesting to explore new phases and phase transitions that occur only in non-equilibrium situations. In these years we explored both situations.

We analyzed [2] the non-equilibrium dynamics of a gas of interacting photons in an array of coupled dissipative nonlinear cavities driven by a pulsed external coherent field. Using a mean-field approach, we showed that the system exhibits a phase transition from a Mott-insulator-like to a superfluid regime. For a given single-photon nonlinearity, the critical value of the photon tunneling rate at which the phase transition occurs increases with the increasing photon loss rate. We checked the robustness of the transition by showing its insensitivity to the initial state prepared by the the pulsed excitation. Moreover we found that the second-order coherence of cavity emission can be used to determine the phase diagram of an optical many-body system without the need for thermalization. Our proposal makes a further link to the physics of quantum quenches [3] which is nowdays attracting inreasing interest. What we showed, in essence, is that under certain circumstances it is possible to reconstruct the equilibrium phase diagram from a quantum quench experiment.

Looking for unique signatures of non-equilibrium dynamics we further introduced [4] cavity arrays with coupling mediated by non-linear elements (see the figure 1) opening the way to study a variety of new possibilities, including correlated photon hopping and finite-range photon blockade. We concentrated on this last point studying the effect of a cross-Kerr non-linearity on the steady state and found a very rich phase diagram. A photon solid characterized by a checkerboard ordering of the average photon number appears for a substantial range of the coupling constants.In addition we see that,

for some choice of the parameters, a finite hopping stabilizes a phase where the crystalline ordering coexists with a globally synchronized dynamics of the cavities, suggesting an analogy to a non-equilibrium supersolid.
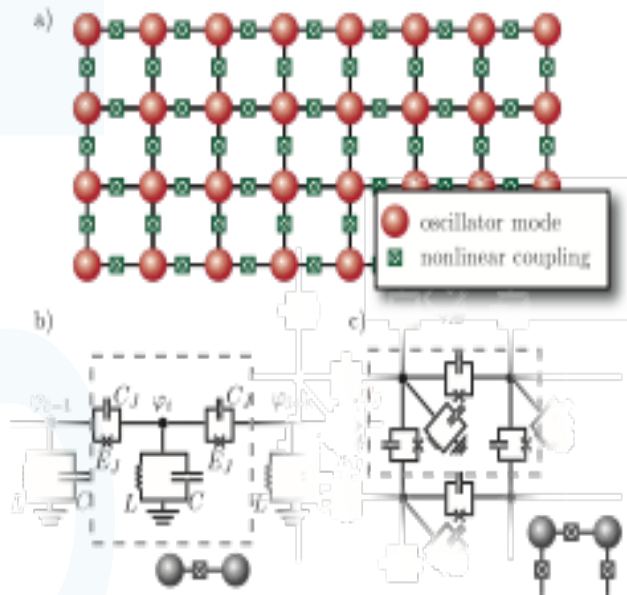

Figure 1. a) An array of QED-cavities described by oscillator modes (red circles) that are coupled via nonlinear elements (crossed boxes). b) and c) Implementation of its building blocks in circuit-QED for one- and two-dimensional lattices.

In some cases it is also possible to engineer the external bath [5]. As a result the steady state of the system under consideration can be "guided" by controlling the interplay between its internal dynamics and the coupling to the environment. We discussed [6] an open driven-dissipative many-body system, in which the competition of unitary Hamiltonian and the dissipative Liouvillian dynamics lead to a non-equilibrium phase transition. This situation shares features of a quantum phase transition in that it is interaction driven, and of a classical phase transition, in that the ordered phase is continuously connected to a thermal state. Within a generalized Gutzwiller approach which includes the description of mixed state density matrices, we characterized the complete phase diagram and the critical behavior at the phase transition approached as a function of time. We found a novel fluctuation induced dynamical instability, which occurs at long wavelength as a consequence of a subtle dissipative renormalization effect on the speed of sound.

In the study of open quantum open systems already understanding the motion of a quantum particle is a complex problem which has a long history. Polarons, originally studied in the context of slow-moving electrons in ionic crystals, and impurities in 3He are two prototypical examples in which the bath is bosonic and fermionic, respectively. Recently, thanks of the realisation of quantum simulators, it has become possible to investigate the real-time dynamics of this problem. Moreover it has become possible to tunel in a controlled fashion the coupling to the bath and the properties of the bath itself.

We studied [6] the impurity dynamics in a one-dimensional bath of interacting bosons numerically by means of a time-dependent density-matrix renormalization group. We have shown that, against the conventional wisdom, a Luttinger-liquid description of the bath is applicable only in a very small

region of parameter space, where the impurity suffers an Abraham-Lorentz radiation-reaction friction. Among the most striking features, we have found a non-monotonic behavior of the damping rate and the large renormalization of the oscillation frequency for attractive impurity-bath interactions. The unveiled signatures of interactions in the bath on the impurity dynamics are amenable to future experimental verification.

References

[1] M.J. Hartmann, F.G.S.L. Brandao, and M.B. Plenio, Nature Phys. **2**, 849 (2006); A.D. Greentree, C. Tahan, J.H. Cole, and L.C.L. Hollenberg, Nature Phys. **2**, 856 (2006); D.G. Angelakis, M.F. Santos, and S. Bose, Phys. Rev. A **76**, 031805(R) (2007).

[2] A. Tomadin, V. Giovannetti, R. Fazio, D. Gerace, I. Carusotto, H.E. Tureci, and A. Imamoglu, Phys. Rev. A **81**, 061801(R) (2010).

[3] A. Polkovnikov, K. Sengupta, A. Silva, and M. Vengalattore, Rev. Mod. Phys. **83**, 863 (2011).

[4] S. Diehl, A. Tomadin, A. Micheli, R. Fazio, and P. Zoller, Phys. Rev. Lett. **105**, 015702 (2010).

[5] J. Jin, D. Rossini, R. Fazio, M. Leib, and M. J. Hartmann, Phys. Rev. Lett., **110**, 163605 (2013).

[6] S. Peotta, D. Rossini, M. Polini, F. Minardi, and R. Fazio, Phys. Rev. Lett. **110**, 015302 (2013).

1.3.11 Quantum transport and Majorana fermions in hybrid systems

Since the first prediction of real solutions to the Dirac equation, known as Majorana fermions, there have been many attempts to demonstrate their occurrence in nature~\cite{WilczekNatPhys2009}, but a clear evidence is still lacking. Besides the natural search for these elusive particles in high-energy physics, it has been recently suggested that Majorana fermions can exist as exotic excitations in certain condensed-matter systems [The field has be recently reviewed in J. Alicea, Rep. Progr. Phys. 75 , 076501 (2012)].

The importance of finding Majorana fermions in condensed-matter systems is not only related to their fundamental interests. It is also rooted in the non-Abelian braiding statistics of these particles which could be exploited as a basis for decoherence-free topological quantum computation [1].

We focused on a specific proposal [2] realized with spin-orbit-coupled semiconducting nanowires in proximity to an *s*-wave superconductor and subjected to an in-plane magnetic field This wire can support Majorana-fermion bound states at its ends when parameters such as chemical potential, magnetic field, and superconducting pairing are properly tuned }. The S-nanowire is said to be in the topological phase when Majorana bound states are present, while it is topologically trivial otherwise.

We have considered [3] a multi-band semiconducting nanowire subjected to spin-orbit coupling, superconducting pairing and a longitudinal Zeeman field.

Depending on the values of such parameters, the nanowire presents a non-trivial topological phase in which a pair of Majorana modes, at an energy equal to the chemical potential, are localized at its ends.
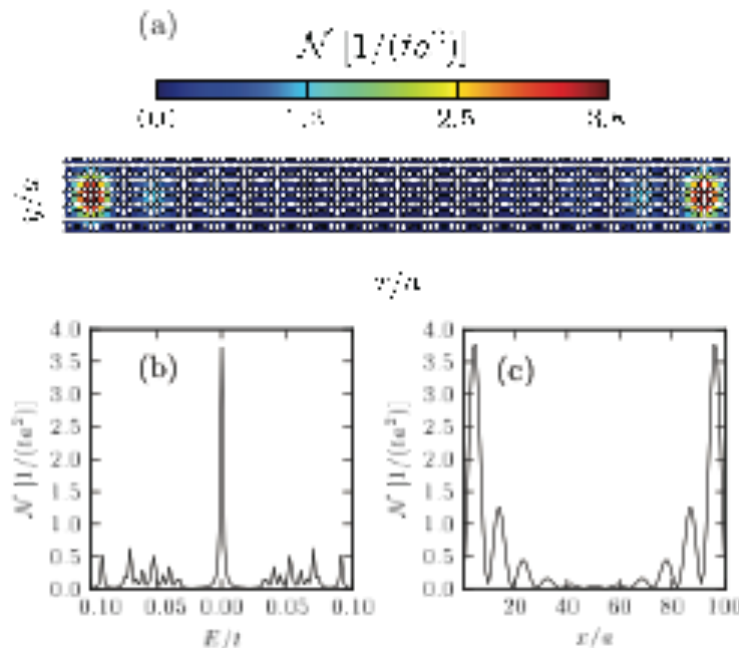

Figure 1 (a) LDOS of an isolated superconducting nanowire in the topologically non-trivial phase at an energy very lose to the chemical potential. Bound states at both ends of the wire are apparent. (b) LDOS at a given position as a function of energy. A sharp peak corresponding to a Majorana bound state is present at zero energy. (c) LDOS at very low energy along the wire.

We have carefully calculated and analyzed the local density of states (LDOS) of such nanowires in the case where they are coupled to normal regions (such as electrodes or links) and we have compared the topologically non-trivial and trivial phases in different situations. This is a situation of particular importance for the experimental detection of Majorana modes.

When the nanowire is coupled to a normal electrode we have found that the peak in the LDOS at zero energy (with respect to the chemical potential), corresponding to the Majorana mode, broadens with increasing coupling strength to the electrode, eventually disappearing for ideal coupling. Interestingly, for finite coupling the peak is also present on the normal electrode, though being of smaller amplitude and broadening more rapidly with the strength of the coupling.

Additional interesting features emerge in realistic wires where the proximity varies along the section of the wire. We have shown that topological adiabatic pumping occurs in a class-D superconducting nanowire connected to a metallic lead [4]. This is the case when the lead supports a single propagating mode or when the nanowire is coupled to the lead through a quantum point contact.
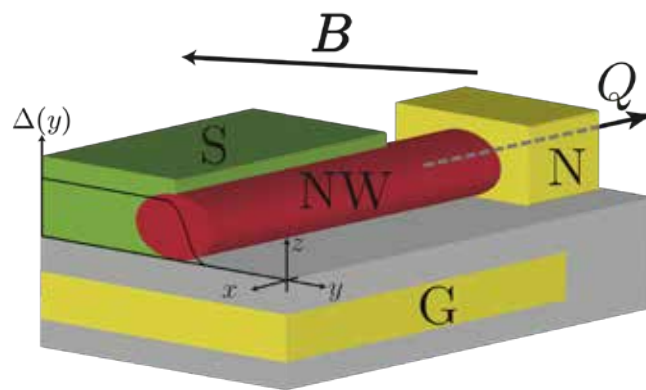
Figure 2. Sketch of the system. A spin-orbit coupled nanowire (NW) is subject to a tilted Zeeman field and in contact with a bulk superconductor (S) which induces a pairing gap. Due to the lateral contact the induced gap is space-dependent as illustrated in the figure. The wire is in contact with a normal lead (N). By changing in time the chemical potential (through the gate voltage) and the Zeeman field a charge Q is pumped through the NW-N interface

The necessary condition to achieve a topological pumped charge is that the phase diagram presents a non-simply connected structure, where isolated non-topological regions are surrounded by connected topological ones. This is possible by allowing both a non-uniform pairing amplitude and a tilted Zeeman field. Non-contractible pumping paths in parameter space can thus be identified within the topological phase. Quantised pumping is very important in view of its metrological applications. In general the quantisation condition requires some fine tuning of the parameters. If, however, quantisation stems from topology, pumping will be immune from errors and robust to unavoidable perturbations and therefore it might lead to current standards of unprecedent accuracy.
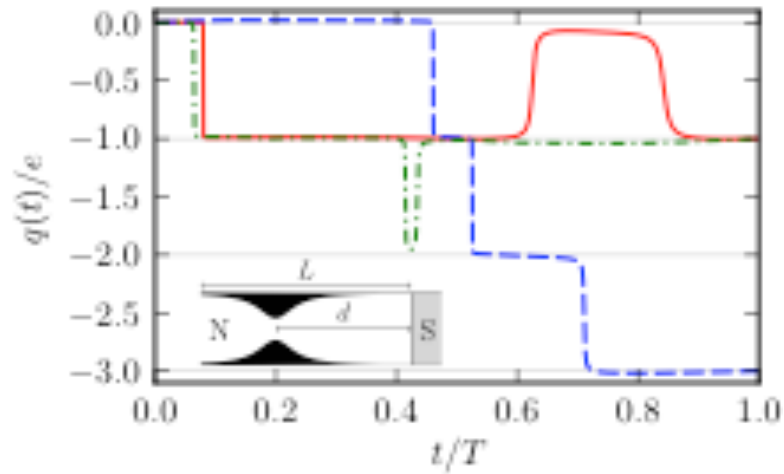
In the figure above we show the cumulative pumped charge (in units of e) as a function of time t (in units of the pumping period T) in the presence of a quantum point contact at a distance from the NS interface. At the end of the cycle the final pumped charge is quantized. Results for different trajectories in parameter space are denoted with distinct line styles. In the inset we have sketched the setup with a QPC at a distance d from the NS boundary in order to restrict the number of propagating modes.

References

[1] C. Nayak, S.H. Simon, A. Stern, M. Freedman, and S. Das Sarma, Rev. Mod. Phys. **80**, 1083 (2008).

[2] R.M. Lutchyn, J.D. Sau, and S. Das Sarma Phys. Rev. Lett. **105**, 077001 (2010); Y. Oreg G. Refael, and F. von Oppen, ibid. **105**, 177002 (2010).

[3] M. Gibertini, F. Taddei, M. Polini and R. Fazio, Phys. Rev. B **85**, 144525 (2012).

[4] M. Gibertini, R. Fazio, M. Polini, and F. Taddei, Phys. Rev. B **88**, 140508(R) (2013).

1.3.12 Quantum thermal machines

The interest in study quantum thermal machines has its roots in the need to understand the relations between thermodynamics and quantum mechanics [1, 2]. The progress in this field has also important applications in the control of heat transport in nano-devices [3]. The fundamental limits to the dimensions of a quantum refrigerator have been found in series of recent works [4-6]. It has been further demonstrated that these machines could still attain Carnot-efficiency [5] thus launching the call for the implementation of the smallest possible quantum refrigerator.

We theoretically designed an electronic quantum refrigerator based on four quantum dots arranged in a square configuration, in contact with as many thermal reservoirs [7]. The system implements the minimal mechanism for acting as a self-contained quantum refrigerator, by operating without the requirement of external time-dependent work and demonstrating heat extraction from the coldest reservoir and the cooling of the nearby quantum-dot. We also discuss the operational nature of the definition of local temperatures in systems out of equilibrium and how important is to discuss reference experimental regimes to define the regime of operation of small quantum thermal machines.
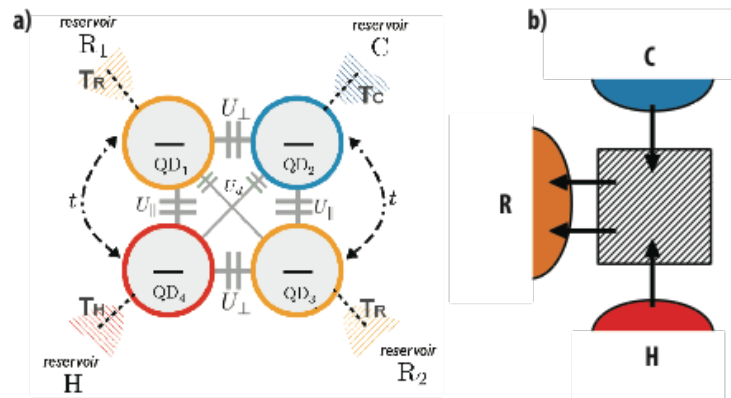
Figure 1: a) The quadridot. Vertical and Horizontal interdot capacitances are considered to be the highest energy scales among those in the figure. Their values are determined by the arrangement of the top gates over the QDs, which are not shown. The four quantum dots are weakly tunnel coupled to the electronic reservoirs H, C, R1, and R2, respectively, which are all grounded but maintained at equilibrium at a well-defined temperatures. No tunneling is possible between dot 1 (orange) and dot 2 (blue), and between dot 4 (red) and dot 3 (orange). b) schematic representation of the heat flux.

Minimal self-contained thermal machines are theoretical systems that perform a cycle based only on the steady-state heat transfer from thermal reservoirs at different temperatures, utilizing as few degree of freedom as possible. In our work we design an implementation of these machines operating by quantum mechanical tunneling, consisting of four quantum dots in a planar square array (named a "quadridot") coupled to independent electron reservoirs as shown in Fig. 1. The couplings and the electrostatics interactions has been carefully chosen so that the quadridot could pump energy from the high temperature reservoir H

and the low temperature reservoir C to the intermediate temperature reservoirs, thereby acting as a "quantum refrigerator" (Fig 1). To show this effect, we explicitly solve the open dynamics of the quadridot and study its asymptotic behavior. In the Born-Markov-Secular limit we write a Lindblad equation for the reduced density matrix of the quadridot, which describes the effective dissipative and coherent interaction between the low-energy states of the system obtained after a Schrieffer-Wolff transformation. Solving numerically the steady state equation we observe that for each TC < TR, there exists a minimal threshold value for TH above which the quadridot extracts heat from the cold reservoir C. This is shown in Fig. 2-a for TR=2 and different values of Ud, the quadridot works as a refrigerator in the blue region. For given TH > TR, there is a minimal temperature (whose approximate value is obtained analytically) for the cold reservoir under which the effect cannot work. Interestingly for large values of TH/TR this value asymptotically converges toward a finite non-zero temperature which can be interpreted as the emergent absolute zero of the model. This refrigeration effect is also accompanied with a cooling of QD2, namely its effective local temperature T(eff)C decreases as TH increases, for sufficiently high TH. However, being the quadridot a nanoscale system out-of-equilibrium, the definition of the local temperature is must be operational. In Fig. 2 we show an example of operation showing that depending on how the refrigeration effect is "switched on" we can achieve very different operational regimes. The QD2 might be either colder (in region I) or hotter (in region II) when the device extract heat from the C reservoir. Conversely, we might achieve a colder QD2 also when the quadridot pumps heat into the colder bath (III).
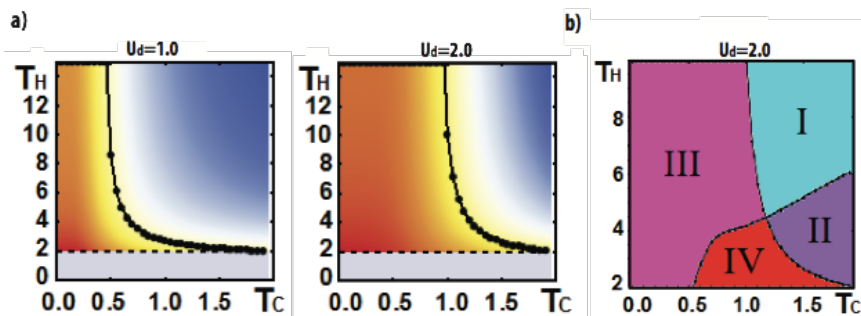
Figure 2: a) Working conditions of the refrigerator. Panels refer to Ud = 1 (left), Ud = 2 (right). The change of sign in the heat flow occurs at a value of TH indicated by the black line. Above this line (blue region) the machine works as a proper refrigerator extracting heat from the C,H-reservoirs and pumping it into R. Black dashed line above the grey region indicates TH = TR=2. Blue/Red background color intensity is proportional to the actual heat pumped to/extracted from C- reservoir. b) Possible temperature regimes for Ud = 2. In regions I/II the refrigerator is working (heat is extracted from C) while in regions III/IV the C bath receives heat. In regions I/III we have an effective decrease of single particle occupation number (i.e. nC < n0C).

In Ref. [8] a completely different approach to quantum thermodynamics was proposed. Specifically in this work, we define thermodynamic configurations and identify two primitives of discrete quantum processes between configurations for which heat and work can be defined in a natural way. This allows us to uncover a general second law for any discrete trajectory that consists of a sequence of these primitives, linking both equilibrium and non-equilibrium

configurations. Moreover, in the limit of a discrete trajectory that passes through an infinite number of configurations, i.e. in the reversible limit, we recover the saturation of the second law. Finally, we show that for a discrete Carnot cycle operating between four configurations one recovers Carnot's thermal efficiency.

References
[1] G. Gemma, M. Michel and G. Mahler, Thermodynamics, Springer (Berlin 2004).
[2] K. Maruyama, F. Nori, and V. Vedral, Rev. Mod. Phys. **81**, 1 (2009).
[3] F. Giazzoto, et al. Rev. Mod. Phys. **78**, 217 (2006).
[4] N. Linden, S. Popescu, and P. Skzypczyk, Phys. Rev. Lett. **105**, 130401 (2010).
[5] P. Skrzypczyk, et al. J. Phys. A Math. Theor. **44**, 492002 (2011).
[6] N. Brunner, et al. Phys. Rev. E **85**, 051117 (2012).
[7] D. Venturelli, V. Giovannetti, and R. Fazio, Phys. Rev. Lett. **110**, 256801 (2013).
[8] J. Anders and V. Giovannetti, New. J. Phys. **15**, 033022 (2013).

1.3.13 Limits and properties of Bosonic Quantum Communication Channels

Bosonic Gaussian channels [1] are ubiquitous in physics. They arise whenever a harmonic system interacts linearly with a number of Bosonic modes which are inaccessible in principle or in practice [2,3]. They provide realistic noise models for a variety of quantum optical and solid state systems when treated as open quantum systems, including models for wave guides and quantum condensates. They play a fundamental role in characterizing the efficiency of a variety of tasks in continuous-variables quantum information processing [4], including quantum communication and cryptography. Most importantly, communication channels such as optical fibers can to a good approximation be described by Gaussian quantum channels.

In our analysis a complete analysis of multi-mode Bosonic Gaussian channels is proposed [5,6]. We clarify the structure of unitary dilations of general Gaussian channels involving any number of Bosonic modes and present a normal form. The maximum number of auxiliary modes that is needed is identified, including all rank deficient cases, and the specific role of additive classical noise is highlighted. By using this analysis, we derive a canonical matrix form of the noisy evolution of n-mode Bosonic Gaussian channels and of their weak complementary counterparts, based on a recent generalization of the normal mode decomposition for non-symmetric or locality constrained situations. It allows us to simplify the weak-degradability classification. Moreover, we investigate the structure of some singular multi-mode channels, like the additive classical noise channel that can be used to decompose a noisy channel in terms of a less noisy one in order to find new sets of maps with zero quantum capacity. Finally, the two-mode case is analyzed in detail. By exploiting the composition rules of two-mode maps and the fact that anti-degradable channels cannot be used to transfer quantum information, we identify sets of two-mode Bosonic channels with zero capacity.

We further present a formulation of the generalized minimal output entropy conjecture for Bosonic Gaussian channels [7]. It asserts that, for states with fixed input entropy, the minimal value of the output entropy of the channel (i.e. the minimal output entropy increment for fixed input entropy) is achieved by Gaussian states. In the case of centered channels (i.e. channels which do not add squeezing to the input state) this implies that the minimum is obtained by thermal (Gibbs) inputs. The conjecture is proved to be valid in some special cases.

A series of analytic upper bounds to the channel capacity C for transmission of classical information in these channels has been provided in [8]. In the practically relevant regimes of high noise and low transmissivity, by comparison with know lower bounds on C, our inequalities determine the value of the capacity up to corrections which are irrelevant for all practical purposes. Examples of such channels are radio communication, infrared or visible-wavelength free space channels. We also provide bounds to active channels that include amplification.

With increasing communication rates via quantum channels, memory effects become unavoidable whenever the use rate of the channel is comparable to the typical relaxation time of the channel environment (see Ref. [9] for a review on the subject – the paper been under consideration for publication by Rev. Mod. Phys.). In Refs. [10,11] we introduce a model of a Bosonic memory channel,

describing correlated noise effects in quantum-optical processes via attenuating or amplifying media. To study such a channel model, we make use of a proper set of collective field variables, which allows us to unravel the memory effects, mapping the n-fold concatenation of the memory channel to a unitarily equivalent, direct product of n single-mode Bosonic channels. We hence estimate the channel capacities by relying on known results for the memoryless setting. Our findings show that the model is characterized by two different regimes, in which the cross correlations induced by the noise among different channel uses are either exponentially enhanced or exponentially reduced.

Finally, still in the context of Bosonic Gaussian Channels in Ref. [12] we consider the problem of quantum communication mediated by an optical refocusing system, which is schematized as a thin lens with a finite pupil. This model captures the basic features of all those situations in which a signal is either refocused by a repeater for long distance communication, or it is focused on a detector prior to the information decoding process. Introducing a general method for linear optical systems, we compute the communication capacity of the refocusing apparatus. Although the finite extension of the pupil may cause loss of information, we show that the presence of the refocusing system can substantially enhance the rate of reliable communication with respect to the free-space propagation. An application of these scheme to the readout of a classical memory is presented in [13,14].

References
[1] A.S. Holevo and R.F. Werner, Phys. Rev. A 63, 032312 (2001)
[2] C. M. Caves and P. D. Drummond, Rev. Mod. Phys. 66, 481 (1994).
[3] A. S. Holevo and V. Giovannetti, Rep. Prog. Phys. 75, 046001 (2012).
[4] S. L. Braunstein and P. van Loock, Rev. Mod. Phys. 77, 513 (2005).
[5] F. Caruso, J. Eisert, V. Giovannetti, and A. S. Holevo, New. J. Phys. 10, 083030 (2008).
[6] F. Caruso, J. Eisert, V. Giovannetti, and A. S. Holevo, Phys. Rev. A 84, 022306 (2011).
[7] V. Giovannetti, A. S. Holevo, S. Lloyd, and L. Maccone, J. Phys. A: Math. Theor. 43, 415305 (2010).
[8] V. Giovannetti, S. Lloyd, L. Maccone, and J. H. Shapiro, Nature Phot. 7, 834 (2013).
[9] F. Caruso, V. Giovannetti, C. Lupo, and S. Mancini, "Quantum channels and memory effects" Eprint arXiv:1207.5435v1 [quant-ph].
[10] C. Lupo, V. Giovannetti, and S. Mancini, Phys. Rev. Lett. 104, 030501 (2010).
[11] C. Lupo, V. Giovannetti, and S. Mancini, Phys. Rev. A 82, 032312 (2010).
[12] C. Lupo, V. Giovannetti, S. Pirandola, S. Mancini, and S. Lloyd, Phys. Rev. A 84, 010303(R) (2011).
[13] S. Pirandola, C. Lupo, V. Giovannetti, S. Mancini, and S. L. Braunstein, New J. Phys. 13, 113012 (2011).
[14] C. Lupo, S. Pirandola, V. Giovannetti, and S. Mancini, Phys. Rev. A 87, 062310 (2013).

1.3.14 Open quantum systems: theoretical characterization and experimental proposals

One of the major achievements of the recently emerged quantum information theory is the introduction and thorough investigation of the notion of quantum channel which is a basic building block of any data-transmitting or data-processing system. This development resulted in an elaborated structural theory [1] and was accompanied by the discovery of a whole spectrum of entropic quantities, notably the channel capacities, characterizing information-processing performance of the channels. The activity of the group in this field covers different research lines which are briefly summarized in the following.

In a series of theoretical papers [2,3,4] we studied the properties of open quantum system dynamics by adopting a collisional model. In particular in [2,3] we derived the general form of a master equation describing the interaction of an arbitrary multipartite quantum system, consisting of a set of subsystems, with an environment, consisting of a large number of sub-envirobments. Each subsystem "collides" with the same sequence of sub-environments which, in between the collisions, evolve according to a map that mimics relaxations effects. No assumption was made on the specific nature of neither the system nor the environment. In the weak coupling regime, we it was shown that the collisional model produces a correlated Markovian evolution for the joint density matrix of the multipartite system: the associated Linblad super-operator contains pairwise terms describing cross correlation between the different subsystems. In Ref. [4] we generalized the above analysis to include also quantum non-Markovian dynamics. In this case we endow the bath with memory by introducing inter-ancillary collisions between next system-ancilla interactions. Our model interpolates between a fully Markovian dynamics and the continuous interaction of the system with a single ancilla, i.e., a strongly non-Markovian process. We show that in the continuos limit one can derive a general master equation, which while keeping such features is guaranteed to describe an unconditionally completely positive and trace-preserving dynamics. We apply our theory to an atom in a dissipative cavity for a Lorentzian spectral density of bath modes, a dynamics which can be exactly solved. The predicted evolution shows a significant improvement in approaching the exact solution with respect to two well-known memory-kernel master equations.

In Ref. [5] we introduced a way to quantify the noise level associated to a given open quantum system transformation. The key mechanism lying at the heart of the proposal is "noise addition": in other words we compute the amount of extra noise we need to add to the system, through convex combination with a reference noisy map or by reiterative applications of the original map, before the resulting transformation becomes entanglement-breaking. We also introduce the notion of entanglement-breaking channels of order n (i.e. maps which become entanglement-breaking after n iterations), and the associated notion of amendable channels (i.e. maps which can be prevented from becoming entanglement-breaking after iterations by interposing proper quantum transformations). Explicit examples were analyzed in the context of qubit and one-mode Guassian channels. For the latter an experimental proposal was also developed in Ref. [6].

In Ref. [7,8] we presented a new decoding procedure to transmit classical information in a quantum channel which, saturating asymptotically the Holevo bound, achieves the optimal rate of the communication line. Differently from previous proposals, it is based on performing a sequence of (projective) YES/NO measurements which in N steps determines which codeword was sent by the sender (N being the number of the codewords). Our analysis shows that as long as N is below the limit imposed by the Holevo bound the error probability can be sent to zero asymptotically in the length of the codewords.

Finally in Ref. [9] we discuss ergodicity in the general case where the fixed point of the open quantum system transformation is not a full-rank (faithful) density matrix. Notably, we show that ergodicity is stable under randomizations, namely that every random mixture of an ergodic channel with a generic channel is still ergodic. In addition, we prove several conditions under which ergodicity can be promoted to the stronger property of mixing. Finally, exploiting a suitable correspondence between quantum channels and generators of quantum dynamical semigroups, we extend our results to the realm of continuous-time quantum evolutions, providing a characterization of ergodic Lindblad generators and showing that they are dense in the set of all possible generators.

References
[1] A. S. Holevo and V. Giovannetti, Rep. Prog. Phys. 75, 046001 (2012).
[2] V. Giovannetti and G. M. Palma, Phys. Rev. Lett. 108, 040401 (2012).
[3] V. Giovannetti and G. M. Palma, J. Phys. B: At. Mol. Opt. Phys. 45, 154003 (2012).
[4] F. Ciccarello, G. M. Palma, and V. Giovannetti, Phys. Rev. A 87, 040103(R) (2013).
[5] A. De Pasquale and V. Giovannetti, Phys. Rev. A 86, 052302 (2012).
[6] A. De Pasquale, A. Mari, A. Porzio, and V. Giovannetti, Phys. Rev. A 87, 062307 (2013).
[7] S. Lloyd, V. Giovannetti, and L. Maccone, Phys. Rev. Lett. 105, 250501 (2011).
[8] V. Giovannetti, S. Lloyd, and L. Maccone, Phys. Rev. A 85, 012302 (2012).
[9] D. Burgarth, G. Chiribella, V. Giovannetti, P. Perinotti, and K. Yuasa, New J. Phys. 15, 073045 (2013).

1.3.15 Quantum Metrology

In classical estimation theory, the central limit theorem implies that the statistical error in a measurement outcome can be reduced by an amount proportional to $n^{-1/2}$ by repeating the measures n times and then averaging. Using quantum effects, such as entanglement, it is often possible to do better, decreasing the error by an amount proportional to $1/n$. Quantum metrology is the study of those quantum techniques that allow one to gain advantages over purely classical approaches [1].

In interferometry, sub-Heisenberg strategies claim to achieve a phase estimation error smaller than the inverse of the mean number of photons employed (Heisenberg bound). In a series of works [2,3] we show that one can achieve a comparable precision without performing any measurement, just using the large prior information that sub-Heisenberg strategies require. For uniform prior (i.e. no prior information), we prove that these strategies cannot achieve more than a fixed gain over Heisenberg-limited interferometry. Analogous results hold for arbitrary single-mode prior distributions. These results extend also beyond interferometry: the effective error in estimating any parameter is lower bounded by a quantity proportional to the inverse expectation value (above a ground state) of the generator of translations of the parameter. In Ref. [4] we analyze the how the sensitivity in optical interferometry is affected by losses during the signal propagation or at the detection stage. The optimal quantum states of the probing signals in the presence of loss were recently found. However, in many cases of practical interest, their associated accuracy is worse than the one obtainable without employing quantum resources (e.g. entanglement and squeezing) but neglecting the detector's loss. In our analysis we detailed an experiment that can reach the latter even in the presence of imperfect detectors: it employs a phase-sensitive amplification of the signals after the phase sensing, before the detection. We experimentally demonstrated the feasibility of a phase estimation experiment able to reach its optimal working regime. Since our method uses coherent states as input signals, it is a practical technique that can be used for high-sensitivity interferometry and, in contrast to the optimal strategies, does not require one to have an exact characterization of the loss beforehand. In Ref. [5] we studied the efficiency of quantum tomographic reconstruction where the system under investigation (quantum target) is indirectly monitored by looking at the state of a quantum probe that has been scattered off the target. In particular we focus on the state tomography of a qubit through a one-dimensional scattering of a probe qubit, with a Heisenberg-type interaction. Via direct evaluation of the associated quantum Cramer-Rao bounds, we compare the accuracy efficiency that one can get by adopting entanglement-assisted strategies with that achievable when entanglement resources are not available. Even though sub-shot noise accuracy levels are not attainable, we have shown that quantum correlations play a significant role in the estimation.

References
[1] V. Giovannetti, S. Lloyd, and L. Maccone, Nat. Phot. 5, 222 (2011).
[2] V. Giovannetti, S. Lloyd, L. Maccone, Phys. Rev. Lett. 108, 260405 (2012).
[3] V. Giovannetti and L. Maccone, Phys. Rev. Lett. 108, 210404 (2012).
[4] N. Spagnolo, C. Vitelli, V. G. Lucivero, V. Giovannetti, L. Maccone, and F. Sciarrino, Phys. Rev. Lett. 108, 233602 (2012).
[5] A. De Pasquale, P. Facchi, V. Giovannetti, and K. Yuasa. J. Phys. A: Math. Theor. 45, 105309 (2012).

1.3.16 Quantum Optomechanics

Theoretical studies and huge technological progresses over the last decades made it possible to reach a considerable level of control over quantum states of matter in a large variety of physical systems, ranging from photons, electrons and atoms to bigger solid state systems such as quantum dots and superconducting circuits. This opened the possibility for novel tests of quantum mechanics and allowed, among other things, to take important steps forward in investigating the quantum regime of macroscopic objects. In this perspective, one of the main goals in today quantum science is controlling nano- and micromechanical oscillators at the quantum level. Quantum optomechanics [1,2], i.e. studying and engineering the radiation pressure interaction of light with mechanical systems, comes as a powerful and well-developed tool to do so.

Parametrically modulated optomechanical systems have been recently proposed as a simple and efficient setting for the quantum control of a micromechanical oscillator: relevant possibilities include the generation of squeezing in the oscillator position (or momentum) and the enhancement of entanglement between mechanical and radiation modes. In tIn Ref. [3] we further investigate this new modulation regime, considering an optomechanical system with one or more parameters being modulated over time. We first apply a sinusoidal modulation of the mechanical frequency and characterize the optimal regime in which the visibility of purely quantum effects is maximal. We then introduce a second modulation on the input laser intensity and analyze the interplay between the two. We find that an interference pattern shows up, so that different choices of the relative phase between the two modulations can either enhance or cancel the desired quantum effects.

In Ref. [4] instead we introduce and characterize two different measures which quantify the level of synchronization of interacting continuous variable quantum systems. The two measures allow to extend to the quantum domain the notions of complete and phase synchronization. The Heisenberg principle sets a universal bound to complete synchronization. The measure of phase synchronization is in principle unbounded, however in the absence of quantum resources (e.g. squeezing) the synchronization level is bounded below a certain threshold. We elucidate some interesting connections between entanglement and synchronization and, finally, discuss an application based on quantum opto-mechanical systems.

References
[1] F. Marquardt and S. M. Girvin, Physics 2, 40 (2009).
[2] M. Aspelmeyer, S. Groblacher, K. Hammerer and N. Kiesel, J. Opt. Soc. Am. B 27, A189 (2010).
[3] A. Farace and V. Giovannetti, Phys. Rev. A 86, 0103820 (2012).
[4] A. Mari, A. Farace, N. Didier, V. Giovannetti, and R. Fazio, Phys. Rev. Lett. 111, 103605 (2013).

1.3.17 Quantum Algorithms

Privacy is a major concern in many information trans- actions. A familiar example is provided by the transac- tions between web search engines and their users. On one hand, the user (say Alice) would typically prefer not to reveal to the server the item she is interested in (user privacy). On the other hand, the server (say Bob) would like not to disclose more information than that Alice has asked for (data privacy). User and data privacy are apparently in conflict: the most straightforward way to obtain user privacy is for Alice to have Bob send her the entire database, leading to no data privacy whatsoever. Conversely, techniques for guaranteeing the server's data privacy typically leave the user vulnerable. At the information theoretical level, this problem has been formalized by Gertner et al. as the Symmetrically-Private Information Retrieval (SPIR) [1]. This is a generalization of the Private Information Retrieval (PIR) problem [2] which deals with user privacy alone. (SPIR is closely related to oblivious transfer [3], in which Bob sends to Alice N bits, out of which Alice can access exactly one–which one, Bob doesn't know.) No efficient solutions in terms of communication complexity [4] are known for SPIR.

In a series of papers [5-7] we proposed a cheat sensitive quantum protocol to perform a private search on a classical database which is efficient in terms of communication complexity. It allows a user to retrieve an item from the server in possession of the database without revealing which item she retrieved: if the server tries to obtain information on the query, the person querying the database can find it out. Furthermore our protocol ensures perfect data privacy of the database, i.e. the information that the user can retrieve in a single queries is bounded and does not depend on the size of the database. With respect to the known (quantum and classical) strategies for private information retrieval, our protocol displays an exponential reduction both in communication complexity and in running-time computational complexity. In Ref. [7] the basic properties of the proposal was experimentally tested using a linear optical implementation.

References
[1] Y. Gertner, Y. Ishai, E. Kushilevitz, and T. Malkin, Jour- nal of Computer Systems Sciences, 60 592 (2000).
[2] B. Chor, O. Goldreich, E. Kushilevitz, and M. Sudan, Journal of the ACM, 45, 965 (1998).
[3] S. Wiesner, ACM SIGACT News, 15(1), 78-88, Winter- Spring (1983).
[4] A. Ambainis, in Proceedings of the 24ht ICALP, Lecture Notes in Computer Science, 1256 401 (1997).
[5] V. Giovannetti, S. Lloyd, and L. Maccone, Phys. Rev. Lett. 100, 230502 (2008).
[6] V. Giovannetti, S. Lloyd, and L. Maccone, EEE TRANSACTIONS ON INFORMATION THEORY, 56 3465 (2010).
[7] F. De Martini, V. Giovannetti, S. Lloyd, L. Maccone, E. Nagali, L. Sansoni, and F. Sciarrino, Phys. Rev. A 80, 010302(R) (2009).

1.4 Publications and patents 2008-2013

In the following publication list, author affiliations are coded as follows:

Laboratorio NEST faculty and postdocs   regular font, black
Laboratorio NEST **students**   bold font, black
CNR@NEST staff   regular font, blue
IIT@NEST staff   regular font, green
Collaborators   italic, black

Note that all publications include authors belonging to Laboratorio NEST in the strict sense (i.e. either SNS faculty or SNS graduate/undergraduate students), but that a close network of collaborations does exist within NEST that involves scientists and students with different affiliations. Other publications with NEST, Scuola Normale Superiore affiliation exist that do not involve Laboratorio NEST people in the former strict sense: these were not included.

NEST publications 2008

1. Tuning transport properties of HIV-1 Tat arginine-rich motif in living cells, Traffic **9**, 528 (2008). **F. Cardarelli**, M. Serresi, R. Bizzarri, and F. Beltram

2. Linewidth enhancement factor of terahertz quantum cascade lasers, Appl. Phys. Lett. **92**, 071106 (2008). R. P. Green, J. Xu, **L. Mahler**, A. Tredicucci, F. Beltram, *G. Giuliani, H. E. Beere,* and *D. A. Ritchie*

3. Acoustic-counter-flow micro-fluidics by surface acoustic waves, Appl. Phys. Lett. **92**, 104103 (2008). M. Cecchini, S. Girardo, *D. Pisignano, R. Cingolani,* and F. Beltram

4. Tailoring light-matter interaction in intersubband microcavities, Phys. E **40**, 1906 (2008). **A. A. Anappara**, A. Tredicucci, F. Beltram, L. Sorba, and *G. Biasiol*

5. Terahertz quantum cascade lasers with quasi-periodic resonators, Phys. E **40**, 2176 (2008). **L. Mahler**, A. Tredicucci, R. P. Green, F. Beltram, *C. Walther, J. Faist, H. E. Beere,* and *D. A. Ritchie*

6. Filling factor dependence of the fractional quantum Hall effect gap, Phys. Rev. Lett. **100**, 196805 (2008). *S. Khrapai, A.A. Shashkin, M.G. Trokina, V.T. Dolgopolov*, V. Pellegrini, F. Beltram, *G. Biasiol*, and L. Sorba

7. Polydimethylsiloxane-LiNbO$_3$ surface acoustic wave hybrid micropump devices for fluid control into microchannels, Lab Chip **8**, 1557 (2008). S. Girardo, M. Cecchini, F. Beltram, *R. Cingolani,* and *D. Pisignano*

8. Cis-trans photoisomerization of fluorescent-protein chromophores. J. Phys. Chem. B **112**, 10714 (2008). **V. Voliani**, R. Bizzarri, R. Nifosì, *S. Abbruzzetti, E. Grandi, C. Viappiani,* and F. Beltram

9. Manipulation and generation of supercurrent in out-of-equilibrium Josephson tunnel nanojunctions. Phys. Rev. Lett. **101**, 077004 (2008). **S. Tirelli**, *A. M. Savin*, **C. P. Garcia**, *J. P. Pekola,* F. Beltram, and F. Giazotto

10. Relevant energy scale in hybrid mesoscopic Josephson junctions, Phys. Rev. B **78**, 052506 (2008). F. Carillo, *D. Born*, V. Pellegrini, *F. Tafuri, G. Biasiol,* L. Sorba, and F. Beltram

11. Magnetic field sensitivity of In$_{0.75}$Ga$_{0.25}$As Hall nano probes, Mater. Sci. Eng. B **147**, 148 (2008). *A. Candini*, F. Carillo, *G. Biasiol*, P. Pingue, *M. Affronte*, and L. Sorba

12. Transport anisotropy in InGaAs 2D electron gases, Physica E **40**, 1392 (2008), *M. Rosini, E. Cancellieri*, D. Ercolani, *G. Biasiol*, L. Sorba, and *C. Jacoboni*

13. Transport anisotropy in In$_{0.75}$Ga$_{0.25}$As two dimensional electron gases, Phys. Rev. B **77**, 235307 (2008). D. Ercolani, *G. Biasiol, E. Cancellieri, M. Rosini, C. Jacoboni*, F. Carillo, S. Heun, L. Sorba, and *F. Nolting*

14. High-resolution poly(ethylene terephthalate) (PET) hot embossing at low-temperature: thermal, mechanical and optical analysis of nanopatterned films, Langmuir **24**, 12581 (2008). M. Cecchini, *F. Signori*, P. Pingue, *S. Bronco, F. Ciardelli*, and F. Beltram

15. PC12 polarity on biopolymer nanogratings. J. Phys. C **100**, 012003 (2008). M. Cecchini, A. Ferrari, and F. Beltram

16. Supercoiling and local denaturation of plasmids with a minimalist DNA model, J. Phys. Chem. B **112,** 13197 (2008). **F. Trovato** and V. Tozzini

17. A molecular state of correlated electrons in a quantum dot, Nature Phys. **4**, 467 (2008). S. Kalliakos, M. Rontani, V. Pellegrini, **C. P. Garcia**, *A. Pinczuk, G.*

Goldoni, E. Molinari, L.N. Pfeiffer, and *K.W. West*

18. The N-terminal domain of ERK1 accounts for the functional differences with ERK2. PLoS One **3**, e3873 (2008). **M. Marchi**, *A. D'Antoni, I. Formentini, R. Parra, R. Brambilla*, G. M. Ratto, and *M. Costa*

19. Epigenetic drugs modulate MeCP2 dynamics in living cells, Cell. Oncology **30**, 264 (2008). **M. Marchi**, *M. Becucci, P. Tognini, M Maffei, N. Landsberger*, G.M. Ratto, and *M. Costa*.

20. Signatures of composite-fermion metals in electron bilayers at ν(T)=1, Physica E 40, 1312 (2008). B. Karmakar, S. Luin, V. Pellegrini, *A. Pinczuk, B.S. Dennis, L.N. Pfeiffer,* and *K.W. West*

21. Optical control of energy-level structure of few electrons in AlGaAs/GaAs quantum dots, Nano Lett. **8**, 577 (2008). S. Kalliakos, V. Pellegrini, **C. P. Garcia**, *A. Pinczuk, L.N. Pfeiffer,* and *K.W. West*

22. Entanglement in Many-Body Systems Rev. Mod. Phys. **80**, 517 (2008). *L. Amico*, R. Fazio, *A. Osterloh*, and *V. Vedral*

23. Condensed-matter physics: Opposite of a superconductor, Nature **452**, 542 (2008). R. Fazio

24. Non abelian superconducting pumps, Phys. Rev. Lett. **100**, 027002 (2008*). V. Brosco*, R. Fazio, *F.W.J. Hekking,* and *A. Joye*

25. Quantum Random Access Memory , Phys. Rev. Lett. **100**, 160501 (2008). V. Giovannetti, *S. Lloyd*, and *L. Maccone*

26. Quantum Private Queries, Phys. Rev. Lett. **100**, 230502 (2008). V. Giovannetti, *S. Lloyd,* and *L. Maccone*

27. Adiabatic Dynamics in Open Quantum Critical Many-Body Systems, Phys. Rev. Lett. **101**, 175701 (2008). *D. Patané, A. Silva, L. Amico*, R. Fazio, and *G.E. Santoro*

28. Quantum illumination with Gaussian states, Phys. Rev. Lett. **101**, 253601 (2008). *S.-H. Tan, B.I. Erkmen,* V. Giovannetti, *S. Guha, S. Lloyd, L. Maccone, S. Pirandola,* and *J.H. Shapiro*

29. Time-dependent current-density-functional theory of spin-charge separation and spin drag in one-dimensional ultracold Fermi gases, Phys. Rev. Lett. **101**, 206402 (2008). *G. Xianlong*, M. Polini, **D. Rainis**, *M.P. Tosi,* and *G. Vignale*

30. Quantum MERA channels, Phys. Rev. Lett. **101**, 180503 (2008). V. Giovannetti, S. Montangero, and R. Fazio

31. Multi-mode bosonic Gaussian channels, New J. Phys. **10**, 083030 (2008). **F. Caruso**, *J. Eisert*, V. Giovannetti, and *A.S. Holevo*

32. Spin chain model for correlated quantum channels, New J. Phys. **10**, 115009 (2008). D. Rossini, V. Giovannetti, and S. Montangero

33. Optimized Cooper pair pump, Phys. Rev. B **77**, 144522 (2008). **S. Safaei**, S. Montangero, F. Taddei, and R. Fazio

34. Spin-drag relaxation time in one-dimensional spin-polarized Fermi gases, Phys. Rev. B **77**, 035113 (2008). **D. Rainis**, M. Polini, *M.P. Tosi,* and *G. Vignale*

35. Multi-channel architecture for electronic quantum-Hall interferometry, Phys. Rev. B **77**, 155320 (2008). V. Giovannetti, F. Taddei, *D. Frustaglia*, and R. Fazio

36. Coulomb-Interaction Effects in Full Counting Statistics of a Quantum-Dot Aharonov-Bohm Interferometer, Phys. Rev. B **78**, 075318 (2008). *D. Urban, J. Koenig*, and R. Fazio

37. Adiabatic quantum dynamics of the Lipkin-Meshkov-Glick model, Phys. Rev. B **78**, 104426 (2008). *T. Caneva*, R. Fazio, and *G.E. Santoro*

38. Adiabatic quenches through an extended quantum critical region., Phys. Rev. B **77**, 140404 (2008). *F. Pellegrini*, S. Montangero*, G.E. Santoro,* and R. Fazio

39. Phase-Dependent Electronic Specific Heat in Mesoscopic Josephson Junctions., Phys. Rev. B **78**, 012503 (2008). *H. Rabani*, F. Taddei, *O. Bourgeois*, R. Fazio, and F. Giazotto

40. Fulde-Ferrell-Larkin-Ovchinnikov superfluidity in one-dimensional optical lattices, Phys. Rev. B **77**, 245105 (2008). *M. Rizzi*, M. Polini, *M.A. Cazalilla, M.R. Bakhtiari, M.P. Tosi*, and R. Fazio

41. Nonequilibrium pairing instability in ultracold Fermi gases with population imbalance, Phys. Rev. A **77**, 033605 (2008). **A. Tomadin**, M. Polini, *M.P. Tosi*, and R. Fazio

42. Bang-Bang control of a qubit coupled to a quantum critical spin bath, Phys. Rev. A **77**, 052112 (2008). D. Rossini, *P. Facchi*, R. Fazio, *G. Florio, D.A. Lidar, S. Pascazio, F. Plastina,* and *P. Zanardi*

43. Architectures for a quantum random access memory, Phys. Rev. A **78**, 052310 (2008). V. Giovannetti, *S. Lloyd*, and *L. Maccone*

44. Qubit channels with small correlations, Phys. Rev. A **77**, 052323 (2008). **F. Caruso** V. Giovannetti, *C. Macchiavello,* and *M.B. Ruskai*

45. Photon and polariton fluctuations in arrays of QED-cavities, EuroPhys. Lett. **83**, 47011 (2008). D. Rossini, R. Fazio, and *G.E. Santoro*

46. Quantum Shared Broadcasting, Quantum Inf. Process. **7**, 55 (2008). V. Giovannetti and *A.S. Holevo*

47. A new approach to characterize qubit channels, Int. J. Quant. Inf. **6**, 621 (2008). **F. Caruso** and V. Giovannetti

48. Density Matrix Renormalization Group for Dummies, J. Comput. Theor. Nanos. **5**, 1277 (2008). *G. De Chiara, M. Rizzi*, D. Rossini, and S. Montangero

49. A protocol For Cooling and Controlling Composite Systems by Local Interactions, Quantum Information and Many Body Quantum Systems, **17** (2008). *D. Burgarth* and V. Giovannetti

NEST publications 2009

50. Vertically emitting microdisk lasers, Nature Photonics **3**, 46 (2009). **L. Mahler**, A. Tredicucci, F. Beltram, *C. Walther, J Faist, B. Witzigmann, H. E. Beere and D. A. Ritchie*

51. Quantitative FRET analysis with the E⁰GFP-mCherry fluorescent protein pair, Photochem. Photobiol*. **85**, 287 (2009)*. **L. Albertazzi**, D. Arosio, **L. Marchetti, F. Ricci**, and F. Beltram

52. The homeotic protein HOXC13 is a member of human DNA pre-replication complexes, Cell. Cycle **8**, 454 (2009). **L. Comelli, L. Marchetti**, D. Arosio, *S. Riva, G. Abdurashidova,* F. Beltram, and *A. Falaschi*.

53. Green Fluorescent Protein-based pH indicators for in vivo use: a review, Anal. Bioanal. Chem. **393**, 1107 (2009). R. Bizzarri, M. Serresi, S. Luin, and F. Beltram

54. Real-time measurement of endosomal acidification by a novel genetically encoded biosensor, Anal. Bioanal. Chem. **393**, 1123 (2009). M. Serresi, R. Bizzarri, **F. Cardarelli**, and F. Beltram

55. Acoustoelectric luminescence from a field-effect n-i-p lateral junction, Appl. Phys. Lett. **94**, 121 (2009). **G. De Simoni**, V. Piazza, L. Sorba, *G. Biasiol*, and F. Beltram

56. Raman Study of Chromophore States in Photochromic Fluorescent Proteins. J. Am. Chem. Soc. **131**, 96 (2009). S. Luin, **V. Voliani**, **G. Lanza**, R. Bizzarri, R. Nifosì, **P. Amat**, V. Tozzini, M. Serresi, and F. Beltram

57. Finite size effects in surface emitting Terahertz quantum cascade lasers, Opt. Exp. **17**, 6703 (2009). **L. Mahler**, A. Tredicucci, F. Beltram, *C. Walther, H.E. Beere,* and *D.A. Ritchie*

58. Signatures of the ultrastrong light-matter coupling regime, Phys. Rev. B **79**, 201303 (2009). **A. A. Anappara**, *S. De Liberato*, A. Tredicucci, *C. Ciuti, G. Biasiol*, L. Sorba, and F. Beltram

59. Impact of classical forces and decoherence in multiterminal Aharonov-Bohm networks, Phys. Rev. B **79**, 195443 (2009). **E. Strambini**, V. Piazza, *G. Biasiol*, L. Sorba, and F. Beltram

60. Tuning non-linear charge transport between integer and fractional quantum Hall states, Phys. Rev. Lett. **103**, 016802 (2009). S. Roddaro, **N. Paradiso**, V. Pellegrini, *G. Biasiol*, L. Sorba, and F. Beltram.

61. YBCO Nanobridges: Simplified Fabrication Process by Using a Ti Hard Mask, IEEE Trans. Appl. Supercond. **19**, 183 (2009). *G. Papari*, F. Carillo, *D. Born,* **L. Bartoloni**, *E. Gambale, D. Stornaiuolo*, P. Pingue, F. Beltram, and *F. Tafuri*.

62. Distributed feedback ring resonators for vertically emitting terahertz quantum cascade lasers, Opt. Exp. **17**, 13031 (2009). **L. Mahler**, *M. I. Amanti, C. Walther*, A. Tredicucci, F. Beltram, *J. Faist, H. E. Beere,* and *D. A. Ritchie*.

63. InAs/InSb nanowires heterostructures grown by chemical beam epitaxy. Nanotechnology **20**, 505605 (2009). D. Ercolani, *F. Rossi*, **A. Li**, S. Roddaro, *V. Grillo, G. Salviati*, F. Beltram, and L. Sorba.

64. Directional PC12 cell migration along plastic nanotracks. IEEE Trans. Biomed. Eng. **56**, 2692 (2009). A. Ferrari, M. Cecchini, R. Degl'Innocenti, F. Beltram.

65. Probing nuclear localization signal-Importin alpha binding equilibria in living cells, J. Biol. Chem. **284**, 36638 (2009). **F. Cardarelli**, R. Bizzarri, M. Serresi, **L. Albertazzi**, and F. Beltram.

66. Differential Near-Field Scanning Optical Microscopy with THz quantum cascade laser sources, Optics Express **17**, 23785 (2009). R. Degl'Innocenti, **M. Montinaro**, J. Xu, V. Piazza, P. Pingue, A. Tredicucci, F. Beltram, *H. E. Beere,* and *D. A. Ritchie*.

67. SDP hound, a Mutual Information-Based Method to Investigate Specificity-Determining Positions, Algorithms **2**, 764 (2009). *S. Bonella*, W. Rocchia, **P. Amat**, R. Nifosì, and V. Tozzini.

68. Complexes of HIV-1 Integrase with HAT proteins: multiscale models, dynamics and hypotheses on allosteric sites of inhibition, Proteins **76**, 946 (2009). A. Di Fenza, W. Rocchia, and V. Tozzini

69. Quantum phase transition of a quantum Hall excitonic state in electron bilayers, International Journal of mod. Phys. B **23**, 2607 (2009). B. Karmakar, V. Pellegrini, *A. Pinczuk, L.N. Pfeiffer,* and *K.W. West*.

70. Probing collective modes of correlated states of few electrons in semiconductor quantum dots. Solid State Comm. **149**, 1436 (2009). S. Kalliakos, *M. Rontani*, V. Pellegrini, *A. Pinczuk, A. Singha*, **C. P. Garcia**, *G. Goldoni, E. Molinari, L.N. Pfeiffer,* and *K.W. West*.

71. First-Order Quantum Phase Transition of Excitons in Quantum Hall Bilayers, Phys. Rev. Lett. **102**, 036802 (2009). B. Karmakar, V. Pellegrini, *A. Pinczuk, L.N. Pfeiffer,* and *K.W. West*

72. Engineering artificial graphene in a two-dimensional electron gas, Phys. Rev. B **79**, 241406 (2009). **M. Gibertini**, A. Singha, V. Pellegrini, M. Polini, *G. Vignale, A. Pinczuk, L.N. Pfeiffer,* and *K.W. West.*

73. Evidence of interlayer correlation in spin excitations of quantum Hall bilayers with negligible tunneling, Phys. Rev. B Rapid Comm. **80**, 241312 (2009) B. Karmakar, V. Pellegrini, *A. Pinczuk, L.N. Pfeiffer,* and *K.W. West.*

74. Probing collective modes of correlated states of few electrons in semiconductor quantum dots, Solid State Comm. **149**, 1436 (2009). S. Kalliakos, *M. Rontani*, V. Pellegrini, *A. Pinczuk*, A. Singha, **C. P. Garcia**, *G. Goldoni, E. Molinari, L.N. Pfeiffer, and K.W. West*

75. Optical anisotropy of electronic excitations in elliptical quantum dots, Appl. Phys. Lett. **94**, 073114 (2009). A. Singha, V. Pellegrini, S. Kalliakos, B. Karmakar, *A. Pinczuk, L.N. Pfeiffer,* and *K.W. West.*

76. Recombination limited energy relaxation in a BCS superconductor, Phys. Rev. Lett. **102**, 017003 (2009). *A.V. Timofeev*, **C. Pascual Garcia**, *N.B. Kopnin, A.M. Savin, M. Meschke*, F. Giazotto*, and *J. P. Pekola*

77. Josephson current in nanofabricated V/Cu/V mesoscopic junctions, Appl. Phys. Lett. **94**, 132508 (2009). **C. Pascual Garcia** and F. Giazotto.

78. The quantum optical Josephson interferometer, Nature Phys. **5**, 281 (2009). *D. Gerace, H.E. Tureci, A. Imamoglu*, V. Giovannetti, and R. Fazio

79. Optimal Control at the Quantum Speed Limit, Phys. Rev. Lett. **103**, 240501 (2009). *T. Caneva, M. Murphy, T. Calarco*, R. Fazio*, S. Montangero, V. Giovannetti, and *G.E. Santoro*

80. Efficient generation of a maximally entangled state by repeated on- and off-resonant scattering of ancilla qubits, New J. Phys. **11**, 123027 (2009). *K. Yuasa, D. Burgarth,* V. Giovannetti, and *H. Nakazato*

81. Adiabatic dynamics of a quantum critical system coupled to an environment: Scaling and kinetic equation approaches, Phys. Rev. B **80**, 024302 (2009) *D. Patané, A. Silva, L. Amico,* R. Fazio, and *G.E. Santoro*

82. Electron tunneling into a quantum wire in the Fabry-Perot regime, Phys. Rev. B **79**, 035121 (2009). **S. Pugnetti**, F. Dolcini, *D. Bercioux,* and *H. Grabert*

83. Critical exponents of one-dimensional quantum critical models by means of MERA tensor network, Phys. Rev. B **80**, 113103 (2009). S. Montangero, *M. Rizzi*, V. Giovannetti, and R. Fazio

84. Optimized single-qubit gates for Josephson phase qubits, Phys. Rev. B **79**, 064524 (2009). **S. Safaei**, S. Montangero, F. Taddei, and R. Fazio

85. Detection of Tiny Mechanical Motion by Means of the Ratchet Effect, Phys. Rev. B **79**, 174516 (2009). **S. Pugnetti**, *Y.M. Blanter*, F. Dolcini, and R. Fazio

86. Nonlocality of Field-Emitted Electrons from a Superconductor, Phys. Rev. B **79**, 180503(R) (2009). *K. Yuasa, P. Facchi*, R. Fazio, *H. Nakazato, I. Ohba, S. Pascazio,* and *S. Tasaki*

87. Andreev reflection in graphene nanoribbons, Phys. Rev. B **79**, 115131 (2009). **D. Rainis**, F. Taddei, F. Dolcini, M. Polini, and R. Fazio

88. Linear response of doped graphene sheets to vector potentials, Phys. Rev. B **80**, 075418 (2009). **A. Principi**, M. Polini, and *G. Vignale*

89. Homogeneous MERA states: an information theoretical analysis, Phys. Rev. A **79**, 052314 (2009). V. Giovannetti, S. Montangero, *M. Rizzi*, and R. Fazio

90. Communication Through a Quantum Link, Phys. Rev. A **79**, 012311 (2009). V. Giovannetti, *D. Burgarth,* and *S. Mancini*

91. Dipole oscillations of confined lattice bosons in one dimension, Phys. Rev. A **79**, 041602(R) (2009). S. Montangero, R. Fazio, *P. Zoller,* and *G. Pupillo*

92. Sub-Rayleigh Quantum Imaging, Phys. Rev. A **79**, 013827 (2009). V. Giovannetti, *S. Lloyd, L. Maccone,* and *J.H. Shapiro*

93. Trap modulation spectroscopy of the Mott-insulator transition in optical lattices, Phys. Rev. A **79**, 041601(R) (2009). *H. Lignier, A. Zenesini, D. Ciampini, O. Morsch, E. Arimondo,* S. Montangero, *G. Pupillo*, and R. Fazio

94. High fidelity state transfer in binary tree networks, Phys. Rev. A **79**, 022313 (2009). **T. Tufarelli** and V. Giovannetti

95. Local controllability of quantum networks, Phys. Rev. A **79**, 060305(R) (2009). *D. Burgarth, S. Bose, C. Bruder*, and V. Giovannetti

96. Experimental Quantum Private Queries with linear optics, Phys. Rev. A **80**, 010302(R) (2009). *F. De Martini*, V. Giovannetti, *S. Lloyd*, *L. Maccone*, *E. Nagali, L. Sansoni,* and *F. Sciarrino*

97. Quantum billiards in optical lattices, EuroPhys. Lett. **88**, 30006 (2009). S. Montangero, *D. Frustaglia, T. Calarco*, and R. Fazio

98. Influence of interface transmissivity and inelastic scattering on the electronic entropy and specific heat of diffusive SNS Josephson junctions, J. Appl. Phys. **105**, 093904 (2009). *H. Rabani*, F. Taddei, F. Giazotto, and R. Fazio

99. Improved resolution in imaging through quantum post-selection, AIP Conf. Proc. 1110, 433 (2009). V. Giovannetti, *S. Lloyd, L. Maccone,* and *J.H. Shapiro*

100. Characterizing electron entanglement in multi-mode mesoscopic conductors., AIP Conf. Proc. 1129, 475 (2009). F. Taddei, V. Giovannetti, *D. Frustaglia*, and R. Fazio

NEST publications 2010
101. Charge pumping in InAs nanowires by surface acoustic waves, Semicond. Sci. Technol. **25**, 024013 (2010). S. Roddaro, **E. Strambini**, V. Piazza, and F. Beltram.

102. Electronic properties of quantum dot systems realized in semiconductor nanowires, Semicond. Sci. Technol. **25**, 024007 (2010). *J. Salfi*, S. Roddaro, D. Ercolani, L. Sorba, *I. Saverlyev, M. Blumin, H.E. Ruda*, and F. Beltram.

103. Single aminoacid replacement makes Aequorea Victoria fluorescent proteins reversibly photoswitchable, J. Am. Chem. Soc. **132**, 85 (2010). R. Bizzarri, M. Serresi, **F. Cardarelli**, *S. Abbruzzetti, B. Campanini, C. Viappiani*, and F. Beltram.

104. The effect of alternative neuronal differentiation pathways on PC12 cell adhesion and neurite alignment to nanogratings, Biomaterials **31**, 2565 (2010). A. Ferrari, P. Faraci, M. Cecchini, and F. Beltram.

105. Selective control of edge channel trajectories by scanning gate microscopy. Physica E **42**, 1038 (2010). **N. Paradiso**, S. Heun, S. Roddaro, *L. N. Pfeiffer, K. W. West*, L. Sorba, *G. Biasiol*, and F. Beltram.

106. Little-Parks effect in single nanoscale $YBa_2Cu_3O_{6+x}$ rings, Phys. Rev. B **81**, 054505 (2010). F. Carillo, *G. Papari, D. Stornaiuolo, D. Born*, P. Pingue, F. Beltram, and *F. Tafuri*.

107. Quasi-periodic distributed feedback laser, Nature Phot. **4**, 165 (2010). **L. Mahler**, A. Tredicucci, F. Beltram, and *D. Wiersma*.

108. Neuronal polarity selection by topography-induced focal-adhesion control, Biomaterials **31**, 4682 (2010). A. Ferrari, M. Cecchini, *D. Pisignano*, and F. Beltram.

109. Singlet-triplet transition in a few-electron lateral $In_{0.75}Ga_{0.25}As/In_{0.75}Al_{0.25}As$ quantum dot, Appl. Phys. Lett. **96**, 142107 (2010). **F. Deon**, V. Pellegrini, F. Carillo, F. Giazotto, *G. Biasiol*, L. Sorba, and F. Beltram.

110. Cantilever deflection measurement and actuation by an interdigitated transducer, Appl. Phys. Lett. **96**, 173505 (2010). **E. Strambini**, V. Piazza, P. Pingue, *G. Biasiol*, L. Sorba, and F. Beltram.

111. Coherent detection of electron dephasing, Phys. Rev. Lett. **104**, 170403 (2010). **E. Strambini**, L. Chirolli, V. Giovannetti, F. Taddei, R. Fazio, V. Piazza, and F. Beltram.

112. Conductance and valley splitting in etched *Si/SiGe* one-dimensional nanostructures, Phys. Rev. B **81**, 195311 (2010). *G. Frucci, L. Di Gaspare, F. Evangelisti, E. Giovine, A. Notargiacomo*, V. Piazza, and F. Beltram.

113. High-power surface emission from terahertz distributed feedback lasers with a dual-slit unit cell, Appl. Phys. Lett. **96**, 191109 (2010). **L. Mahler**, A. Tredicucci, F. Beltram, *C. Walther, J. Faist, H. E. Beere,* and *D. A. Ritchie*.

114. Dendrimer Internalization and Intracellular Trafficking in Living Cells, Mol. Pharm. **7**, 680 (2010). **L. Albertazzi**, M. Serresi, **A. Albanese**, and F. Beltram.

115. Simultaneous intracellular chloride and pH measurements using a GFP-based sensor, Nature Methods **7**, 516 (2010). D. Arosio, **F. Ricci**, **L. Marchetti**, **R. Gualdani**, **L. Albertazzi** and F. Beltram.

116. Surface-acoustic-wave counterflow micropumps for on-chip liquid motion in two-dimensional microchannel arrays. Lab Chip **10**, 1997 (2010). **L. Masini**, M. Cecchini, *S. Girardo, D. Pisignano*, and F. Beltram.

117. Tuning a distributed feedback laser with a coupled microcavity. Optics Express **18**, 19185 (2010). **L. Mahler**, A. Tredicucci, F. Beltram, *H. E. Beere, and D. A. Ritchie*.

118. Pd–assisted growth of InAs nanowires, Crystal Growth and Design **10**, 4197 (2010). S. Heun, *B. Radha*, D. Ercolani, *G. U. Kulkarni, F. Rossi, V. Grillo, G. Salviati*, F. Beltram, and L. Sorba.

119. Faceting of InAs-InSb heterostructured nanowires, Crystal Growth and Design **10**, 4038 (2010). **L. Lugani**, D. Ercolani, *F. Rossi, G. Salviati*, F. Beltram, and L. Sorba.

120. Delocalized-localized transition in a semiconductor two-dimensional honeycomb lattice, Appl. Phys. Lett. **97**, 132113 (2010). **G. De Simoni**, A. Singha, **M. Gibertini**, B. Karmakar, M. Polini, V. Piazza, *L. N. Pfeiffer, K. W. West,* F. Beltram, and V. Pellegrini.

121. Photoswitching of E222Q GFP mutants: "concerted" mechanism of chromophore isomerization and protonation, Photochem Photobiol. Sci. **9**, 1307 (2010). *S. Abbruzzetti*, R. Bizzarri, S. Luin, R. Nifosì, **B. Storti**, *C. Viappiani*, and F. Beltram.

122. Tuning a distributed feedback laser with a coupled microcavity, Opt. Express **18**, 19185 (2010). **L. Mahler**, A. Tredicucci, F. Beltram, *H. E. Beere, and D. A. Ritchie*.

123. Coexistence of Vapor-Liquid-Solid and Vapor-Solid-Solid Growth Modes in Pd-Assisted InAs Nanowires, Small **6**, 1935 (2010). S. Heun, *B. Radha*, D. Ercolani, *G. U. Kulkarni, F. Rossi, V. Grillo, G. Salviati*, F. Beltram, and L. Sorba

124. Single-step bifunctional coating for selectively conjugable nanoparticles, Nanoscale **2**, 2783 (2010). **V. Voliani**, S. Luin, **F. Ricci**, and F. Beltram.

125. Delivery and Subcellular Targeting of Dendrimer-Based Fluorescent pH Sensors in Living Cells, J. Am. Chem. Soc. **132**, 18158 (2010). **L. Albertazzi**, **B. Storti**, **L. Marchetti**, and F. Beltram.

126. Homeotic proteins partecipate in the function of human-DNA replication origins, Nucl. Acid Res. **38**, 8105 (2010). **L. Marchetti**, *L. Comelli, B. D'Innocenzo, L. Puzzi*, S. Luin, D. Arosio, *M. Calvello, R. Mendoza, F. Peverali*, **F. Trovato**, *S. Riva, G. Biamonti, G. Abdurashidova*, F. Beltram, and *A. Falaschi*.

127. Electronic implementations of interaction-free measurements, Phys. Rev. B **82**, 045403 (2010). L. Chirolli, **E. Strambini**, V. Giovannetti, F. Taddei, V. Piazza, R. Fazio, F. Beltram, and *G. Burkard.*

128. An excitatory loop with astrocytes contributes to drive neurons to seizure threshold, PLoS Biol **8**, e1000352 (2010). *M. Gómez-Gonzalo, G. Losi, A. Chiavegato, M. Zonta, M. Cammarota*, **M. Brondi**, *F. Vetri, L. Uva, T. Pozzan, M. de Curtis,* G.M. Ratto, and *G. Carmignoto*.

129. Polarity-Sensitive Coumarins Tailored to Live Cell Imaging, J Am Chem Soc **132**, 1276 (2010). G. Signore, R. Nifosi, **L. Albertazzi**, **B. Storti**, and R. Bizzarri.

130. Observation of magnetophonon resonance of Dirac fermions in graphite, Phys. Rev. Lett. **105**, 227401 (2010). *J. Yan*, **S. Goler**, *T.D. Rhone, M. Han, R. He, P. Kim*, V. Pellegrini, and *A. Pinczuk*.

131. Impact of nonequilibrium phonons on the electron dynamics in terahertz quantum cascade lasers, Appl. Phys. Lett. **97**, 033110 (2010). *R. C. Iotti, F. Rossi*, M. S. Vitiello, *G. Scamarcio*, **L. Mahler**, and A. Tredicucci.

132. Intersubband polaritons in a one-dimensional surface plasmon photonic crystal, Appl. Phys. Lett. **97**, 231123 (2010). **S. Zanotto**, *G. Biasiol*. R. Degl'Innocenti, L. Sorba, and A. Tredicucci.

133. Submegahertz frequency stabilization of a terahertz quantum cascade laser to a molecular absorption line, Appl. Phys. Lett. **96**, 071112 (2010). *H. Richter, S.G. Pavlov, A.D. Semenov,* **L. Mahler**, A. Tredicucci, *H.E. Beere, D.A. Ritchie,* and *H.-W. Hübers*.

134. Scanning probe nanoimprint lithography, Nanotechnology **21**, 075305 (2010). *F. Dinelli, C. Menozzi, P. Baschieri, P. Facci*, and P. Pingue.

135. Ability to Adapt: Different Generations of PAMAM Dendrimers Show Different Behaviors in Binding siRNA. J Phys Chem B **114**, 2667 (2010). *G. M. Pavan*, **L. Albertazzi**, and *A. Danani*.

136. Preparation of stable dispersion of barium titanate nanoparticles: Potential applications in biomedicine. Colloid Surf B-Biointerfaces **76**, 535 (2010). *G. Ciofani, S. Danti, S. Moscato*, **L. Albertazzi**, *D. D'Alessandro, D. Dinucci, F. Chiellini, M. Petrini,* and *A. Menciassi*.

137. ERK1 nucleocytoplasmic shuttling rate depends on specific N-terminal aminoacids. Biochem. Bioph. Res. Comm. **398**, 166 (2010). **M. Marchi**, *L. Pancrazi, M. Maffei*, G. M. Ratto, and *M. Costa*.

138. Capacities of lossy bosonic memory channels, Phys. Rev. Lett. **104**, 030501 (2010). *C. Lupo*, V. Giovannetti, *S. Mancini*

139. Many-body orbital paramagnetism in doped graphene sheets, Phys. Rev. Lett. **104**, 225503 (2010). **A. Principi**, M. Polini, *G. Vignale,* and *M.I. Katsnelson*

140. Dynamical Phase Transitions and Instabilities in Open Atomic Many-Body Systems., Phys. Rev. Lett. 105, 015702 (2010). *S. Diehl*, **A. Tomadin**, *A. Micheli*, R. Fazio, and *P. Zoller*

141. Teleportation-induced correlated quantum channels, Phys. Rev. Lett. **104**, 020503 (2010). **F. Caruso**, V. Giovannetti, and *G.M. Palma*

142. Blockade and counterflow supercurrent in exciton-condensate Josephson junctions, Phys. Rev. Lett. **104**, 027004 (2010). F. Dolcini, **D. Rainis**, F. Taddei, M. Polini, R. Fazio, and *A.H. MacDonald*

143. Homogeneous MERA tensor networksor quantum critical systems, New J. Phys. **12**, 075018 (2010). *M. Rizzi,* S. Montangero, **P. Silvi**, V. Giovannetti, and R. Fazio

144. Electron-electron interactions in decoupled graphene layers. Rev. B **82**, 085443 (2010). *R.E.V. Profumo*, M. Polini, *R. Asgari*, R. Fazio, and *A.H. MacDonald*, Phys

145. Velocity-modulation control of electron-wave propagation in graphene, Phys. Rev. B **81**, 073407 (2010). *A. Raoux*, M. Polini, *R. Asgari, A.R. Hamilton*, R. Fazio, and *A.H. MacDonald*

146. Electron density distribution and screening in rippled graphene sheets, Phys. Rev. B **81**, 125437 (2010). **M. Gibertini**, **A. Tomadin**, M. Polini, *A. Fasolino,* and *M.I. Katsnelson*

147. Quantum dynamics of a driven three-level Josephson-atom maser, Phys. Rev. B **82**, 214507 (2010). N. Didier and *Y.M. Blanter, F.W.J. Hekking*

148. Quantum Private Queries: securety analysis, IEEE Trans. Inf. Th. **56**, 3465 (2010). V. Giovannetti, *S. Lloyd,* and *L. Maccone*

149. Communication at the quantum speed limit along a spin chain, Phys. Rev. A **82**, 022318 (2010). *M. Murphy,* S. Montangero, V. Giovannetti, and *T. Calarco*

150. Quantum Defragmentation Algorithm, Phys. Rev. A **82**, 024302 (2010). *D. Burgarth* and V. Giovannetti

151. Memory effects in attenuation and amplification quantum processes, Phys. Rev. A **82**, 032312 (2010). *C. Lupo,* V. Giovannetti, and *S. Mancini*

152. Non-equilibrium phase transition in driven-dissipative nonlinear cavity arrays, Phys. Rev. A **81**, 061801 (2010). **A. Tomadin**, V. Giovannetti, R. Fazio, *D. Gerace, I. Carusotto, H.E. Tureci,* and *A. Imamoglu*

153. Homogeneous binary trees as ground states of quantum critical Hamiltonians, Phys. Rev. A **81**, 062335 (2010). **P. Silvi**, V. Giovannetti, S. Montangero, *M. Rizzi, J.I. Cirac,* and R. Fazio

154. SQUID Detection of Quantized Mechanical Motion, EuroPhys. Lett. **90**, 48007 (2010). **S. Pugnetti**, *Y.M. Blanter*, and R. Fazio

155. Entanglement renormalization and boundary critical phenomena, J. Stat. Mech., L03001 (2010). **P. Silvi**, V. Giovannetti, *P. Calabrese, G.E. Santoro*, and R. Fazio

156. Generalized minimal output entropy conjecture for one-mode Gaussian channels: definitions and some exact results, J. Phys. A: Math. Theor. **43**, 415305 (2010). V. Giovannetti, *A.S. Holevo, S. Lloyd,* and *L. Maccone*

NEST publications 2011

157. Cooling electrons from 1 to 0.4K with V-based nanorefrigerators, Appl. Phys. Lett. **98**, 032501 (2011). O. Quaranta, P. Spathis, F. Beltram, and F. Giazotto.

158. High efficiency coupling of Terahertz micro-ring quantum cascade lasers to the low-loss optical modes of hollow metallic waveguides, Opt. Express **19**, 1122 (2011). M. S. Vitiello, J. Xu, **M. Kumar**, F. Beltram, A. Tredicucci, *O. Mitrofanov, H.E. Beere,* and *D. A. Ritchie.*

159. Hybrid InAs nanowire-vanadium proximity SQUID, Nanotechnology **22**, 105201 (2011). P. Spathis, S. Biswas, S. Roddaro, L. Sorba, F. Giazotto, and F. Beltram.

160. Nanotopographic control of neuronal polarity, Nanoletters **11**, 505 (2011). A. Ferrari, M. Cecchini, *A. Dhawan, S. Micera*, I. Tonazzini, *R. Stabile, D. Pisignano*, and F. Beltram

161. Probing the Gate-Voltage-Dependent Surface Potential of Individual InAs Nanowires Using Random Telegraph Signals, ACS Nano **5**, 2191 (2011). *J. Salfi*, **N. Paradiso**, S. Roddaro, S. Heun, *S. V. Nair, I. G. Savelyev, M. Blumin*, F. Beltram, and *H. E. Ruda*.

162. Quantitative analysis of Tat peptide binding to import carriers reveals unconventional nuclear transport properties, J. Biol. Chem. **286**, 12292 (2011). **F. Cardarelli**, M. Serresi, **A. Albanese**, R. Bizzarri, and F. Beltram

163. Spatially resolved analysis of edge-channel equilibration in quantum Hall circuits, Phys. Rev. B **83**, 155305 (2011). **N. Paradiso**, S. Heun, S. Roddaro, **D. Venturelli**, F. Taddei, V. Giovannetti, R. Fazio, *G. Biasiol*, L. Sorba, and F. Beltram.

164. Magnetotransport investigation of conducting channels and spin splitting in high-density AlGaN/AlN/GaN two-dimensional electron gas, Phys. Rev. B **83**, 155318 (2011). **D. Spirito**, *L. Di Gaspare, G. Frucci, F. Evangelisti, A. Di Gaspare, A. Notargiacomo, E. Giovine*, S. Roddaro, and F. Beltram.

165. Probing the local temperature of a two-dimensional electron gas microdomain with a quantum dot: measurement of electron-phonon interaction. Phys. Rev. B **83**, 201306 (2011). **S. Gasparinetti**, **F. Deon**, *G. Biasiol*, L. Sorba, F. Beltram, and F. Giazotto.

166. Quantum dot spectroscopy of proximity-induced superconductivity in a two-dimensional electron gas, Appl. Phys. Lett. **98**, 132101 (2011). **F. Deon**, V. Pellegrini, F. Giazotto, *G. Biasiol*, L. Sorba, and F. Beltram.

167. Manipulation of electron orbitals in hard-wall InAs/InP nanowire quantum dots, Nanoletters **11**, 1695 (2011). S. Roddaro, **A. Pescaglini**, D. Ercolani, L. Sorba, and F. Beltram.

168. Growth mechanism of InAs–InSb heterostructured nanowires grown by chemical beam epitaxy, J Crystal Growth **323**, 304 (2011). **L. Lugani**, D. Ercolani, F. Beltram, and L. Sorba.

169. Engineering the excited state of fluorophores for high resolution imaging of bio- and soft-matter, Eur Biophys. J. **40**, 147 (2011). R. Bizzarri, G. Signore, *P. Bianchini*, **G. Abbandonato**, A. Battisti, *A. Pucci*, R. Nifosì, *A. Diaspro*, and F. Beltram.

170. Microfluidic chip with temporal and spatial concentration generation capabilities for biological applications, Microelec. Eng. **88**, 1689 (2011). R. Sahai, *C. Martino, P. Castrataro, A. Menciassi, A. Ferrari*, F. Beltram, and M. Cecchini.

171. Self-assembly and electron-beam-induced direct etching of suspended graphene nanostructures, J. Appl. Phys. **110**, 064308 (2011). **S. Goler**, V. Piazza, S. Roddaro, V. Pellegrini, F. Beltram, and P. Pingue.

172. Cis–trans photoisomerization properties of GFP chromophore analogs, Eur Biophys J. **40**, 1205 (2011). **G. Abbandonato**, G. Signore, R. Nifosì, **V. Voliani**, R. Bizzarri, and F. Beltram

173. Proximity effect in a two-dimensional electron gas probed with a lateral quantum dot, Phys. Rev. B **84**, 100506 (2011). **F. Deon**, V. Pellegrini, F. Giazotto, *G. Biasiol*, L. Sorba, and F. Beltram.

174. Guiding a terahertz quantum cascade laser into a flexible silver-coated waveguide, J. Appl. Phys. **110**, 063112 (2011). M. Vitiello, J. Xu, F. Beltram, A. Tredicucci, *O. Mitrofanov, J. A. Harrington, H. E. Beere and D. A. Ritchie*.

175. Anti-bunched photons from a lateral light-emitting diode, Appl. Phys. Lett. **99**, 131103 (2011). **T. Lunghi**, **G. De Simoni**, V. Piazza, *C. A. Nicoli*, *H. E. Beere, D. A. Ritchie*, and F. Beltram

176. Controlled coupling of spin-resolved quantum Hall edge states, Phys. Rev. Lett. **107**, 236804 (2011). B. Karmakar, **D. Venturelli**, L. Chirolli, F. Taddei, V. Giovannetti, R. Fazio, S. Roddaro, *G. Biasiol*, L. Sorba, V. Pellegrini, and F. Beltram.

177. Multiphoton molecular photorelease in click-chemistry-functionalized gold nanoparticles, Small **7**, 3271 (2011). **V. Voliani**, **F. Ricci**, G. Signore, R. Nifosì, S. Luin, and F. Beltram

178. Dendrimer-based fluorescent indicators: in vitro and in vivo applications, PLoS ONE **6**, e28450 (2011). **L. Albertazzi**, **M. Brondi**, *G.M. Pavan*, **S. Sulis Sato**, G. Signore, **B. Storti**, G.M. Ratto, and F. Beltram.

179. Quantum transport in low-dimensional AlGaN/GaN systems, J. Nanoparticle Res. **13**, 5699 (2011). **D. Spirito**, *G. Frucci, A. Di Gaspare, L. Di Gaspare, E. Giovine, A. Notargiacomo*, S. Roddaro, F. Beltram, and F. Evangelisti.

180. Lasing in planar semiconductor diodes, Appl. Phys. Lett. **99**, 261110 (2011). **G. De Simoni**, **L. Mahler**, V. Piazza, A. Tredicucci, *C. Nicoll, H. Beere*, and F. Beltram.

181. Impact of electron heating on the equilibration between quantum Hall edge channels, Phys. Rev. B **84**, 235318 (2011). **N. Paradiso**, S. Heun. S. Roddaro, L. Sorba, F. Beltram, and *G. Biasiol*.

182. Microfluidic chip for spatially and temporally controlled biochemical gradient generation in standard cell-culture Petri dishes, Microfluidics and Nanofluidics **11**, 763 (2011). R. Sahai, M. Cecchini, M. Klingauf, A. Ferrari, *C. Martino, P. Castrataro, V. Lionetti, A. Menciassi*, and F. Beltram.

183. Hot-electron effects in InAs nanowire Josephson junctions, Nano Research **4**, 259 (2011). S. Roddaro, **A. Pescaglini**, D. Ercolani, L. Sorba, F. Giazotto, and F. Beltram.

184. A Josephson quantum electron pump, Nature Phys. **7**, 857 (2011). F. Giazotto, P. Spathis, S. Roddaro, S. Biswas, F. Taddei, *M. Governale*, and L. Sorba.

185. Multifunctional Trackable Dendritic Scaffolds and Delivery Agents, Angew Chem Int Edit **50**, 3425 (2011). *R.J. Amir*, **L. Albertazzi**, *J. Willis, A. Khan, T. Kang,* and *C.J. Hawker*.

186. Photonic engineering of surface-emitting terahertz quantum cascade lasers, Laser & Photonics Rev **5**, 647 (2011). **L. Mahler** and A. Tredicucci.

187. The short-time structural plasticity of dendritic spines is altered in a model of Rett syndrome, Scientific Reports **1**, 45 (2011). S. Landi, E. Putignano, *E.M. Boggio, M. Giustetto, T. Pizzorusso*, and G.M. Ratto.

188. Nanoscale Viscoelastic Behavior of the Surface of Thick Polystyrene Films as a Function of Temperature, Macromolecules **44**, 987 (2011). *F. Dinelli, A. Ricci, T. Sgrilli, P. Baschieri*, P. Pingue, *M. Puttaswamy, and P. Kingshott*.

189. Control of initial endothelial spreading by topographic activation of focal adhesion kinase, Soft Matter **7**, 7313 (2011). *D. Franco*, M. Klingauf, *M. Bednarzik*, M. Cecchini, *V. Kurtcuoglu, J. Gobrecht, D. Poulikakos,* and A. Ferrari.

190. Ictal but not interictal epileptic discharges activate astrocyte endfeet and elicit cerebral arteriole responses, Front Cell Neurosci **5**, 8 (2011). *M. Gómez-Gonzalo, G. Losi*, **M. Brondi**, *L. Uva*, **S. Sulis Sato**, *M. de Curtis*, G.M. Ratto, and *G. Carmignoto*.

191. High quality factor HTS Josephson junctions on low loss substrates, Supercond. Sci. Technol. **24**, 045008 (2011). *D. Stornaiuolo*, G. Papari, *N. Cennamo*, F. Carillo, *L. Longobardi, D. Massarotti, A. Barone,* and *F. Tafuri*.

192. Switching ultrastrong light–matter coupling on a subcycle scale, J. Appl. Phys. **109**, 102418 (2011). *R. Huber*, **A. A. Anappara**, *G. Günter, A. Sell, S. De Liberato, C. Ciuti, G. Biasiol*, L. Sorba, A. Tredicucci, and *A. Leitenstorfer*.

193. One-dimensional surface-plasmon gratings for the excitation of intersubband polaritons in suspended membranes, Solid State Commun. **151**, 1725 (2011). R. Degl'Innocenti, **S. Zanotto**, A. Tredicucci, *G. Biasiol*, and L. Sorba.

194. Two-dimensional Mott-Hubbard electrons in an artificial honeycomb lattice., Science 332, 1176 (2011). A. Singha, **M. Gibertini**, B. Karmakar, *S. Yuan*, M. Polini, *G. Vignale, M.I. Katsnelson, A. Pinczuk, L.N. Pfeiffer, K.W. West*, and V. Pellegrini

195. Advances in Quantum Metrology, Nature Photon. **5**, 222 (2011). V. Giovannetti, *S. Lloyd,* and *L. Maccone*

196. Beauty and the noisy beast., Nature Phys. **7**, 376 (2011). *L. Maccone* and V. Giovannetti

197. Persistent spin oscillations in a spin-orbit-coupled superconductor, Phys. Rev. Lett. **107**, 077004 (2011). A. Agarwal, M. Polini, R. Fazio, and *G. Vignale*

198. Closed timelike curves via post-selection: theory and experimental test of consistency, Phys. Rev. Lett. **106**, 040403 (2011). *S. Lloyd, L. Maccone, R. Garcia-Patron*, V. Giovannetti, *Y. Shikano, S. Pirandola, L.A. Rozema, A. Darabi, Y. Soudagar, L.K. Shalm,* and *A.M. Steinberg*

199. Sequential projective measurements for channel decoding, Phys. Rev. Lett. **106**, 250501 (2011). *S. Lloyd*, V. Giovannetti, and *L. Maccone*

200. The quantum mechanics of time travel through post-selected teleportation, Phys. Rev. D **84**, 025007 (2011). *S. Lloyd, L. Maccone, R. Garcia-Patron*, V. Giovannetti, and *Y. Shikano*

201. Generating topological order from a 2D cluster state using a duality mapping, New J. Phys. **13**, 065010 (2011). *B.J. Brown, W. Son, C.V. Kraus*, R. Fazio, and *V. Vedral*

202. Quantum Reading Capacity, New J. Phys. **13**, 113012 (2011*). S. Pirandola, C. Lupo*, V. Giovannetti, *S. Mancini,* and *S.L. Braunstein*

203. Edge channel mixing induced by potential steps in an integer quantum Hall system, Phys. Rev. B **83**, 075315 (2011). **D. Venturelli**, V. Giovannetti, F. Taddei, R. Fazio, *D. Feinberg, G. Usaj,* and *C.A. Balseiro*

204. Drude weight, plasmon dispersion, and a.c. conductivity in doped graphene sheets, Phys. Rev. B **84**, 045429 (2011). *S.H. Abedinpour, G. Vignale*, **A. Principi**, M. Polini, *W.-K. Tse,* and *A.H. MacDonald*

205. Gauge fields and interferometry in folded graphene, Phys. Rev. B **83**, 165403 (2011). **D. Rainis**, F. Taddei, M. Polini, *G. León, F. Guinea,* and *V.I. Falko*

206. Phase diagram of hard-core bosons on a zig-zag ladder, Phys. Rev. B **83**, 155106 (2011). D. Rossini, *V. Lante, A. Parola,* and *F. Becca*

207. Detecting phonon blockade with photons, Phys. Rev. B **84**, 054503 (2011). N. Didier, **S. Pugnetti**, *Y.M. Blanter*, and R. Fazio

208. Spin-supersolid phase in Heisenberg chains: A characterization via Matrix Product States with periodic boundary conditions, Phys. Rev. B **83**, 140411(R) (2011). D. Rossini, V. Giovannetti, and R. Fazio

209. Floquet theory of Cooper pair pumping, Phys. Rev. B **83**, 214508 (2011). *A. Russomanno*, **S. Pugnetti**, *V. Brosco*, and R. Fazio

210. Dissipative spin dynamics near a quantum critical point: Numerical Renormalization Group and Majorana diagrammatics, Phys. Rev. B **84**, 155110 (2011). *S. Florens*, **D. Venturelli**, and *R. Narayanan*

211. Josephson current in a four terminal superconductor - exciton condensate - superconductor system, Phys. Rev. B **84**, 184528 (2011). **S. Peotta, M. Gibertini**, F. Dolcini, F. Taddei, M. Polini, *L.B. Ioffe*, R. Fazio, and *A.H. MacDonald*

212. Quantum Quenches, Thermalization and Many-Body Localization, Phys. Rev. B **83**, 094431 (2011). **E. Canovi**, D. Rossini, R. Fazio, *G.E. Santoro,* and *A. Silva*

213. The optimal unitary dilation for bosonic Gaussian channels, Phys. Rev. A **84**, 022306 (2011). **F. Caruso**, *J. Eisert*, V. Giovannetti, and *A.S. Holevo*

214. Speeding up critical system dynamics through optimized evolution, Phys. Rev. A **84**, 012312 (2011). *T. Caneva, T. Calarco*, R. Fazio, *G.E. Santoro,* and S. Montangero

215. Statistical mechanics of the cluster Ising model, Phys. Rev. A **84**, 022304 (2011). *P. Smacchia, L. Amico, P. Facchi*, R. Fazio, *G. Florio, S. Pascazio,* and *V. Vedral*

216. Enhanced Quantum Communication via Optical Refocusing, Phys. Rev. A **84**, 010303(R) (2011). *C. Lupo*, V. Giovannetti, *S. Pirandola, S. Mancini,* and *S. Lloyd*

217. Quantum phase transition between cluster and antiferromagnetic states., EuroPhys. Lett. **95**, 50001 (2011). *W. Son, L. Amico*, R. Fazio, *A. Hamma, S. Pascazio,* and *V. Vedral*

218. Ground-state factorization and correlations with broken symmetry, EuroPhys. Lett. **96**, 27002 (2011). *B. Tomasello*, D. Rossini, *A. Hamma,* and *L. Amico*

219. Errors in quantum optimal control and strategy for the search of easily implementable control pulses, J. Phys. B: At. Mol. Opt. Phys. **44**, 154012 (2011). **A. Negretti**, R. Fazio, and *T. Calarco*

220. Stiffness in 1D Matrix Product States with periodic boundary conditions, J. Stat. Mech., P05021 (2011). D. Rossini, V. Giovannetti, and R. Fazio

221. Applicability of the generalized Gibbs ensemble after a quench in the quantum Ising chain, J. Stat. Mech., P07015 (2011). *T. Caneva,* **E. Canovi**, D. Rossini, *G. E. Santoro,* and *A. Silva*

222. Interaction between hopping and static spins in a discrete network, Phys. Lett. A **375**, 2538 (2011). F. Ciccarello

223. Acoustic plasmons and composite hole-acoustic plasmon satellite bands in graphene on a metal gate, Solid State Commun. **151**, 1627 (2011). **A. Principi**, *R. Asgari*, and M. Polini

224. Quantitative entanglement witnesses of Isotropic-and Werner-class via local measurements., J. Phys. A: Math. Theor. **44**, 145303 (2011). **P. Silvi**, F. Taddei, R. Fazio, and V. Giovannetti

NEST publications 2012

225. Biocompatible noisy nanotopographies with specific directionality for controlled anisotropic cell cultures, Soft Matter **8**, 1109 (2012). **S. Meucci**, I. Tonazzini, F. Beltram, and M. Cecchini.

226. Room temperature Terahertz detectors based on semiconductor nanowire field-effect transistors, Nano Letters **12**, 96 (2012). M. S. Vitiello, *D. Coquillat,* **L. Viti**, D. Ercolani, *F. Teppe*, A. Pitanti, F. Beltram, L. Sorba, *W. Knap*, and A. Tredicucci

227. Single particle tracking of acyl carrier protein (ACP)-tagged TrkA receptors in PC12nnr5 cells, J. Neurosci. Methods **204**, 82 (2012). **A. Callegari**, S. Luin, **L. Marchetti**, *A. Duci*, *A. Cattaneo*, and F. Beltram

228. Fluorescence recovery after photobleaching (FRAP) analysis of nuclear export rates indentifies intrinsic features of nucleocytoplasmic transport, J. Biol. Chem. **287**, 5554 (2012). F. Cardarelli, **L. Tosti**. M. Serresi, F. Beltram, and R. Bizzarri.

229. High critical current density and scaling of phase-slip processes in YBaCuO nanowires, Superconductor Sci & Technol **25**, 035011 (2012). G. Papari, F. Carillo, *D. Stornaiuolo, L. Longobardi*, F. Beltram, and *F. Tafuri*.

230. Interaction-free, automatic, on-chip fluid routing by surface acoustic waves, Lab on a chip **12**, 2621 (2012). **M. Travagliati**, G. De Simoni, **C. M. Lazzarini**, V. Piazza, F. Beltram, and M. Cecchini.

231. Intact microtubules preserve transient receptor potential vanilloid 1 TRPV1 functionality through receptor binding, J. Biol. Chem. **287**, 7803 (2012). **B. Storti**, R. Bizzarri, F. Cardarelli, and F. Beltram.

232. Peptidic coating for gold nanospheres multifunctionalizable with photostable and photolabile moieties, J. Materials Chem. **22**, 14487 (2012). **V. Voliani, F. Ricci**, S. Luin, and F. Beltram.

233. Growth of InAs/InAsSb heterostructured nanowires, Nanotechnology **23**, 115606 (2012). D. Ercolani, M. Gemmi, *L. Nasi, F. Rossi,* M. Pea, **A. Li**, *G. Salviati*, F. Beltram, and L. Sorba.

234. Imaging Fractional Incompressible Stripes in Integer Quantum Hall Systems, Phys. Rev. Lett. **108**, 246801 (2012). **N. Paradiso**, S. Heun, S. Roddaro, L. Sorba, F. Beltram, *G. Biasiol, L. N. Pfeiffer,* and *K.W. West*.

235. Fuorescence recovery after photobleaching reveals the biochemistry of nucleocytoplasmic exchange, Anal. Bioanal. Chem. **403**, 2339 (2012) R. Bizzarri, F. Cardarelli, M. Serresi, and F. Beltram.

236. Semiconductor nanowires for highly sensitive, room-temperature detection of Terahertz quantum cascade laser emission, Appl. Phys. Lett. **100**, 241101 (2012). M. S. Vitiello, **L. Viti**, **L. Romeo**, D. Ercolani, *G. Scalari, J. Faist*, F. Beltram, L. Sorba, and A. Tredicucci.

237. Intracellular pH measurements made simple by fluorescent protein probes and the phasor approach to fluorescence lifetime imaging, Chem. Comm. **48**, 5127 (2012). A. Battisti, *M. Digman, E. Gratton*, **B. Storti**, F. Beltram, and R. Bizzarri.

238. Electron beam induced current in InSb-InAs nanowire type-III heterostructures, Appl. Phys. Lett. **101**, 063116 (2012). *C. Y. Chen*, *A. Shik*, A. Pitanti, A. Tredicucci, D. Ercolani, L. Sorba, F. Beltram, and *H. E. Ruda*.

239. Imaging backscattering through impurity-induced antidots in quantum Hall constrictions, Phys. Rev. B **86** (2012). **N. Paradiso**, S. Heun, S. Roddaro, *G. Biasiol*, L. Sorba, D. Venturelli, F. Taddei, V. Giovannetti, and F. Beltram.

240. Coherent transport in extremely underdoped $Nd_{1.2}Ba_{1.8}Cu_3O_z$ nanostructures, New J Phys. **14**, 083025 (2012). F. Carillo, *G. N. De Luca*, **D. Montemurro**, G. Papari, *M. Salluzzo, D. Stornaiuolo, F. Tafuri*, and F. Beltram

241. Electrostatic spin control in InAs/InP nanowire quantum dots, Nano Lett. **12**, 4490 (2012). **L. Romeo**, S. Roddaro, A. Pitanti, D. Ercolani, L. Sorba, and F. Beltram.

242. Non-equilibrium longitudinal and transverse optical phonons in terahertz quantum cascade lasers, Appl. Phys. Lett. **100**, 091101 (2012). M. S. Vitiello, *R. C. Iotti, F. Rossi*, **L. Mahler**, A. Tredicucci, *H. E. Beere, D. A. Ritchie,* and *Q. Hu*, *G. Scamarcio*

243. Terahertz confocal microscopy with a quantum cascade laser source, Opt. Exp. **20**, 21924 (2012). **U. Siciliani de Cumis**, J. Xu, **L. Masini**, R. Degl'Innocenti, P. Pingue, F. Beltram, A. Tredicucci, M. S. Vitiello, *P. Benedetti, H. E. Beere,* and *D. A. Ritchie.*

244. Terahertz detection by heterostructured InAs/InSb nanowire based field effect transistors, Appl. Phys. Lett. **101**, 141103 (2012). A. Pitanti, *D. Coquillat*, D. Ercolani, L. Sorba, *F. Teppe, W. Knap*, G. De Simoni, F. Beltram. A. Tredicucci, and M.S. Vitiello.

245. A novel chimeric cell-penetrating peptide with membrane-disruptive properties for efficient endosomal escape, J. Controlled Release **163**, 293 (2012). **F. Salomone**, F. Cardarelli, M. Di Luca, C. Boccardi, R. Nifosì, G. Bardi, *L. Di Bari*, M. Serresi, and F. Beltram.

246. Rotating-polarization CARS microscopy: combining chemical and molecular orientation sensitivity, Optics Exp. **20**, 29369 (2012). **G. de Vito,** A. Bifone, and V. Piazza.

247. Enhanced Bioactivity of Internally Functionalized Cationic Dendrimers with PEG Cores, Biomacromol. **13,** 4089 (2012). **L. Albertazzi,** *F.M. Mickler, G. M. Pavan,* **F. Salomone,** G. Bardi, **M. Panniello,** *E. Amir, T. Kang, K. L. Killops, C. Brauchle, R.J. Amir,* and *C.J. Hawker.*

248. Ordered rippling of polymer surfaces by nanolithography: influence of scan pattern and boundary effects, Nanotechnology **23,** 475301 (2012). *S. Napolitano, M. D'Acunto, P. Baschieri, E. Gnecco,* and P. Pingue

249. Ultrafast optical bleaching of intersubband cavity polaritons Phys. Rev. B **86,** 201302 (2012). **S. Zanotto**, R. Degl'Innocenti, J-H. Xu, L. Sorba, A. Tredicucci, and *G. Biasiol*

250. Energy scales in YBaCuO grain boundary biepitaxial Josephson junctions Physica C **479,** 74 (2012). *F. Tafuri, D. Stornaiuolo, P. Lucignano, L. Galletti, L. Longobardi, D. Massarotti,* **D**. **Montemurro,** G. Papari, *A. Barone,* and *A. Tagliacozzo*

251. Dextran-Catechin Conjugate: A Potential Treatment Against the Pancreatic Ductal Adenocarcinoma, Pharmaceutical Res. **29,** 2601 (2012). O. Vittorio, *G. Cirillo, F. Iemma, G. Di Turi,* E. Jacchetti, *M. Curcio, S. Barbuti, N. Funel, O.I. Parisi, F. Puoci,* and *N. Picci*

252. Raman spectroscopy of magneto-phonon resonances in graphene an d graphite Solid State Comm. **152,** 1289 (2012). **S. Goler,** *J. Yan,* V. Pellegrini, and *A. Pinczuk*

253. Nanotopography induced contact guidance of the F11 cell line during neuronal differentiation: a neuronal model cell line for tissue scaffold development Nanotechnology **23** 275102 (2012). *P. Wieringa,* I. Tonazzini, *S. Micera,* and M. Cecchini

254. Raman sensitivity to crystal structure in InAs nanowires Appl. Phys. Lett. **100,** 143101 (2012). *J.K. Panda, A. Roy, A. Singha,* M. Gemmi, D. Ercolani, V. Pellegrini, and L. Sorba

255. High-performance and site-directed in utero electroporation by a triple-electrode probe. Nature Commun **3**, 960 (2012). *M. dal Maschio, D. Ghezzi, G. Bony, A. Alabastri, G. Deidda*, **M. Brondi, S. Sulis Sato**, *R. Proietti Zaccaria, E. Di Fabrizio*, G.M. Ratto, and *L. Cancedda*.

256. Escape dynamics in moderately damped Josephson junctions. Low Temp. Phys. **38,** 263 (2012). *D. Massarotti, L. Longobardi, L. Galletti*, *D. Stornaiuolo,* **D**. **Montemurro,** *G. Pepe, G. Rotoli, A. Barone,* and *F. Tafuri*

257. Large-Area Ohmic Top Contact to Vertically Grown Nanowires Using a Free-Standing Au Microplate Electrode ACS Appl. Mat. & Int. **4,** 1860 (2012). *B. Radha, D. Jayaraj, G.U. Kulkarni,* S. Heun, D. Ercolani, and L. Sorba

258. Contacts shielding in nanowire field effect transistors J. Appl. Phys. **111,** 064301 (2012). A. Pitanti, S. Roddaro, M. S. Vitiello, and A. Tredicucci

259. Modeling of InAs-InSb nanowires grown by Au-assisted chemical beam epitaxy, Nanotechnology **23** 095602 (2012). **L. Lugani,** D. Ercolani, L. Sorba, *N. V. Sibirev, M. A. Timofeeva,* and *V.G. Dubrovskii*

260. Flexible, Low-loss Waveguide Designs for Efficient Coupling to Quantum Cascade Lasers in the Far infrared, J. Infrared Millimeter and Terahertz Waves **33,** 319 (2012). **U. Siciliani de Cumis,** J.H. Xu, *C.M. Bledt, J.A. Harrington,* A. Tredicucci, and M.S. Vitiello

261. Se-doping dependence of the transport properties in CBE-grown InAs nanowire field effect transistors, Nanoscale Res. Lett. **7,** 1 (2012). **L. Viti**, M.S. Vitiello, D. Ercolani, L. Sorba, and A. Tredicucci

262. Nonadiabatic switching of a photonic band structure: Ultrastrong light-matter coupling and slow-down of light, Phys. Rev. B **85,** 081302 (2012). *M. Porer, J.M. Menard, A. Leitenstorfer, R. Huber,* R. Degl'Innocenti, **S. Zanotto,** *G. Biasiol,* L. Sorba, and A. Tredicucci

263. Analysis of line shapes and strong coupling with intersubband transitions in one-dimensional metallodielectric photonic crystal slabs, Phys. Rev. B **85,** 035307 (2012). **S. Zanotto,** R. Degl'Innocenti, L. Sorba, A. Tredicucci, and *G. Biasiol*

264. Minimalist Models for Biopolymers: Open Problems, Latest Advances and Perspectives, AIP Conf. Proc. **1456** 187 (2012). **F. Trovato** and V. Tozzini

265. Terahetz detection by heterostructed InAs/InSb nanowire based field effect transistors, Appl. Phys. Lett. **101** 141103 (2012). A. Pitanti, *D. Coquillat*, D. Ercolani, L. Sorba, *F. Teppe, W. Knap,* G. De Simoni, F. Beltram, A. Tredicucci, and M. S. Vitiello

266. Graphene field-effect transistors as room-temperature terahertz detectors, Nat. Mat. **11**, 865 (2012). **L. Vicarelli**, M.S. Vitiello, *D. Coquillat, A. Lombardo, A.C. Ferrari,W. Knap*, M. Polini, V. Pellegrini, and A. Tredicucci

267. High-fidelity quantum driving, Nature Phys. **8**, 147 (2012). *M.G. Bason, M. Viteau, N. Malossi, P. Huillery, E. Arimondo, D. Ciampini*, R. Fazio, V. Giovannetti, *R. Mannella,* and *O. Morsch*

268. Quantum channels and their entropic characteristics, Rep. Prog. Phys. **75**, 046001 (2012). *A.S. Holevo* and V. Giovannetti

269. Quantum interferometry for noisy detectors, Phys. Rev. Lett. **108**, 233602 (2012). *N. Spagnolo, C. Vitelli, V.G. Lucivero*, V. Giovannetti, *L. Maccone,* and *F. Sciarrino*

270. Quantum measurement bounds beyond the uncertainty relations, Phys. Rev. Lett. **108**, 260405 (2012). V. Giovannetti, *S. Lloyd,* and *L. Maccone*

271. Master equations for correlated quantum channels, Phys. Rev. Lett. **108**, 040401 (2012). V. Giovannetti and *G.M. Palma*

272. Photon production from the vacuum close to the super-radiant transition: When Casimir meets Kibble-Zurek, Phys. Rev. Lett. **108**, 093603 (2012). *G. Vacanti*, **S. Pugnetti**, N. Didier, *M. Paternostro*, *G.M. Palma*, R. Fazio, and *V. Vedral*

273. Sub-Heisenberg estimation strategies are ineffective, Phys. Rev. Lett. **108**, 210404 (2012). V. Giovannetti and *L. Maccone*

274. Optimal correlations in many-body quantum systems, Phys. Rev. Lett. **108**, 240503 (2012). *L. Amico*, D. Rossini, *A. Hamma,* and *V.E. Korepin*

275. Short-time spin dynamics in strongly correlated few-fermion systems, Phys. Rev. Lett. **108**, 245302 (2012). **S. Peotta**, D. Rossini, *P. Silvi, G. Vignale*, R. Fazio, and M. Polini

276. Drude weight, cyclotron resonance, and the Dicke model of graphene cavity QED, Phys. Rev. Lett. **109**, 267404 (2012). L. Chirolli, M. Polini, V. Giovannetti, and *A.H. MacDonald*

277. Phase diagram of the extended Bose Hubbard model, New J. Phys. **14**, 065012 (2012). D. Rossini and R. Fazio

278. Many-body localization and thermalization in the full probability distribution function of observables, New J. Phys. **14**, 095020 (2012). **E. Canovi**, D. Rossini, R. Fazio, *G.E. Santoro,* and *A. Silva*

279. Theory of Coulomb drag for massless Dirac fermions, New J. Phys. **14**, 063033 (2012). **M. Carrega**, *T. Tudorovskiy*, **A. Principi**, *M.I. Katsnelson*, and M. Polini

280. Local density of states in metal-topological superconductor hybrid systems, Phys. Rev. B **85**, 144525 (2012). **M. Gibertini**, F. Taddei, M. Polini, and R. Fazio

281. Geometric phases in superconducting qubits beyond the two-level-approximation, Phys. Rev. B **85**, 220502(R) (2012). *S. Berger, M. Pechal*, **S. Pugnetti**, *A.A. Abdumalikov Jr, L. Steffen, A. Fedorov, A. Wallraff,* and *S. Filipp*

282. Scattering theory of topological invariants in nodal superconductors, Phys. Rev. B **86**, 174520 (2012). *J.P. Dahlhaus*, **M. Gibertini**, and *C.W.J. Beenakker*

283. Proposal for a Datta-Das transistor in the quantum Hall regime, Phys. Rev. B **85**, 155317 (2012). L. Chirolli, D. Venturelli, F. Taddei, R. Fazio, and V. Giovannetti

284. Electron-hole puddles in the absence of charged impurities, Phys. Rev. B **85**, 201405(R) (2012). **M. Gibertini**, A. Tomadin, *F. Guinea, M.I. Katsnelson*, and M. Polini

285. Probing Cooper Pairs with Franson Interferometry, Phys. Rev. B **86**, 115429 (2012). V. Giovannetti and *K. Yuasa*

286. Macroscopic quantum tunneling in quartic and sextic potentials: application to a phase qubit, Phys. Rev. B **85**, 104522 (2012). N. Didier and *F.W.J. Hekking*

287. Plasmons and Coulomb drag in Dirac-Schrà dinger hybrid electron systems., Phys. Rev. B **86**, 085421 (2012). **A. Principi, M. Carrega**, *R. Asgari*, V. Pellegrini, and M. Polini

288. Quantifying the noise of a quantum channel by noise addition, Phys. Rev. A **86**, 052302 (2012). A. De Pasquale and V. Giovannetti

289. Creating quantum correlations through local non-unitary memoryless channels, Phys. Rev. A **85**, 010102(R) (2012). F. Ciccarello and V. Giovannetti

290. Teleportation can only transfer speakable quantum information, Phys. Rev. A **86**, 010304(R) (2012). *G. Chiribella*, V. Giovannetti, *L. Maccone,* and *P. Perinotti*

291. Achieving the Holevo bound via sequential measurements, Phys. Rev. A **85**, 012302 (2012). V. Giovannetti, *S. Lloyd,* and *L. Maccone*

292. Local-channel-induced rise of quantum correlations in continuous-variable systems, Phys. Rev. A **85**, 022108 (2012). F. Ciccarello and V. Giovannetti

293. Geometric phase kickback in a mesoscopic qubit-oscillator system, Phys. Rev. A **85**, 022129 (2012). *G. Vacanti*, R. Fazio, *M.S. Kim, G.M. Palma, M. Paternostro,* and *V. Vedral*

294. Classical to quantum in large number limit, Phil. Trans. R. Soc. A **370**, 4810 (2012). *K. Modi*, R. Fazio, *S. Pascazio, V. Vedral,* and *K. Yuasa*

295. Capacities of linear quantum optical systems, Phys. Rev. A **85**, 062314 (2012). *C. Lupo*, V. Giovannetti, *S. Pirandola, S. Mancini,* and *S. Lloyd*

296. Enhancing Quantum Effects via Periodic Modulations in Optomechanical Systems, Phys. Rev. A **86**, 013820 (2012). **A. Farace** and V. Giovannetti

297. Master equation for cascade quantum channels: a collisional approach, J. Phys. B: At. Mol. Opt. Phys. **45**, 154003 (2012). V. Giovannetti and *G.M. Palma*

298. Statistical distribution of the local purity in a large quantum system, J. Phys. A: Math. Theor. **45**, 015308 (2012). A. De Pasquale, *P. Facchi*, V. Giovannetti, *G. Parisi, S. Pascazio,* and *A. Scardicchio*

299. The tunneling density-of-states of interacting massless Dirac fermions, Solid State Commun. **152**, 1456 (2012). **A. Principi**, M. Polini, *R. Asgari,* and *A.H. MacDonald*

300. Entanglement-assisted tomography of a quantum target, J. Phys. A: Math. Theor. **45**, 105309 (2012). A. De Pasquale, *P. Facchi*, V. Giovannetti, and *K. Yuasa*

301. Invariant measures on multimode quantum Gaussian states, J. Math. Phys. **53**, 122209 (2012). *C. Lupo, S. Mancini*, A. De Pasquale, *P. Facchi, G. Florio, S. Pascazio*

302. Quantum discord in a spin system with symmetry breaking, Int. J. Mod. Phys. B **26**, 1243002 (2012). *B. Tomasello*, D. Rossini, *A. Hamma, and L. Amico*

303. Matrix Product State representation for Slater Determinants and Configuration Interaction States, Int. J. Mod. Phys. B **27**, 1245029 (2012). **P. Silvi**, D. Rossini, R. Fazio, *G.E. Santoro*, and V. Giovannetti

NEST publications 2013

304. Fast spatiotemporal correlation spectroscopy to determine protein lateral diffusion laws in live cell membranes, PNAS **110**(30), 12307 (2013). **C. Di Rienzo**, *E. Gratton*, F. Beltram, F. Cardarelli.

305. Electrical properties and band diagram of InSb-InAs nanowire type-III heterojunctions, J Appl. Phys. **113**, 104307 (2013). *A. Shik, C. Y. Chen*, A. Pitanti, A. Tredicucci, D. Ercolani, L. Sorba, F. Beltram, and *H. E Ruda*.

306. Unveiling LOX-1 receptor interplay with nanotopography: mechanotransduction and atherosclerosis onset, Scientific Reports **3**, 1141 (2013). **C. Di Rienzo**, E. Jacchetti, F. Cardarelli, R. Bizzarri, F. Beltram, and M. Cecchini

307. Fractal TiO2 Nanostructures by Nonthermal Laser Ablation at Ambient Pressure, The Journal of Physical Chemistry C **117**, 23305 (2013). *E. Cavaliere, G. Ferrini*, P. Pingue, and *L. Gavioli*

308. Use of polystyrene brushes to investigate the role of interface between substrates and thin homogeneous films, Journal of Polymer Science Part B: Polymer Physics **51**, 1149 (2013). *F. Dinelli, T. Sgrilli, A. Ricci, P. Baschieri*, P. Pingue, *M. Puttaswamy,* and *P. Kingshott*

309. Revealing the atomic structure of the buffer layer between SiC (0001) and epitaxial graphene, Carbon 249 (2013). **S. Goler**, C. Coletti, V. Piazza, P. Pingue, **F. Colangelo**, V. Pellegrini, *K. V Emtsev, S. Forti, U. Starke*, F. Beltram, and S. Heun

310. Extracellular matrix inhibits structural and functional plasticity of dendritic spines in the adult visual cortex, Nature Communications **4**, 1484 (2013). *L. De Vivo*, S. Landi, **M. Panniello,** *L. Baroncelli, S. Chierzi,* **L. Mariotti,** *M. Spolidoro, T. Pizzorusso,* L. Maffei, and G.M. Ratto

311. Synthesis, Cellular Delivery and In vivo Application of Dendrimer-based pH Sensors, Journal of visualized experiments **79**. **L. Albertazzi**, **B. Storti, M. Brondi, S. Sulis Sato**, G. M. Ratto, G. Signore and F. Beltram

312. The influence of graphene curvature on hydrogen adsorption: A study for future hydrogen storage devices, J. Phys. Chem. C **117** 11506 (2013). **S. Goler**, C. Coletti, V. Tozzini, V. Piazza, T. Mashoff, F. Beltram, V. Pellegrini, and S. Heun

313. A minimalist model of proteins diffusion and interaction: the GFP within the cytoplasm, Macromolecules **46**, 8311 (2013). **F. Trovato**, R. Nifosì, *A. Di Fenza*, and V. Tozzini

314. Evolutionary algorithm in the optimization of a coarse-grained force field, J. Chem. Theor. Comput. **9**, 4874 (2013). *F. Leonarski*, **F. Trovato**, V. Tozzini, *A. Le´s,* and *J. Trylska*
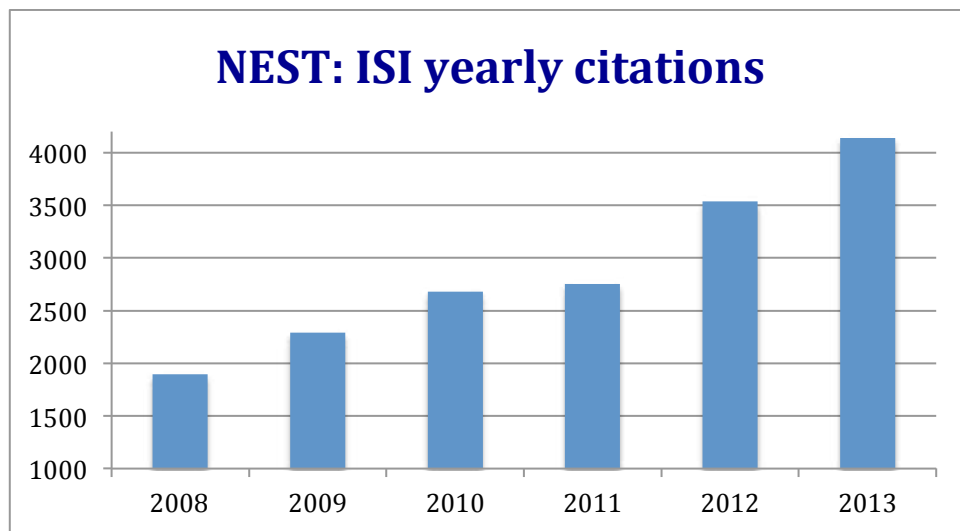
315. Fabrication, Operation and Flow Visualization in Surface-acoustic-wave-driven Acoustic-counterflow Microfluidics, Journal of visualized experiments: JoVE 78, e50524 (2013). **M. Travagliati**, R. Shilton, F. Beltram, and M. Cecchini

316. Accelerated endothelial wound healing on microstructured substrates under flow, Biomaterials **34**, 1488 (2013). *D. Franco, F. Milde,* M. Klingauf, *F. Orsenigo, E. Dejana, D. Poulikakos*, M. Cecchini, *P. Koumoutsakos*, *A. Ferrari*, and *V. Kurtcuoglu*

317. Endothelial differentiation of mesenchymal stromal cells: when traditional biology meets mechanotransduction, Integrative Biology **5**, 291(2013). O. Vittorio, E. Jacchetti, *S. Pacini*, and M. Cecchini

318. Neuronal differentiation on anisotropic substrates and the influence of nanotopographical noise on neurite contact guidance, Biomaterials **34**, 6027 (2013). I. Tonazzini, **S. Meucci**, P. Faraci, F. Beltram, and M. Cecchini

319. Cell Guidance on Nanogratings: A Computational Model of the Interplay between PC12 Growth Cones and Nanostructures, PloS one **8** 70304 (2013). *P.N. Sergi, I.M. Roccasalvo*, I. Tonazzini, M. Cecchini, and *S. Micera*

320. Easy Monitoring of Velocity Fields in Microfluidic Devices Using Spatiotemporal Image Correlation Spectroscopy, Anal. Chem **85**, 8080 (2013). **M. Travagliati**, *S. Girardo, D. Pisignano*, F. Beltram, and M. Cecchini

321. Interaction of SH-SY5Y Cells with Nanogratings During Neuronal Differentiation: Comparison with Primary Neurons, Adv. health. Mat. DOI: 10.1002/adhm.201300216, (2013). I. Tonazzini, **A. Cecchini**, *Y. Elgersma*, and M. Cecchini

322. Suppression of lateral growth in InAs/InAsSb heterostructured nanowires Original Research Article, J. Cryst. Growth **366**, 8 (2013). M. Pea, D. Ercolani, **A. Li**, M. Gemmi, *F. Rossi*, F. Beltram, and L. Sorba

323. Readsorption Assisted Growth of InAs/InSb Heterostructured Nanowire Arrays, Cryst. Growth Des., **13**, 878 (2013). **A. Li**, *N. V. Sibirev*, D. Ercolani, *V. G. Dubrovskii*, and L. Sorba

324. Crystal phase induced bandgap modifications in AlAs nanowires probed by resonant Raman scpectroscopy, ACS Nano **7**, 1400 (2013). *S. Funk*, **A. Li**, D. Ercolani, M. Gemmi, L. Sorba, and *I. Zardo*

325. Laser-Light Polarization Plastic Visualizer: Light-Scattering Distribution and Anisotropy, RSC Advances **3**, 7677 (2013). *A. Shalit, D. E. Lucchetta, L. Criante, F. Vita, J. Tasseva, F. Simoni, L. Franco*, R. Bizzarri, P. Faraci, *R. Conte, L. Viti, R. Kaner*, and R. Castagna

326. Nanowire-based field effect transistors for terahertz detection and imaging systems, Nanotechnology **24**, 214005 (2013). **L. Romeo**, *D. Coquillat*, M. Pea, D. Ercolani, F. Beltram, L. Sorba, *W. Knap*, A. Tredicucci, and M. S. Vitiello

327. Electrostatic tailoring of magnetic interference in quantum point contact ballistic Josephson junctions, Phys. Rev. B **87**, 134506 (2013). M. Amado, **A. Fornieri**, F. Carillo, *G. Biasiol*, L. Sorba, V. Pellegrini, and F. Giazotto

328. A ballistic quantum ring Josephson interferometer, Nanotechnology **24**, 245201 (2013). **A. Fornieri**, M. Amado, F. Carillo, *F. Dolcini, G. Biasiol*, L. Sorba, V. Pellegrini, and F. Giazotto

329. Hydrogen sulfide in the mouse ductus arteriosus: a naturally occurring relaxant with potential EDHF function, Am. J. Physiol. Heart-C **304**, H927 (2013). *B. Baragatti, E. Ciofini, D. Sodini*, S. Luin, *F. Scebba,* and *F. Coceani*

330. Internal field induced enhancement and effect of resonance in Raman scattering of InAs nanowires, Solid State Commun **160**, 26 (2013). *J. K. Panda, A. Roy, A. Singha*, M. Gemmi, D. Ercolani, V. Pellegrini, and L. Sorba.

331. Oscillatory Vertical Coupling between a Whispering-Gallery Resonator and a Bus Waveguide, Phys. Rev. Lett. **110**, 163901 (2013). *M. Ghulinyan, F. Ramiro-Manzano, N. Prtljaga, R. Guider, I. Carusotto*, A. Pitanti, *G. Pucker,* and *L. Pavesi*

332. Evidence of interlayer interaction in magnetoluminescence spectra of electron bilayers, Phys. Rev. B **87**, 161303 (2013). **I. Aliaj**, V. Pellegrini, A. Gamucci, *B. Karmakar, A. Pinczuk, L. N. Pfeiffer,* and *K. W. West*

333. Imaging the static dielectric constant in vitro and in living cells by a bioconjugable GFP chromophore analog, Chem. Commun **49**, 1723 (2013). G. Signore, **G. Abbandonato, B. Storti**, *M. Stockl, V. Subramaniam*, and R. Bizzarri

334. Electronic band structure of wurtzite GaP nanowires via temperature dependent resonance Raman spectroscopy, Appl. Phys. Lett. **103**, 23108 (2013). J. *Kumar Panda, A. Roy*, M. Gemmi, E. Husanu, **A. Li**, D. Ercolani, and L. Sorba

335. In Vivo Distribution and Toxicity of PAMAM Dendrimers in the Central Nervous System Depend on Their Surface Chemistry, Mol. Pharm **10**, 249 (2013). *L. Albertazzi, L. Gherardini*, **M. Brondi, S. Sulis Sato**, A. Bifone, *T. Pizzorusso*, G. M. Ratto, and G. Bardi

336. Mouse aortic muscle cells respond to oxygen following cytochrome P450 3A13 gene transfer, Can. J. Physiol. Pharm. **91**, 369 (2013). *E. Ciofini*, *F. Scebba*, S. Luin, *D. Sodini, D. Angeloni,* and *F. Coceani*

337. Micro-superconducting quantum interference devices based on V/Cu/V Josephson nanojunctions, Appl. Phys. Lett. **103**, 52603 (2013). **A. Ronzani**, *M. Baillergeau*, C. Altimiras, and F. Giazotto

338. Giant Thermovoltage in Single InAs Nanowire Field-Effect Transistors, Nano Lett. **13**, 3638 (2013). S. Roddaro, D. Ercolani, M. A. Safeen, *S. Suomalainen*, F. Rossella, F. Giazotto, L. Sorba, and F. Beltram

339. Iron (III)/multiacrylate-based holographic mixtures, J. Appl. Phys. **114**, 193101 (2013). *D. E. Lucchetta*, **L. Nucara**, *L. Criante, F. Simoni,* A. Boni, J.H. Xu, R. Bizzarri, and R. Castagna

340. Tuning of quantum interference in top-gated graphene on SiC, Phys. Rev. B **88**, 235406 (2013), A. Iagallo, *S. Tanabe*, S. Roddaro, *M. Takamura, H. Hibino*, S. Heun

341. Hydrogen storage with titanium-functionalized grapheme, Appl. Phys. Lett. **103**, 13903 (2013). T. Mashoff, *M. Takamura, S. Tanabe, H. Hibino*, F. Beltram, and S. Heun

342. Ligand signature in the membrane dynamics of single TrkA receptor molecules, J. Cell Sci. **126**, 4445 (2013). L. Marchetti, **A. Callegari**, S. Luin, G. Signore, A. Viegi, F. Beltram, and A. Cattaneo

343. Optical critical coupling into highly confining metal-insulator-metal resonators, Appl. Phys. Lett. **103**, 091110 (2013). *J.M. Manceau,* **S. Zanotto**, *I. Sagnes, G. Beaudoin,* and *R. Colombelli*

344. Barium titane core-gold shell nanoparticles for hyperthermia treatments, International Journal of Nanomedicine 2319 (2013), *E. FarrokhTakin*, *G.*

Ciofani, G.L. Puleo, **G. de Vito**, *C. Filippeschi, B. Mazzolai*, V. Piazza, and *V. Mattoli*

345. In Vitro Efficient Transfection by CM18-Tat11 Hybrid Peptide: A New Tool for Gene-Delivery Applications, PLoS ONE **8**, 70108 (2013). **F. Salomone**, F. Cardarelli, G. Signore, C. Boccardi, and F. Beltram

346. Imaging intracellular viscosity by a new molecular rotor suitable for phasor analysis of fluorescence lifetime Optical Nanosensing in Cells, Analytical and Bioanalytical Chemistry **405**, 6223 (2013). A. Battisti, **S. Panettieri, G. Abbandonato**, E. Jacchetti, F. Cardarelli, G. Signore, F. Beltram, and R. Bizzarri

347. Cancer phototherapy in living cells by multiphoton release of doxorubicin from gold nanospheres, Journal of Materials Chemistry **1**, 4225 (2013). V. Voliani, G. Signore, O. Vittorio, P. Faraci, S. Luin, *J. Perez-Prieto*, and F. Beltram

348. Spectral "fine" tuning in fluorescent proteins: the case of the gfp-like chromophore in the anionic protonation state, J Chem Theory Comput **9**, 497 (2013), **P. Amat** and R. Nifosì

349. Anderson localization of entangled photons in an integrated quantum walk, Nature Phot. **7**, 322 (2013). *A. Crespi, R. Osellame, R. Ramponi*, V. Giovannetti, R. Fazio, *L. Sansoni, F. De Nicola, F. Sciarrino,* and *P. Mataloni*

350. Electromagnetic channel capacity for practical purposes, Nature Phot. (2013). V. Giovannetti, *S. Lloyd, L. Maccone,* and *J.H. Shapiro*

351. Measures of quantum synchronization in continuous variable systems, Phys. Rev. Lett. **111**, 103605 (2013). **A. Mari, A. Farace**, N. Didier, V. Giovannetti, and R. Fazio

352. Wick's theorem for matrix product states, Phys. Rev. Lett. **110**, 040401 (2013). *R. Huebener*, **A. Mari**, and *J. Eisert*

353. Quantum Breathing of an Impurity in a One-dimensional Bath of Interacting Bosons, Phys. Rev. Lett. **110**, 015302 (2013). **S. Peotta**, D. Rossini, M. Polini, *F. Minardi*, and R. Fazio

354. Minimal self-contained quadridot quantum refrigeration machine, Phys. Rev. Lett. **110**, 256801 (2013). D. Venturelli, R. Fazio, and V. Giovannetti

355. Extracting quantum work statistics and fluctuation theorems by single qubit interferometry, Phys. Rev. Lett. **110**, 230601 (2013). *R. Dorner, S.R. Clark, L. Heaney*, R. Fazio, *J. Goold,* and *V. Vedral*

356. Environment-governed dynamics in driven quantum systems, Phys. Rev. Lett. **110**, 150403 (2013). *S. Gasparinetti*, *P. Solinas*, S. Pugnetti, R. Fazio, and *J.P. Pekola*

357. Photon Solid Phases in Driven Arrays of Nonlinearly Coupled Cavities, Phys. Rev. Lett. **110**, 163605 (2013). J. Jin, D. Rossini, R. Fazio, *M. Leib, M.J. Hartmann*

358. Interactions in electronic Mach-Zehnder interferometers with co-propagating edge channels, Phys. Rev. Lett. **111**, 036801 (2013). L. Chirolli, F. Taddei, R. Fazio, and V. Giovannetti

359. Parity dependent Josephson current through a helical Luttinger liquid, New J. Phys. **15**, 085025 (2013**). S. Barbarino**, R. Fazio, *M. Sassetti*, and F. Taddei

360. Robustness of quantum memories based on Majorana zero modes., Phys. Rev. B **88**, 205142 (2013). Leonardo Mazza, *Matteo Rizzi, Mikhail D. Lukin,* and *J. Ignacio Cirac*

361. Josephson-Majorana cycle in topological single-electron hybrid transistors, Phys. Rev. B **88**, 024512 (2013). N. Didier, **M. Gibertini**, *A.G. Moghaddam, J. Koenig*, and R. Fazio

362. Spin filtering and entanglement detection due to spin-orbit interaction in carbon nanotube cross-junctions, Phys. Rev. B **88**, 195403 (2013). **F. Mazza**, *B. Braunecker, P. Recher,* and *A.L. Yeyati*

363. Photoemission spectra of massless Dirac fermions on the verge of exciton condensation, Phys. Rev. B **87**, 075418 (2013). S. Rist, *A.A. Varlamov, A.H. MacDonald*, R. Fazio, and M. Polini

364. Impact of disorder on Dirac plasmon losses, Phys. Rev. B **88**, 121405(R) (2013). **A. Principi**, *G. Vignale*, **M. Carrega**, and M. Polini

365. XXZ spin-1/2 representation of a finite-U Bose-Hubbard chain at half-integer filling, Phys. Rev. B **87**, 035104 (2013). *D. Giuliano*, D. Rossini, *P. Sodano, and A. Trombettoni*

366. Topological pumping in the one-dimensional Bose-Hubbard model, Phys. Rev. B **87**, 085131 (2013). D. Rossini, **M. Gibertini**, V. Giovannetti, and R. Fazio

367. Microscopic theory of polariton lasing via vibronically assisted scattering Phys. Rev. B **88**, 075321 (2013). **L. Mazza**, *S. Kéna-Cohen, P. Michetti,* and *G.C. La Rocca*

368. Topological pumping in class-D superconducting wires, Phys. Rev. B **88**, 140508(R) (2013). **M. Gibertini**, R. Fazio, M. Polini, F. Taddei

369. Coherent edge mixing and interferometry in quantum Hall bilayers, Phys. Rev. B **87**, 075321 (2013). S. Roddaro, *L. Chirolli*, F. Taddei, M. Polini, and V. Giovannetti

370. Quantum parameter estimation affected by unitary disturbance, Phys. Rev. A **052117**, 88 (2013). A. De Pasquale, D. Rossini, *P. Facchi*, and V. Giovannetti

371. Measuring quantumness via anticommutators, Phys. Rev. A **87**, 052132 (2013). R. Fazio, *K. Modi, S. Pascazio, V. Vedral,* and *K. Yuasa*

372. Collision-model-based approach to non-Markovian quantum dynamics Phys. Rev. A **87**, 040103(R) (2013). *F. Ciccarello, G.M. Palma*, and V. Giovannetti

373. Amendable Gaussian channels Phys. Rev. A **87**, 062307 (2013). A. De Pasquale, A. Mari, *A. Porzio*, and V. Giovannetti,

374. Quantum reading capacity under thermal and correlated noise, Phys. Rev. A **87**, 062310 (2013). *C. Lupo, S. Pirandola*, V. Giovannetti, and *S. Mancini*

375. Speeding up and slowing down the relaxation of a qubit by optimal control Phys. Rev. A **88**, 062326 (2013). V. Mukherjee, A. Carlini, A. Mari, *T. Caneva, S. Montangero, T. Calarco*, R. Fazio, and V. Giovannetti

376. Single-site- and single-atom-resolved measurement of correlation functions, Appl. Phys. B **113**, 27 (2013). *M. Endres, M. Cheneau, T. Fukuhara, C. Weitenberg, P. Schauß, C. Gross*, **L. Mazza**, *M. C. Bañuls, L. Pollet, I. Bloch,* and *S. Kuhr*

377. A quantum non-Markovian collision model: incoherent swap case, Phys. Scr. **T153**, 014010 (2013). *F. Ciccarello* and V. Giovannetti

It may be of interest to examine the evolution of NEST citations during these years. The following histogram provides data from ISI database and shows the positive evolution of the impact of NEST publications in the scientific community (data were collected in February 2014).

NEST: ISI yearly citations

Year	Citations
2008	~1900
2009	~2300
2010	~2680
2011	~2750
2012	~3550
2013	~4130

Laboratorio NEST patents

Patent name	Patent authors	Owner(s)	SNS %	Status
THz semiconductor laser incorporating a controlled plasmon confinement waveguide	A. Tredicucci, F. Beltram, *H. E. Beere, A.G. Davies*, **R. Koehler**, *E.H.Linfield*	SNS	100%	IT Patent: active UE Patent: active USA Patent: active PCT: in progress
Circular semiconductor laser having lattices for vertical emission	**L. Mahler**, A. Tredicucci, F. Beltram	SNS	100%	IT Patent: active UE Patent: in progress USA Patent: in progress PCT: in progress
Metodo e dispositivo per misure di posizione e di massa	F. Beltram, *G. Biasiol*, V. Piazza, P. Pingue, L. Sorba, **E. Strambini**	SNS	100%	IT Patent: in progress
Multiphoton photoreleasing system, based on click-chemistry functionalized gold nanoparticles, for biological applications	F. Beltram, S. Luin, **V. Voliani**, **F. Ricci**, G. Signore, R. Nifosì	Fond. IIT CNR SNS	27%	IT Patent: in progress PCT: in progress
Automatic passive control of liquid positioning in microfluidic chips	V. Piazza, F. Beltram, **M. Travagliati**, M. Cecchini, **G. De Simoni**	Fond. IIT CNR SNS	20%	IT Patent: in progress PCT: in progress
Method for the fabrication of dispersible three-dimensional nanoresonators for biological, medical and environmental applications	A. Bifone, A. Boni, *V. Clericò, F. Recchia*, A. Tredicucci, P. Pingue	Fond. IIT SSSUP CNR SNS	10%	IT Patent: in progress

1.5 Funding

In this section we summarize funding sources for NEST activities indicating separately:

- SNS funding (SNS)
- National ministerial and private funding (ITA)
- European research programs (EU)
- Industrial cooperative projects (ICP)

Laboratorio NEST funding
(k€)
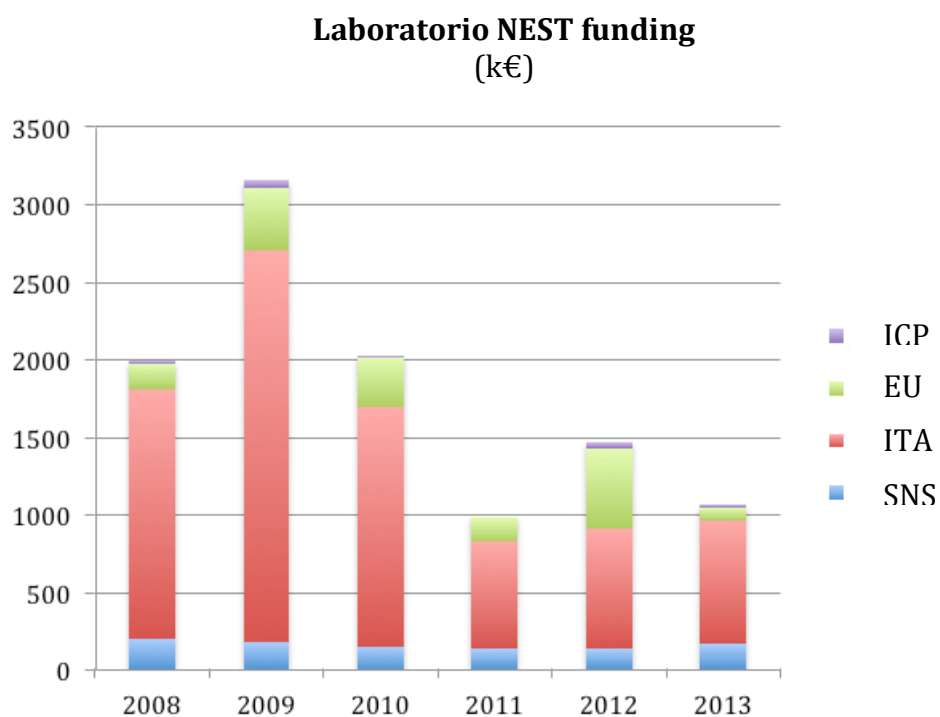
Only funding directly managed by Scuola Normale Superiore is included so that all resources available to the activity at NEST but managed by CNR and IIT are not visibile even if they are the dominant part of the overall budget of the NEST initiative.

1.6 Main collaborations

In the following we list some of the institutions with which NEST people formally collaborated in the period. By "formally" it is intended groups with which we have joint publications in the reference period, groups with which we have carried out projects funded by some entity (European Commission, Italian Ministries, etc.), groups that have hosted NEST students as part of their training.

CANADA. Harry E. Ruda, University of Toronto, Toronto; Marie D'Iorio, National Research Council of Canada, Ottawa

FINLAND. Jukka Pekola, Aalto University, Aalto; Mikko Paalanen, Helsinki University of Technology, Helsinki

FRANCE. Cristiano Ciuti and Carlo Sirtori, Université Paris Diderot, Paris

GREECE. Ilias Perakis, University of Crete and Foundation for Research and Technology - Hellas, Heraklion

GERMANY. Alfred Leitenstorfer University of Konstanz, Konstanz; R. Huber, University of Regensburg G. Abstreiter (TU Muenchen); H.-W. Hübers, Institute for Planetary Research, Berlin; Joachim Spatz, Max Planck Institute for Metals Research, Munich

INDIA. Giridhar U. Kulkarni, Jawaharlal Nehru Centre for Advanced Scientific Research, Bangalore; Anushree Roy, Indian Institute of Technology, Kharagpur.

ITALY. Giorgio Biasiol, IOM-CNR, Trieste; Francesco Tafuri, Seconda Università di Napoli; Giancarlo Salviati, IMEM-CNR, Parma; Diederik Wiersma and Paolo De Natale, CNR-INO, Florence; Tullio Pozzan, IN-CNR, Padova

JAPAN. Yasuhiko Arakawa, University of Tokyo; Hiroki Hibino, NTT Basic Research Laboratories, Morinosato-Wakamiya, Atsugi, Kanagawa

RUSSIA. Eduard Deviatov, V. T. Dolgopolov and V. Khrapai, Institute of Solid State Physics, Russian Academy of Sciences, Chernogolovka. V. Dubroskii, Ioffe Institut, St. Petersburg

SERBIA. Pavle Andjus, University of Belgrade

SPAIN. Francisco Guinea, CSIC, Madrid.

SWEDEN. Lars Samuelson**,** Lund University

SWITZERLAND. Jérôme Faist, ETH, Zurich; Aldo Ferrari, ETH, Zurich

THE NETHERLANDS Mikhail I. Katsnelson and J. K. Maan, Radboud University of Nijmegen, Nijmegen.

UNITED KINGDOM. David A. Ritchie and Jeremy Baumberg, University of Cambridge, Cambridge; University of Nottingham; Giles Davies, University of Leeds**;** University of Sheffield

USA. Enrico Gratton University of California at Irvine; Craig J. Hawker, University of California at Santa Barbara; Allan H. MacDonald, University of Texas, Austin TX; Loren Pfeiffer, Princeton University, Princeton NJ; Aron Pinczuk, Columbia University, New York NY; Robert Westervelt, Harvard University; Paul Alivisatos, University of California at Berkeley; Oskar Painter, California Institute of Technology, Caltech

WITHIN SCUOLA NORMALE. Vincenzo Barone, Giuseppe Brancato, Antonino Cattaneo, Anna Cereseto, Arturo Falaschi

1.7 Undergraduate and graduate training @ NEST

We list here graduate and undergraduate students that carried out their thesis work totally or partially at NEST under the supervision of NEST staff in the period of reference.

2008

Francesca Pacini - Laurea in Fisica
Determinazione delle caratteristiche ottiche e termiche di un laser THz a cascata quantica

Luca Masini - Laurea Magistrale in Fisica
Realizzazione di emettitori Terahertz nanostrutturati a cascata quantica

Giuseppe Valletta - Laurea Magistrale in Fisica
Laser a cascata quantica modulati da onde acustiche

Roberta Gualdani - Laurea Magistrale in Chimica
E2Red: una sonda proteica per la misura combinata del cloruro e del pH

Stefano Tirelli - Laurea Magistrale in Fisica
Modulation of Josephson current in out of equilibrium superconductors

Sebastian Sulis Sato - Laurea Magistrale in Scienze e Tecnologie biomolecolari
Studio in vivo dell'interazione tra astrociti e neuroni nella genesi e nella propagazione dello stato epilettico

Umberto Terranova - Laurea Magistrale in Fisica applicata
Il ruolo dell'architettura delle proteine fluorescenti nel promuovere la formazione del cromoforo: un approccio di dinamica molecolare

Giulia Privitera - Laurea Magistrale in Fisica
Studio delle proprietà di materiali nanostrutturati mediante tecniche di microscopia a forza elettrica

Alessandro Farace – Laurea triennale in Fisica
Dinamica fuori dall'equilibrio di cavit`a QED accoppiate

Giampiero Caruso – Laurea in Fisica
Percolazione di entanglement in network quantistici

Tommaso Tufarelli – Laurea in Fisica
Quantum state transfer with spin chains of polaritonic qubits

Aji Anappara - Perfezionamento in Fisica della Materia condensata
Light-matter interaction in intersubband microcavities

Filippo Caruso – Perfezionamento in Fisica
Quantum Information Transfer over Quantum Channels

2009

Efisio Gigliotti - Laurea Magistrale in Fisica Applicata
Realizzazione di strutture periodiche e guide d'onda integrate per l'osservazione di polaritoni intersottobanda

Daniele Costantini - Laurea Magistrale in Fisica
Analysis of transport properties and photoconductive response of single InAs nanowires

Leonardo Bartoloni - Laurea Magistrale in Fisica
Fabbricazione e caratterizzazione di nanofili di YBaCuO

Michele Montinaro - Laurea Magistrale in Fisica
Microscopio THz a scansione differenziale

Andrea Ursic - Laurea Magistrale in Chimica
Conversione a due fotoni della proteina fluorescente EYQ1

Mara Barucco - Laurea in Fisica
Spettroscopia Raman di singola molecola: le proteine fotocromiche EYQ1

Chiara Martino - Laurea Magistrale in Ingegneria biomedica
Design and development of a microfluidic biochip for chemical and physical cell stimulation

Riccardo Metere - Laurea in Fisica
Trasporto acustoelettrico indotto da onde acustiche di superficie in eterostrutture GaAs/AlGaAs

Ugo Siciliani de Cumis - Laurea in Fisica
Trasporto elettronico coerente in nanostrutture multiterminali

Laura Pistoia - Laurea in Scienze Biologiche Molecolari
Calibrazione e clonaggio di un sensore geneticamente codificato per misure intracellulari di Cloro e pH a due fotoni

Sara Malara - Laurea in Scienze Biologiche Molecolari
Imaging del calcio a due fotoni in vivo

Giuseppe De Vito - Laurea in Scienze Biologiche Molecolari
Imaging a due fotoni in vivo di attività interictale nella corteccia visiva del topo

Lorenzo Romeo - Laurea di primo livello in Fisica
Trasporto acustoelettrico in nanofili semiconduttori

Sebastiano Peotta – Laurea in Fisica
Josephson currents in graphene bilayers

Stefano Valentini – Laurea triennale in Fisica
Effetti quantistici nello sviluppo di algoritmi per accesso remoto

Francesco Cardarelli - Perfezionamento in Biofisica Molecolare
Nanostructuring HIV-1 Tat arginine-rich motif for targeted cellular delivery

Matilde Marchi - Perfezionamento in Biofisica Molecolare
Dynamic imaging of the intracellular trafficking of ERK suggest a novel mechanism at the basis of the functional differences between ERK1 and 2

Alberto Albanese – Perfezionamento in Biologia Molecolare
Intranuclear trafficking of HIV – fluorescent particles

Shabnam Safaei – Perfezionamento in Fisica
Quantum Optimal Control of Josephson-Based Circuits

Andrea Tomadin – Perfezionamento in Fisica
Dynamical instabilities of many-body systems

2010

Ilaria Sanzari - Laurea Ingegneria Biomedica
Trasporto di Microparticelle in Sistemi Fluidici Integrati basati su Onde Acustiche di Superficie

Sandro Meucci - Laurea Magistrale Ingegneria Biomedica
Neuronal Differentiation on nanoengineered Scaffolds: Focal Adhesion Sensing of Noisy Nanotopographies,

Davide Raffaele Ceratti - Laurea in Chimica
Sintesi e spettroscopia di composti cumarinici fotolizzabili. Un passo preliminare alla creazione di nanosistemi per il drug delivery

Anna Bochicchio - Laurea in Fisica
Dinamica molecolare di peptidi per il trasporto intracellulare

Lorenzo Lugani - Laurea Magistrale in Scienza dei materiali
Growth and Structural Study of InAs-InSb heterostructured Nanowires

Greta Pintacuda - Laurea in Scienze Biologiche Molecolari
TIRF-Imaging in tempo reale dell'internalizzazione di HIV-1 Tat-EGFP

Luca Tosti - Laurea in Scienze Biologiche Molecolari
Analisi FRAP per la determinazione di parametri biochimici relativi alla traslocazione nucleo-citoplasma

Nicolò Grilli - Laurea in Fisica Generale
Effetto Tunnel Risonante in nanofili eterostrutturati

Alessandro La Chioma - Laurea in Scienze Biologiche Molecolari
Studio in vivo delle alterazioni morfo-funzionali della circuiteria neuronale corticale, indotte dalla digestione della matrice extracellulare

Luigi Federico Rossi - Laurea in Scienze Biologiche Molecolari
Strategie molecolari per la trasduzione in vivo di un sensore geneticamente codificato

Letizia Mariotti - Laurea Magistrale in Neurobiologia
Utilizzo di un sensore geneticamente codificato per lo studio delle dinamiche spazio-temporali dell'anione cloruro

Emanuela Ligarò - Laurea Magistrale in Fisica.
Coerenza elettronica e trasporto acustoelettrico in nanodispositivi

Tommaso Lunghi - Laurea Magistrale in Fisica applicata
Osservazione di emissione di singolo fotone da giunzione planari

Simone Gasparinetti - Laurea Magistrale in Fisica
Quantum dot Thermometry

Andrea Pescaglini - Laurea Magistrale in Fisica
Modulazione della supercorrente in giunzioni S-nanowire-S tramite elettrodi iniettori

Marco Travagliati – Laurea Magistrale in Fisica
Fabrication and time-resolved optical investigation of hypersonics phononic christals

Alessandro Farace – Laurea in Fisica
Non classical states of an oscillator in optomechanical systems

Angelo Di Marco - Laurea in Fisica
Quantum Optimal Control of Superconducting Charge Qubits

Gianluca Micchi – Laurea triennale in Fisica
Correlazioni quantistiche in processi di scattering elettronico

Laura Marchetti – Perfezionamento in Biologia Molecolare
Dynamics and interactions of an oncogenic homeotic protein within human human replicative complexes

Elio Profumo - Perfezionamento in Fisica
Interaction effects in decoupled graphene layers

Elena Canovi - Perfezionamento in Fisica (SISSA)
Quench dynamics of many-body systems

2011

Mariangela Panniello - Laurea Magistrale in Neurobiologia
La matrice extracellulare come fonte di inibizione della plasticità sinaptica: effetti della sua degradazione in corteccia visiva, in vivo.

Daniela Camillo - Laurea Magistrale in Neurobiologia
Utilizzo di un sensore geneticamente codificato per l'imaging del cloro in modelli fisiopatologici

Giuseppe De Vito - Laurea Magistrale in Biologia applicata alla Biomedicina
Studio sperimentale degli effetti della radiazione Terahertz sulla permeabilità cellulare

Sara Conti – Laurea in Scienze Biologiche Molecolari
Ruolo degli astrociti nel processamento di input visivi tramite microscopia a due fotoni in vivo

Carmine Di Rienzo - Laurea Specialistica in Chimica
Topografie anisotrope aumentano la diffusività di LOX-1 in cellule HUVEC con un meccanismo contrattilità dipendente e ne inibiscono la dimerizzazione

Nicola Di Mitri - Laurea Magistrale in Fisica
Interazione tra onde acustiche di superficie e microparticelle in sistemi microfluidici integrati

Carlo Maria Lazzarini - Laurea in Fisica
Cavità acustiche in sistemi microfluidici basati su onde acustiche di superficie

Miriam Palmiero - Laurea in Biologia
Studio morfo-funzionale di cellule HUVEC coltivate su substrati nanoingegnerizzati

Lorenzo Romeo - Laurea Magistrale in Fisica
Controllo elettrostatico dello spin in punti quantici di InAs

Silvio Panettieri - Laurea in Chimica
Synthesis and characterization of viscosity-dependent fluorophores for bioanalytical use

Francesco Colangelo - Laurea in Fisica
Processi ossido-riduttivi spazialmente risolti su grafene cresciuto mediante tecnica Chemical Vapor Deposition

Diana Di Paolo - Laurea Magistrale in Fisica
Impact of PAMAM dendrimers on the photophysics of linked fluorophores: a spectroscopy and microscopy approach

Diego Scarabelli - Laurea in Fisica
Optical Probing of Spin States of Manganese Atoms in GaAs Quantum Well

Gianluca Micchi - Laurea in Fisica
A superconducting laser in the strong coupling regime

Stefano Valentini – Laurea in Fisica
Electronic Quantum Interference-Diffraction Effects

Elia Strambini - Perfezionamento in Fisica della Materia condensata
Coherent transport in multi-terminal Aharonov-Bohm rings

Lorenzo Albertazzi - Perfezionamento in Biofisica Molecolare
Dendrimers for Drug Delivery and Molecular Imaging

Stefano Pugnetti – Perfezionamento in Fisica
Quantum Transport in Wires and Nanoelectromechanical Systems

Davide Venturelli – Perfezionamento in Fisica (SISSA)
Channel Mixing and Spin Transport in the Integer Quantum Hall Effect

Pietro Silvi – Perfezionamento in Fisica
Tensor Networks: a quantum-information perspective on numerical renormalization groups

2012

Davide Ceratti - Laurea Magistrale in Chimica
Sintesi e caratterizzazione rilassometrica di agenti di contrasto paramagnetici-superparamagnetici ibridi per Risonanza Magnetica

Leonardo Viti - Laurea Magistrale in Fisica
Rivelazione Terahertz con Nanofili a Semiconduttore

Leonardo Vicarelli - Laurea Magistrale in Fisica
 THz Photodetection in Graphene Field Effect Transistors -

Ugo Siciliani de Cumis - Laurea Magistrale in Fisica
Terahertz confocal microscopy with a quantum cascade laser source

Valerio Talora - Laurea Magistrale in Fisica
Laser a Cascata Quantica in quasicristalli fotonici bidimensionali

Fulvio Bonsignore - Laurea Magistrale in Biologia molecolare e cellulare
Nuovi costrutti inducibili per l'analisi biofisica delle dinamiche di singoli recettori di membrana: applicazione a P75^{NTR}

Simone Surdi – Laurea Magistrale in Fisica
Nanofabbricazione di reticoli artificiali a semiconduttore e studio spettroscopico delle eccitazioni collettive

Ilirjan Aliaj – Laurea Magistrale in Fisica della Materia
Evidence of inter-layer interaction in magneto-luminescence spectra of electron double layers

Marco Pagliazzi - Laurea Magistrale in Fisica Medica
Spatio-Temporal Image Correlation Spectroscopy measurements of microparticle dynamics in surface acoustic waves Lab-on-a-Chip devices

Luigi Federico Rossi - Laurea Magistrale in Biologia applicata alla Biomedicina
Imaging neuron-astrocyte interaction in visual processing

Antonella Negro - Laurea Magistrale in Biologia applicata alla Biomedicina
Imaging in vivo a due fotoni della concentrazione di cloro e del pH in corteccia cerebrale di topo

Silvia Ferrara - Laurea Magistrale in Biologia applicata alla Biomedicina
Imaging a due fotoni dell'attività epilettiforme in vivo

Luca Nucara – Laurea Magistrale in Chimica organica
Preparazione di organo(trialcossi)silani e loro impiego nella funzionalizzazione superficiale di ossido di silicio per immobilizzazione covalente di grafene

Nicola Paradiso – Perfezionamento in Fisica della Materia Condensata
Tomography and manipulation of quantum Hall edge channels

Valerio Voliani - Perfezionamento in Biofisica Molecolare
Metal nanoparticles for biomedical applications: engineered coatings for multifunctionalization and controlled release

Fernanda Ricci - Perfezionamento in Biofisica Molecolare
Clophensor: a novel genetically encoded probe of intracellular ions

2013

Francesco Trovato - Laurea Magistrale in Biotecnologie Molecolari ed Industriali
Sviluppo di un sensore fluorescente per la rilevazione della attività della ricombinasi Cre

Marco Galimberti – Laurea Magistrale in Fisica Medica
Simulazioni di dinamica molecolare classica con modelli a bassa risoluzione della proteasi di HIV-1

Giulia Spampinato - Laurea Magistrale in Fisica della Materia condensata
A Minimalist Model for Simulation of Structure and Dynamics of Helical Polypeptides

Anna Bochicchio - Laurea Magistrale in Fisica della Materia condensata
Multi–Scale simulations of -2microglobulin Supervisor

Francesco Tavanti - Laurea Magistrale in Fisica Medica
Dinamica molecolare delle rodopsine con modelli multi-scala

Davide Toniolo – Laurea in Chimica
Analisi statistica della morfologia di nanofili a semiconduttore

Lorenzo Baldacci – Laurea Specialistica in Fisica
Coherent enhancement of absorption in metal-semiconductor structures

Francesco Gobbo – Laurea in Biologia molecolare e cellulare
Space-resolved mRNA imaging in living cells and subcellular control of its localization in neuronal cell models

Alessandra Cecchini - Laurea Magistrale in biotecnologie molecolari e industriali
Correlazione tra meccanotrasduzione e sistema dopaminergico: studio in un modello neuronale umano attraverso l'utilizzo di substrati nanostrutturati

Martino Alfredo Cappelluti - Laurea Magistrale in biologia molecolare
Studio delle interazioni tra substrati nanostrutturati di polietilene tereftalato (PET) e cellule staminali mesenchimali umane derivate da midollo osseo (hBM MSC)

Antonio Fornieri – Laurea Magistrale in Fisica
Josephson effect in ballistic semiconductor nanostructures

Giorgio de Simoni – Perfezionamento in Fisica della Materia Condensata
From anti-bunching to lasing: planar junctions in semiconductor heterostructures

Lukas Mahler - Perfezionamento in Fisica della Materia Condensata
Photonic structures for Terahertz Quantum Cascade Lasers

Fabio Trovato – Perfezionamento in Biofisica Molecolare
Molecular Dynamics Simulations of biopolymers within the cell environment: Minimalist models for the Nucleic Acids and Green Fluorescent Proteins in the cytoplasm

Riccardo Parra – Perfezionamento in Neurobiologia
Analysis of trafficking properties of ERK1 and ERK2 in neural cells

Marco Gibertini – Perfezionamento in Fisica
Quantum transport and many-body effects in graphene and topological superconductor

Diego Rainis – Perfezionamento in Fisica
Electronic Transport in Graphene Hybrid Structures

Sebastiano Peotta – Perfezionamento in Fisica
Nonequilibrium dynamics of strongly correlated one-dimensional ultracold quantum gases

Alessandro Principi – Perfezionamento in Fisica
Electron-electron interactions in few-layer graphene systems

2. Scientific proposal

2014-2018

2.1 Strategic development lines for the NEST initiative

2.1.1 Institutional development

Scuola Normale Superiore objective of making NEST and the San Silvestro facility a reference center for research in nanoscience has so far successfully attracted other institutions, namely the Consiglio Nazionale delle Ricerche, the Istituto Italiano di Tecnologia, and, very recently, Scuola Superiore Sant'Anna. This last addition (in 2013) led to the creation of nanoPlant@NEST that will expand the scope of NEST activities to plant biology. We regard this as a significant development from at least two points of view. Firstly this is the first joint initiative of the Scuola Normale Superiore and Scuola Superiore Sant'Anna, two sister institutions that will much benefit from a closer collaboration and for teaming up to reach critical mass. Secondly this opens NEST to *green* biology, an important development line and a wide range of opportunities for the whole NEST community and its methodologies.

Furthermore, contacts are in progress with Fondazione Pisana per la Scienza - ONLUS, a newly established non-profit private-research organization, for its joining the NEST initiative. This would complete the nanobiotech effort at NEST by adding a group with proteomics and genomics research activities with marked clinical interests. We regard this as a very important opportunity for the NEST community since it would stimulate translational research and help apply NEST research to the actual clinical world.

2.1.2 Technology transfer

NEST scientists have consistently investigated and demonstrated novel methods and techniques that can have an impact on industrial development and innovation. This is a characteristic property of nanoscience and it is known to have a very large potential both for the establishment of novel product lines and for the "injection" of innovation and competitive advantage in more "mature" industries. Today the latter represent the backbone of Tuscany industry.

While this proposal is being written a Regional-Government funded technology transfer initiative is being established at NEST. The "Centro di Competenza NEST per le nanotecnologie" opened in 2013 with 950 k€ funding made available by Regione Toscana. Its objective is to facilitate the transfer of innovative ideas and technologies generated by NEST research activities from the laboratory to industrial applications, and to support industrial research and development activity by making available its state-of-the-art instrumentation. The "Centro di Competenze NEST per le Nanotecnologie" is expected to focus on three main technology-transfer activities: 1) nanofabrication, 2) analysis and characterization, 3) nanocertification.

Nanofabrication, analysis and characterization activities will be made possible by NEST Clean Room facility through instruments and equipment that allow nm-scale resolution both in fabrication and in topographical-structural-compositional imaging and analysis. Nanocertification activity will be developed together with the industrial partners in order to certify structure and function of nanomaterials or technologies. This last task is expected to be crucial for the use of nanomaterials at a large-scale industrial production, where the final product is

directly employed by consumers and the effectiveness of nanomaterials and/or their presence and/or their active role in the properties of a new material must be tested before commercialization.

Finally, while this report is being written talks are in progress for another joint initiative involving NEST, the Regione Toscana and the Capannori (Lucca) administration. The purpose of these interaction is the creation of a Science Park in Capannori with the support of Regione Toscana where NEST will provide technical expertise both in the selection of the new startups to be hosted in the Science Park and in providing technical support for their activity.

It is much hoped that after about ten years of successful activity as a research center, NEST will prove ready to play a role as a driver of economic growth in the area.

2.1.3 People and facilities

Data in Sec. 1.2.1 clearly show that most of the senior staff at NEST is affiliated to the partner institutions (i.e. IIT and CNR), while Scuola Normale Superiore is mostly present with students and fellows. While this approach will continue in the following years, SNS must ensure a continued leadership and presence in the Laboratory research areas. At present one full professor and one tenured assistant professor are active in the lab, and two professors (one associate and one full professor) carry out theoretical research. All of them have a background in condensed matter physics. It is felt that the very minimum necessity of another professor –at the full or associate level- in biophysics must be considered urgently.

Laboratorio NEST proved able to generate funds to hire the necessary fellows and to establish joint projects with CNR and IIT people to create a dynamic and healthy research environment. There are no reasons to believe that this trend will not continue, so that no further specific personnel requirements are mentioned. The only concern stems from the recent cancellation of the tenured ricercatore position in the Italian university system. They may lead to the need for additional professorial staff or to a further dependence from the hiring policies (and, above all, personnel quality) of the partner institutions. For what concerns technical staff, if technology transfer activities increase and so do collaborative projects with industry, it may be necessary to hire additional specialized staff. Should this be the case, however, we expect that dedicated funding will be made available by the regional authorities and will not require specific funding from the SNS.

For what concerns facilities, NEST never relied on SNS funding to purchase instrumentation. At present the lab expansion planned appears adequate for the whole five-year period of this proposal. Proponents regard as particularly positive the close proximity to the Scuola Normale Superiore BioLab and the Chemistry group: this is expected to favor multidisciplinary training and research. The major change in equipment during the next period is expected to stem from a transition to cryo-free setups. This will be made possible by the current advancements in the available technologies and is strongly motivated by the significant expenses for cryogenic fluids at NEST. A continued, timely update

of imaging and nanofabrication equipment is expected thanks to research-project funding.

2.2 Research lines

The development lines at NEST are constantly kept at the forefront of nano(bio)technology so that writing this report/proposal at the end of 2013 does not demand to rethink or drastically update the scope of the activity.
Indeed, we feel that NEST research lines are up to date and at the state of the art. Certainly a different emphasis is put on different aspects and it is felt that specific issues must be highlighted today (and will deserve specia attention in the coming several years). It is important to state that at NEST emphasis is mostly put on student training *through* research. We accept the price of a broad range of issues concurrently under investigation in order to generate individual challenges for our students, graduate students in particular, as a tool to stimulate their rapid growth into independent young scientists.

Two main directions can be identified for the coming years: (i) semiconductor, hybrid semiconductor-superconductor nanostructures, and solid-state quantum computation on one hand, and (ii) molecular biophysics on the other. These two research lines naturally correspond to the two PhD programs available at NEST, Fisica della Materia Condensata (Condensed Matter Physics) and Scienze Biofisiche (Biophysical Sciences), respectively.
These two lines will be discussed separately.

Condensed matter physics research
Semiconductor-nanowire and graphene-based nanostructures, hybrid semiconductor-superconductor and other phase-sensitive systems together with quantum information and its connection to condensed matter will be the main research directions in the incoming years. Semiconductor nanowires are produced at NEST and are fundamental building blocks for electron transport studies, hybrid nanosystem fabrication and nanodevice production. An extensive materials-science research work is ongoing that provides NEST scientists with novel material combinations and research opportunities. Different catalysts, As- and Sb-based binary and ternary alloys are made available that allow electron transport studies in low dimensions (with an emphasis on ballistic transport), thermoelectrics and piezoelectrics investigations in these artificial systems. The fact that nanowires represent self-contained stable nanostructures makes them ideal candidates for the integration with superconductor systems. Also here, materials science efforts are dedicated to optimizing the fabrication of ideal semiconductor-superconductor interfaces. Both *in-situ* and *ex-situ* protocols will be tested to obtain high-transparency junctions suitable for the experimental study of proximized low-dimensional systems. This activity is carried out in collaboration with CNR personnel and benefits from IIT characterization facilities. Hybrid nanodevices are also investigated as very promising hosts of Majorana zero-mode excitations. This last activity will be developed in the more general framework of quantum information, its implementations in condensed matter and the realization of quantum simulators of many-body systems.

Important stimuli for these activities stem from the ongoing investigations of more formal aspects of quantum computation and communication.

The second research line to be mentioned is based on graphene. This system is currently attracting much interest and NEST groups are directly involved in the European flagship initiative on this material system. Our peculiar interest is on hydrogen storage and to this end a dedicated scanning tunneling microscopy system was set up for the study H-graphene interaction, but activities are ongoing also for radiation detectors and electron transport that take advantage of the peculiar electronic properties of this material. At present most of these latter experimental investigations are carried out based on flakes produced with simple mechanical methods starting from graphite, but an intense effort in ongoing to synthesize graphene on various substrates by chemical vapor deposition thanks to the existing IIT facility available at NEST.

We expect to investigate electronic transport and optoelectronic properties and devices also starting from heterostructures (mostly III-V) acquired through our collaborations that will be processed and studied at NEST. Our expertise and equipment allow us to fabricate a very broad range of devices optimized for implementation of model systems of interest or for the realization of specific device prototypes.

Physics of biological systems - nanomedicine

This research field has rapidly grown at NEST in these past years. The development lines envisioned at present include the investigation of drug-delivery fundamentals, studies on new high-sensitivity high-resolution microscopy approaches with an emphasis on single-molecule studies and on the development of novel sensing nanoprobes (useful also for diagnostic purposes), and microfluidics within lab-on-chip architectures.

A significant body of knowledge was acquired at NEST in these last years on endosomes and their trafficking, and on the exploitation of this constitutive mechanism for the purpose of delivery of a variety of payloads into the cytoplasm (some of these activities can be found in Sec. 1.3.2). In the incoming years we intend to build on these results and on the further study on the molecular details of endocytosis in order to develop novel vectors capable of driving cell internalization via endocytosis followed by efficient endosomal escape. It is felt that this field offers unique opportunities for NEST since it combines high biomedical relevance with a number of methodological issues that can challenge the diverse background of NEST people. Novel imaging techniques will be required, novel carriers of organic and/or biological origin (*e.g.* exosomes) will be investigated, cell selectivity will be targeted as well based also on our recent results on aptamers.

In line with current trends in nanobiotechnology, we view these as some of the modules of more complex architectures like the one schematically sketched in the cartoon on the left. Apart from the "Targeting" element, at NEST the "Sensor" module was implemented with GFP-derived mutants and dendrimer-based architectures capable of probing intracellular pH and Cl$^-$ (both in cultured cells and *in vivo*), additionally polarity and viscosity sensors were

shown. Research on this module is expected to continue. We plan to investigate one additional module: "Contrast Agents" such as nanoparticles suitable for MRI, although the bulk of our experiments will continue to be based on fluorescent probes both at cell-level and *in vivo*. No activity is planned on the "Drugs" module, although existing molecules were employed in innovative configurations (e.g., doxorubicin). In this context, we plan to collaborate with other groups that may make available new molecules of pharmaceutical relevance. In fact an important aspect of the activity of the coming years is a planned increased collaboration with partners that can assist us with medical expertise and samples. We are currently performing some first tests together with Fondazione Monasterio in Pisa. The ongoing contacts with Fondazione Pisana per la Scienza were already mentioned in Sec. 2.1.1.

For what concerns imaging, the laboratory is equipped with a rather large set of microscopy systems and in this context we intend to develop new probes and new methodologies capable of yielding single-molecule sensitivity, access to molecular properties (e.g. diffusivity, interactions), and *in vivo* applicability. Recent examples in this direction are represented by ref. 304 and the setup of a CARS facility. We shall also investigate the use of coated metallic nanoparticle probes (based on their optical properties such as plasmonic resonances or surface enhanced raman scattering - SERS) and/or of spectroscopic based diagnostic tools, e.g. for the identification and separation of specific exosomes. Activity is not limited to optical microscopy, however, and electron microscopy of biological samples is available thanks to the collaboration with NEST IIT groups.

For what concerns lab-on-chip technologies, the next few years will be dedicated to assess the actual practical applicability of our surface-acoustic-wave pumping method described in Sec. 1.3.3. Specific demonstrators of automated diagnostic systems will be targeted, whenever possible integrating in these systems the sensing elements developed at NEST. In this context the role of SAW-induced mixing is envisioned as an important mean to induce increased sensitivity in conventional or nanoparticle-based optical sensing architectures, with or without SAW pumping included in the overall architecture. This research line will be discontinued if no realistic implementation is achieved within the period of the present proposal. Somewhat along the same lines, we feel that our extensive work on guided cell differentiation and growth (Sec. 1.3.7) is now mature to be put to the final *in vivo* test. Collaborations with Pisa and Manchester (UK) groups were recently established to apply our patterning techniques to guide neuronal regeneration in rodents.